USGS
science for a changing world

Prepared in cooperation with the
NATIONAL PARK SERVICE

Characterization of Near-Surface Geology and Possible Voids Using Resistivity and Electromagnetic Methods at the Gran Quivira Unit of Salinas Pueblo Missions National Monument, Central New Mexico, June 2005

Scientific Investigations Report 2006–5176

U.S. Department of the Interior
U.S. Geological Survey

Characterization of Near-Surface Geology and Possible Voids Using Resistivity and Electromagnetic Methods at the Gran Quivira Unit of Salinas Pueblo Missions National Monument, Central New Mexico, June 2005

By Lyndsay B. Ball, Jeffrey E. Lucius, Lewis A. Land, and Andrew P. Teeple

Prepared in cooperation with the National Park Service

Scientific Investigations Report 2006–5176

U.S. Department of the Interior
U.S. Geological Survey

U.S. Department of the Interior
DIRK KEMPTHORNE, Secretary

U.S. Geological Survey
P. Patrick Leahy, Acting Director

U.S. Geological Survey, Reston, Virginia: 2006

For product and ordering information:
World Wide Web: http://www.usgs.gov/pubprod
Telephone: 1-888-ASK-USGS

For more information on the USGS--the Federal source for science about the Earth, its natural and living resources, natural hazards, and the environment:
World Wide Web: http://www.usgs.gov
Telephone: 1-888-ASK-USGS

Suggested citation:
Ball, L.B., Lucius, J.E., Land, L.A, Teeple, A.P., 2006, Characterization of near-surface geology and possible voids using resistivity and electromagnetic methods at the Gran Quivira Unit of Salinas Pueblo Missions National Monument, central New Mexico, June 2005: U.S. Geological Survey Scientific Investigations Report 2006–5176, 101 p.

Contents

Figures

Tables

Conversion Factors, Abbreviations, and Datums

Multiply	By	To obtain
	Length	
centimeter (cm)	0.3937	inch (in.)
kilometer (km)	0.6214	mile (mi)
meter (m)	3.281	foot (ft)
	Area	
hectare (ha)	2.471	acre
hectare (ha)	0.003861	square mile (mi^2)
square kilometer (km^2)	247.1	acre
square kilometer (km^2)	0.3861	square mile (mi^2)

Vertical coordinate information is referenced to the North American Vertical Datum of 1988 (NAVD 88).

Horizontal coordinate information is referenced to North American Datum of 1983 (NAD 83).

Elevation, as used in this report, refers to distance above the vertical datum.

Additional Abbreviations

1-D	one-dimensional
2-D	two-dimensional
3-D	three-dimensional
DC	direct current
EM	electromagnetic
FDEM	frequency-domain electromagnetic
GPS	global positioning system
Hz	hertz
NPS	National Park Service
ohm-m	ohm-meter
ppm	parts per million
RMS	root mean square
RTK	real-time kinematic
Rx	receiver
TDEM	time-domain electromagnetic
Tx	transmitter
USGS	U.S. Geological Survey

Characterization of Near-Surface Geology and Possible Voids Using Resistivity and Electromagnetic Methods at the Gran Quivira Unit of Salinas Pueblo Missions National Monument, Central New Mexico, June 2005

By Lyndsay B. Ball[1], Jeffrey E. Lucius[2], Lewis A. Land[3], and Andrew P. Teeple[1]

Abstract

At the Gran Quivira Unit of Salinas Pueblo Missions National Monument in central New Mexico, a partially excavated pueblo known as Mound 7 has recently become architecturally unstable. Historical National Park Service records indicate both natural caves and artificial tunnels may be present in the area. Knowledge of the local near-surface geology and possible locations of voids would aid in preservation of the ruins. Time-domain and frequency-domain electromagnetic as well as direct-current resistivity methods were used to characterize the electrical structure of the near-surface geology and to identify discrete electrical features that may be associated with voids.

Time-domain electromagnetic soundings indicate three major electrical layers; however, correlation of these layers to geologic units was difficult because of the variability of lithologic data from existing test holes. Although resistivity forward modeling was unable to conclusively determine the presence or absence of voids in most cases, the high-resistivity values (greater than 5,000 ohm-meters) in the direct-current resistivity data indicate that voids may exist in the upper 50 meters. Underneath Mound 7, there is a possibility of large voids below a depth of 20 meters, but there is no indication of substantial voids in the upper 20 meters. Gridded lines and profiled inversions of frequency-domain electromagnetic data showed excellent correlation to resistivity features in the upper 5 meters of the direct-current resistivity data. This technique showed potential as a reconnaissance tool for detecting voids in the very near surface.

Introduction

Gran Quivira, known to the Spanish colonists of New Mexico as the Pueblo de las Humanas, was occupied by Native Americans between 1300 A.D. and 1672 A.D. (Hayes and others, 1981). The Gran Quivira Unit of Salinas Pueblo Missions National Monument is a mixed assemblage of Native American pueblo ruins and colonial-era Spanish missions located in central New Mexico (fig. 1*A*). Excavation and partial reconstruction of some of these pueblo ruins have taken place over the past century, with excavations of the largest of the house mounds, Mound 7 (fig. 1*B*), occurring in the 1960s. Recently, the structures of Mound 7 have become architecturally unstable, and the National Park Service (NPS) has proposed backfilling the base of these structures to preserve structural integrity (Steven DeVore, NPS, oral commun., 2005).

The near-surface geology of the area surrounding the Gran Quivira Unit is composed primarily of carbonates and evaporites (Clebsch, 1957; Titus, 1960). As water infiltrates the subsurface, dissolution of carbonates and evaporites along joints and bedding planes can occur over time, leading to the formation of open caverns. Frequently, as these caverns increase in size, the overlying material can no longer be supported, causing surface collapse and the formation of sinkholes. An historic NPS report refers to a vertical shaft, excavated by treasure hunters in the late 19th century in the apse of San Isidro Church (fig. 1*B*), that had intersected a natural cave system. The shaft has since been backfilled. The report also refers to an artificial horizontal tunnel that extended from the vertical shaft in a northwest direction toward San Buenaventura Mission. The report also states that this tunnel intersected features “similar to those found in Carlsbad Caverns,” (Attwell, NPS, written commun., 1932, on record at Salinas Pueblo Missions National Monument Headquarters Archive, Mountainair, N. Mex.). Knowledge of the local near-surface geology and the possible location of open voids in the area surrounding the Gran Quivira Unit is essential to the effective preservation and resource management of Salinas Pueblo Missions National Monument.

[1] U.S. Geological Survey, Lincoln, Nebraska.

[2] U.S. Geological Survey, Lakewood, Colorado.

[3] New Mexico Bureau of Geology & Mineral Resources and the National Cave & Karst Research Institute, Carlsbad, New Mexico.

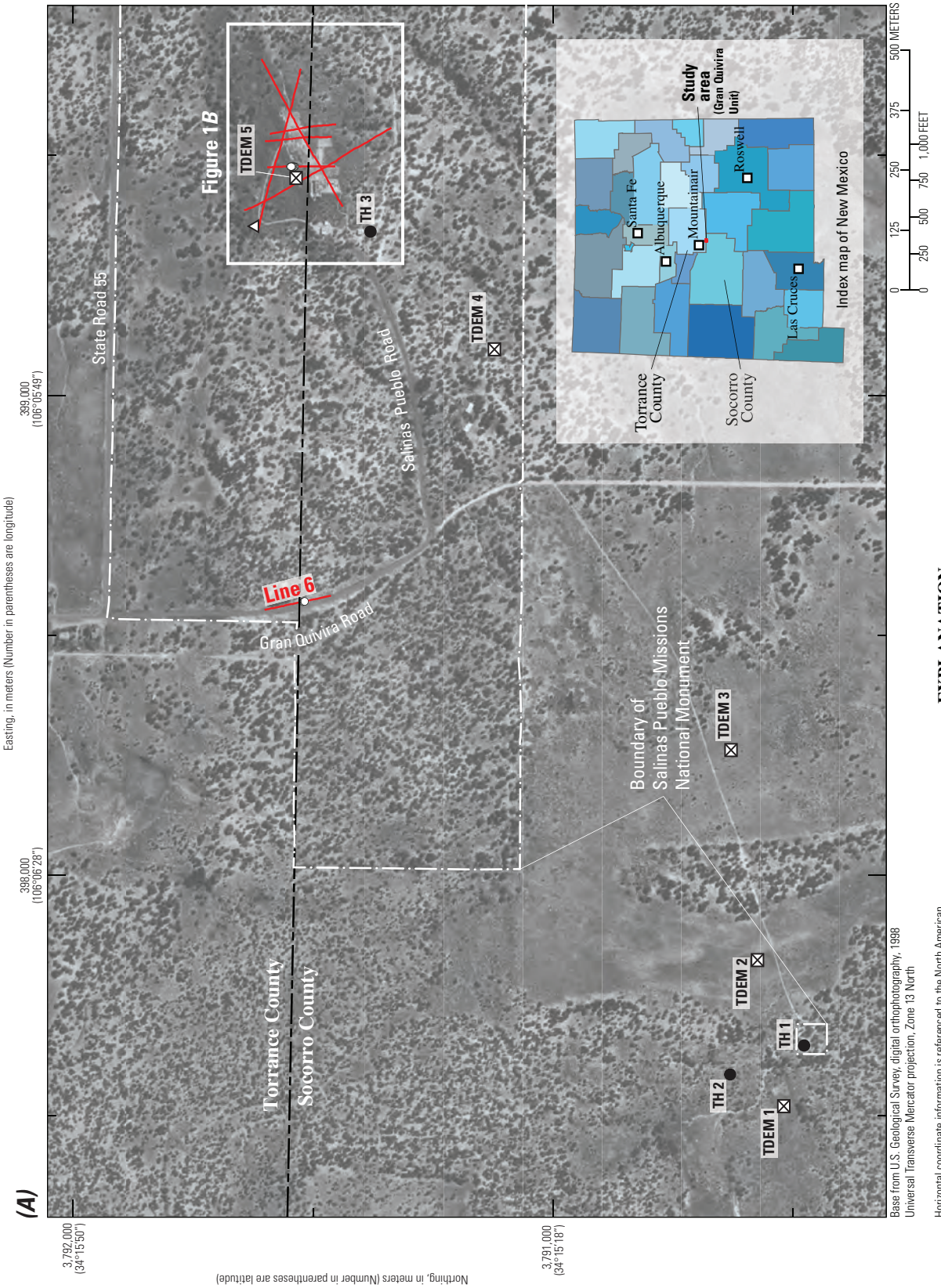
(A)
Easting, in meters (Number in parentheses are longitude)
398,000 (106°06'28")
399,000 (106°05'49")
3,792,000 (34°15'50")
3,791,000 (34°15'18")
Northing, in meters (Number in parentheses are latitude)
State Road 55
Figure 1B
TDEM 5
TH 3
TDEM 4
Salinas Pueblo Road
Line 6
Gran Quivira Road
Torrance County
Socorro County
Boundary of Salinas Pueblo Missions National Monument
TDEM 3
TDEM 2
TH 2
TH 1
TDEM 1
Index map of New Mexico
Study area (Gran Quivira Unit)
Santa Fe
Albuquerque
Mountainair
Roswell
Las Cruces
Torrance County
Socorro County
0 125 250 500 750 1,000 FEET
0 250 500 375 500 METERS
Base from U.S. Geological Survey, digital orthophotography, 1998
Universal Transverse Mercator projection, Zone 13 North
Horizontal coordinate information is referenced to the North American Datum of 1983 (NAD 83)
EXPLANATION
Line 1 Direct-current resistivity and profiled frequency-domain electromagnetic line and number
TDEM 1 Time-domain electromagnetic sounding and map identifier
Igneous intrusion—location approximate
GEM-2 calibration point
Adobe-lined pit—location approximate
TH 1 Test hole and map identifier—location approximate

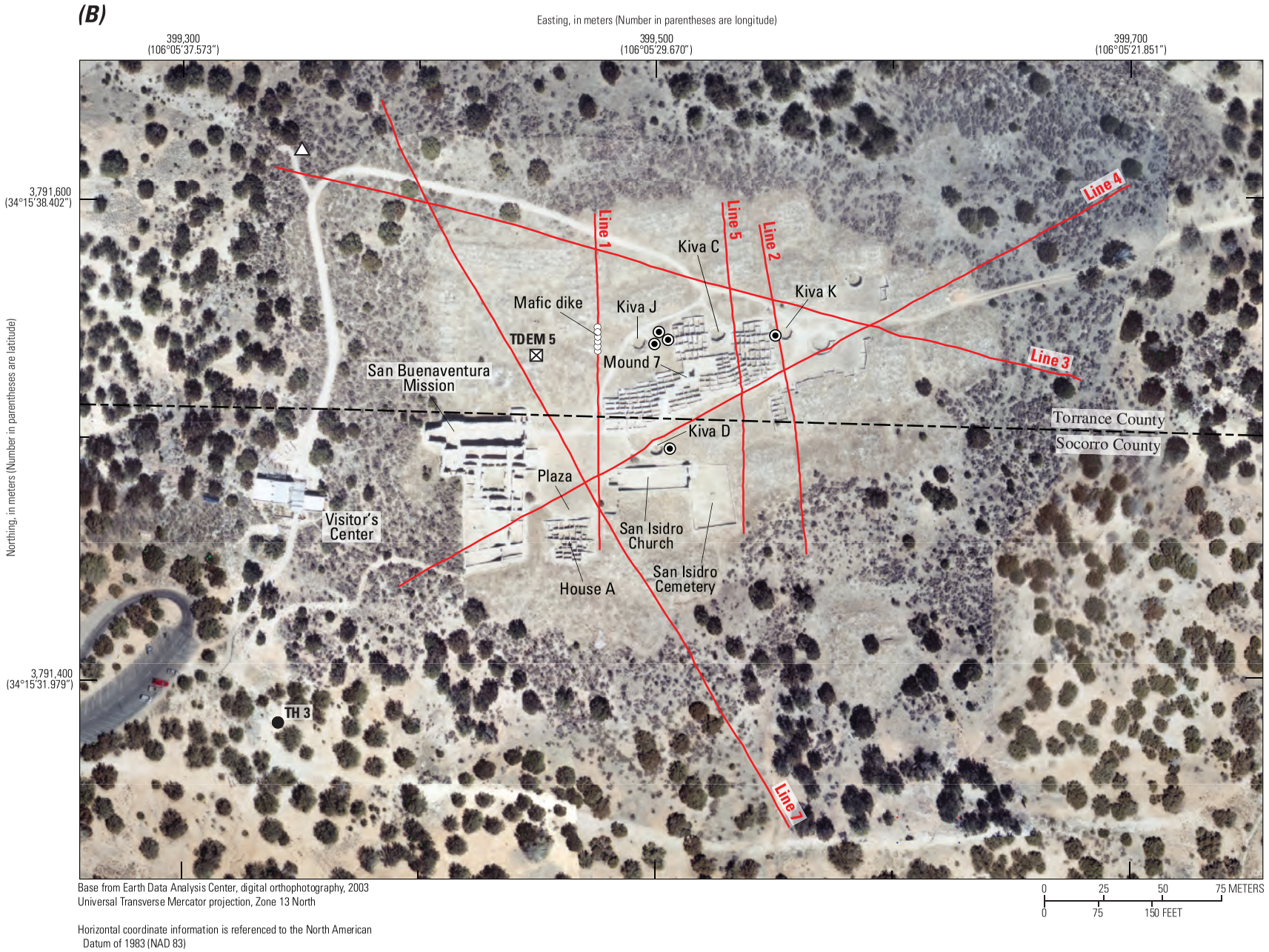

Figure 1. Location of *(A)* study area and *(B)* data-collection sites at the Gran Quivira Unit, Salinas Pueblo Missions National Monument, central New Mexico.

A typical geologic mapping study would collect information by test-hole drilling and surficial geologic mapping techniques. The risk of damage to valuable subsurface cultural resources often found on archeological sites is too great when invasive and potentially destructive data-collection techniques such as drilling are used, and the presence of extensive archeological features can hide outcropping geologic structures. Extensive drilling also can be time intensive and costly, and frequently test holes are drilled too far apart to adequately characterize small areas and discrete features such as open voids. In contrast, surface-geophysical methods provide quick, nonintrusive, and relatively inexpensive alternatives for collecting more continuous subsurface geologic information.

Surface-geophysical methods provide information about the spatial distribution of subsurface physical properties, such as electrical conductivity (or its inverse, resistivity), dielectric permittivity, magnetic permeability, density, and elasticity. For geophysical methods to detect specific subsurface features, such as voids, there must be sufficient physical contrast between the feature and the surrounding material. For example, because the resistivity of air in an open void is very high, approximately $4x10^{13}$ ohm-m (Lide, 2004), a void may produce a measurable contrast with the surrounding rock where resistivity values typically range from hundreds to thousands of ohm-meters. This electrical contrast may be detected using surface electrical geophysical methods. The U.S. Geological Survey (USGS), in cooperation with NPS, used electromagnetic and resistivity surface-geophysical methods at the Gran Quivira Unit to identify electrical anomalies that could be associated with open voids in the subsurface.

Purpose and Scope

This report presents the results of a surface-geophysical investigation at the Gran Quivira Unit of Salinas Pueblo Missions National Monument, conducted in June 2005, to characterize near-surface geology and determine the presence of possible open subsurface voids. Time-domain and frequency-domain electromagnetic (EM) techniques were used in conjunction with two-dimensional (2-D) direct-current (DC) resistivity to characterize the electrical structure of the local subsurface geology, as well as to identify electrical anomalies that could be associated with open subsurface voids in the immediate area of the ruins at Gran Quivira.

Site Description

The Gran Quivira Unit is one of three archaeological sites included within Salinas Pueblo Missions National Monument. The site is on the Torrance-Socorro County line in central New Mexico, approximately 100 km southeast of Albuquerque and 45 km south of Mountainair (fig. 1*A*). Land-surface elevation on the site ranges between 1,975 and 1,990 m, and steep, rocky mounds of remaining unexcavated ruins create highly variable local topography. The site is dominantly vegetated by desert scrubland, although cactus, juniper, and pinon pine are found on the side slopes near the boundary of the study area.

The most prominent features of the Gran Quivira Unit are the remains of two Spanish churches, San Buenaventura Mission (fig. 2*A*) and San Isidro Church (fig. 2*B*), and the large, partially excavated and stabilized pueblos known as Mound 7 (fig. 2*C*) and House A. The flat, open area between Mound 7, San Isidro Church, and San Buenaventura Mission is known as "the plaza." Several kivas (partially underground, circular ceremonial structures) and house walls are also exposed at the surface throughout the study area. Irregular topography and the distribution of artifacts indicate that many additional unexcavated pueblos, kivas, and other structures may be present in the shallow subsurface (fig. 2*D*), the extent of which can be seen most clearly in aerial photography (fig. 1*B*).

Legal-Description System

Test-hole locations in this report were derived from the published locations originally described using the surveyed land subdivisions of township, range, and section, as defined by the U.S. Bureau of Land Management's Public Land Survey System for New Mexico. Each location is represented by a number with four segments separated by periods. The first three segments describe the township, range, and section, respectively. The letter "S" denotes that the township lies south of the New Mexico Base Line; the letter "E" denotes that the range lies east of the New Mexico Principal Meridian. The fourth segment contains three numbers and locates the test hole to a 4-ha (10-acre) area within the section. The section is initially quartered and numbered from left to right and top to bottom. This quartering and numbering continues until the 4-ha area has been defined (fig. 3).

Hydrogeology

The Gran Quivira Unit of the Salinas Pueblo Missions National Monument is in the Gran Quivira 7.5-minute quadrangle on the northwest flank of the Chupadera Mesa, a wide tableland that covers about 4,400 km^2 of central New Mexico (fig. 1*A*). The Gran Quivira Unit stands on the western end of a low ridge, one of a series of east-west trending ridges separated by wide valleys (Bates and others, 1947). No perennial streams are in the area surrounding the Gran Quivira Unit. Intermittent streams are typically short, and runoff gathers in small depressions where it either evaporates or disappears into the subsurface (Clebsch, 1957).

The Yeso Formation of Permian age is the principal water-bearing formation of the area (Clebsch, 1957). Water quality is variable, with analysis of dissolved solids in a test well southwest of the Gran Quivira Unit indicating that the water is slightly saline (Titus, 1960). The Yeso Formation consists of siltstone, sandstone, gypsum, and limestone. Although outcrops occur about 20 km west-southwest of the study area, the depth to the Yeso Formation was found to be

(A) San Buenaventura Mission

(B) San Isidro Church

(C) Mound 7

(D) Unexcavated mounds

Figure 2. Photographs taken at Gran Quivira Unit in June 2005 showing *(A)* San Buenaventura Mission, *(B)* San Isidro Church, *(C)* Mound 7, and *(D)* unexcavated mounds typical of study area.

nearly 140 m in test hole 3 (TH 3) at the Gran Quivira Unit (fig. 4*C*, appendix 1–3; Clebsch, 1957), which is below the depth of investigation for this study. Also below the depth of investigation is an interval described as "no record" in the lithologic description from TH 3. It could be speculated that this represents a loss of circulation or a void encountered during drilling; however, the true meaning of this description is not known and could not be determined on the basis of the age of the log (circa 1932 and 1933).

The San Andres Limestone of late-Permian age is exposed at the surface over a substantial part of the Chupadera Mesa, including the area immediately surrounding the Gran Quivira Unit. Smith (1957) described the San Andres as being divided into three members in the vicinity of Torrance County—an upper fine-grained clastic member, a middle limestone member, and the lower Glorieta Sandstone member. The upper clastic member, although eroded from the majority of the Chupadera Mesa, may appear as the small layer of yellow sandstone described in TH 1 (fig. 4*A*, appendix 1–1). The middle limestone member is described by Bates and others (1947) as gray, thickly bedded to slabby limestone containing numerous solution cavities, gypsum, and white sandstone. The gypsum in the formation has a tendency to be massive and typically is easily dissolved, which Bates and others (1947) indicate as the cause of the uneven surface topography and abundant sinkholes found on the Mesa. The lower extent of the San Andres Limestone consists of the medium-grained, white to brown Glorieta Sandstone. The San Andres Limestone is estimated to extend to a depth of more than 120 m in the area surrounding the Gran Quivira Unit and is not known to be water bearing, although some zones of local perching may exist (Clebsch, 1957).

Numerous igneous mafic dikes and sills, estimated by Bates and others (1947) to be of Tertiary age, intrude through the Permian sedimentary layers of the Yeso Formation and San Andres Limestone throughout the Gran Quivira quadrangle. Evidence of one of these intrusions can be seen at the Gran Quivira Unit about 20 m west of the northwestern

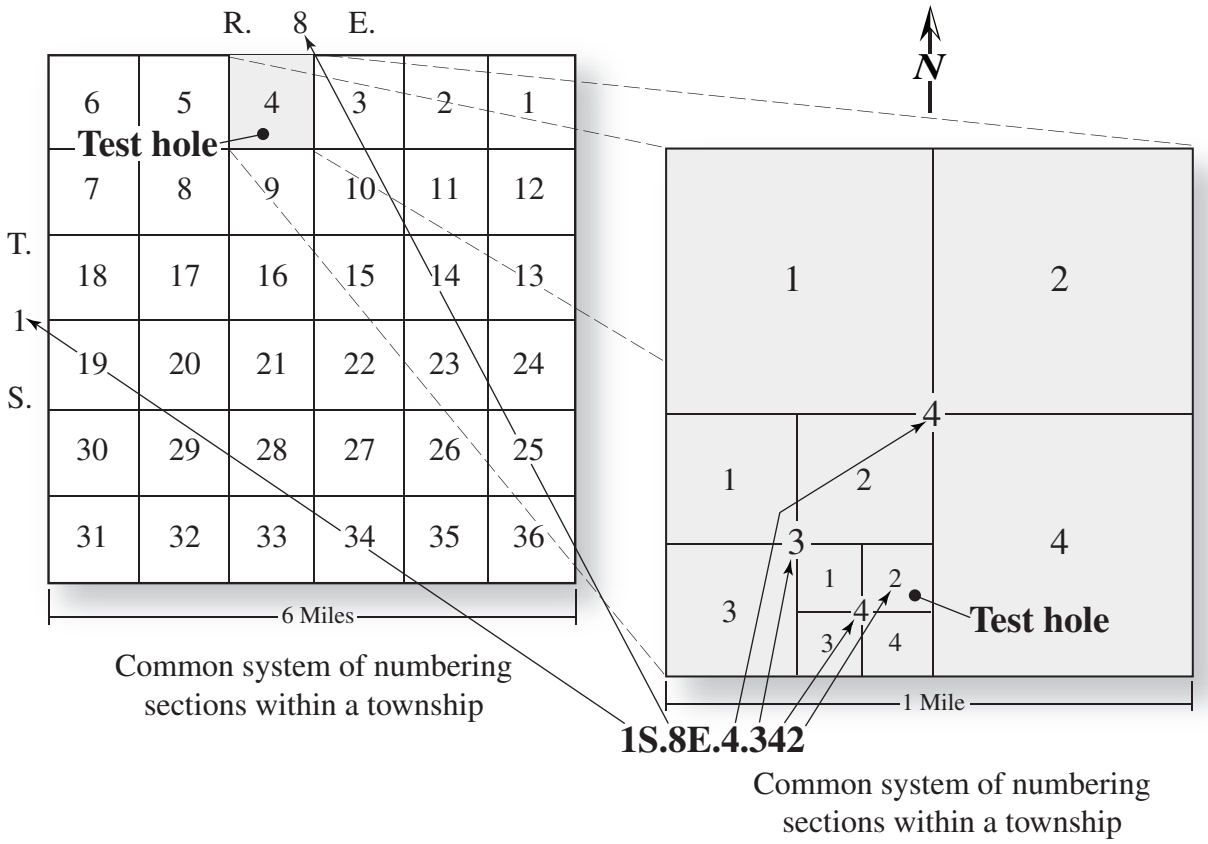

Figure 3. Legal-description system used in New Mexico.

corner of the excavated walls of Mound 7 (fig. 1*B*). Bates and others (1947) associated folds in the Glorieta Sandstone and Yeso Formation with these intrusions, although they also documented folds in the San Andres Limestone, Glorieta Sandstone, and Yeso Formation to be tentatively associated with differential solution of gypsum. Bates and others (1947) also described numerous places on the Chupadera Mesa where the San Andres Limestone is steeply tilted, suggesting folding, and is capped with additional, flat-lying limestone, leaving what superficially looks like an anticline. However, the steep tilting is more likely caused by the dissolution of gypsum leading to a draping of the limestone over the underlying strata (Bates and others, 1947).

Quaternary alluvial sediment, ranging from silt to moderately coarse gravel, can be found in the valleys and in undrained depressions in the area. Although existing test holes provide little information on the thickness of the alluvium, Clebsch (1957) describes a well in the valley northwest of the Gran Quivira Unit in which at least 21 m of alluvium were encountered and were found to be water bearing.

Substantial local geologic variation occurs in the area surrounding the Gran Quivira Unit; this is exemplified by the lithologic descriptions from TH 1 and TH 2 (figs. 4*A*, 4*B*, appendix 1–1, 1–2), which are estimated from legal descriptions to be within 280 m of each other (fig. 1*A*). TH 1 describes the San Andres Limestone as interbedded limestone and caliche layers underlain by the Glorieta Sandstone. TH 2 describes five layers of igneous intrusions within the upper 85 m of the San Andres Limestone that are absent at TH 1, and no caliche or any other secondary mineral accumulation is identified. This extreme variability among test-hole lithologies can make the correlation of geologic units to surface-geophysical data difficult.

Acknowledgments

The authors extend their appreciation to Marc LeFrancois and Tobin Roop, NPS Salinas Pueblo Missions National Monument (Mountainair, N. Mex.), for their efforts in securing access to the study area and for providing vital information on the geology and historical record of the Gran Quivira Unit. Special thanks also are extended to Steven DeVore, NPS Midwest Archeological Center (Lincoln, Nebr.), for his coordination efforts. The authors also thank James Holmlund, Western Mapping Company (Tucson, Ariz.), and Andrew Waggener, NPS Salinas Pueblo Missions National Monument (Mountainair, N. Mex.), for providing field maps and digital data of the study area, as well as John Hawley, Hawley Geomatters (Albuquerque, N. Mex.), for sharing his extensive knowledge of the geology of central New Mexico.

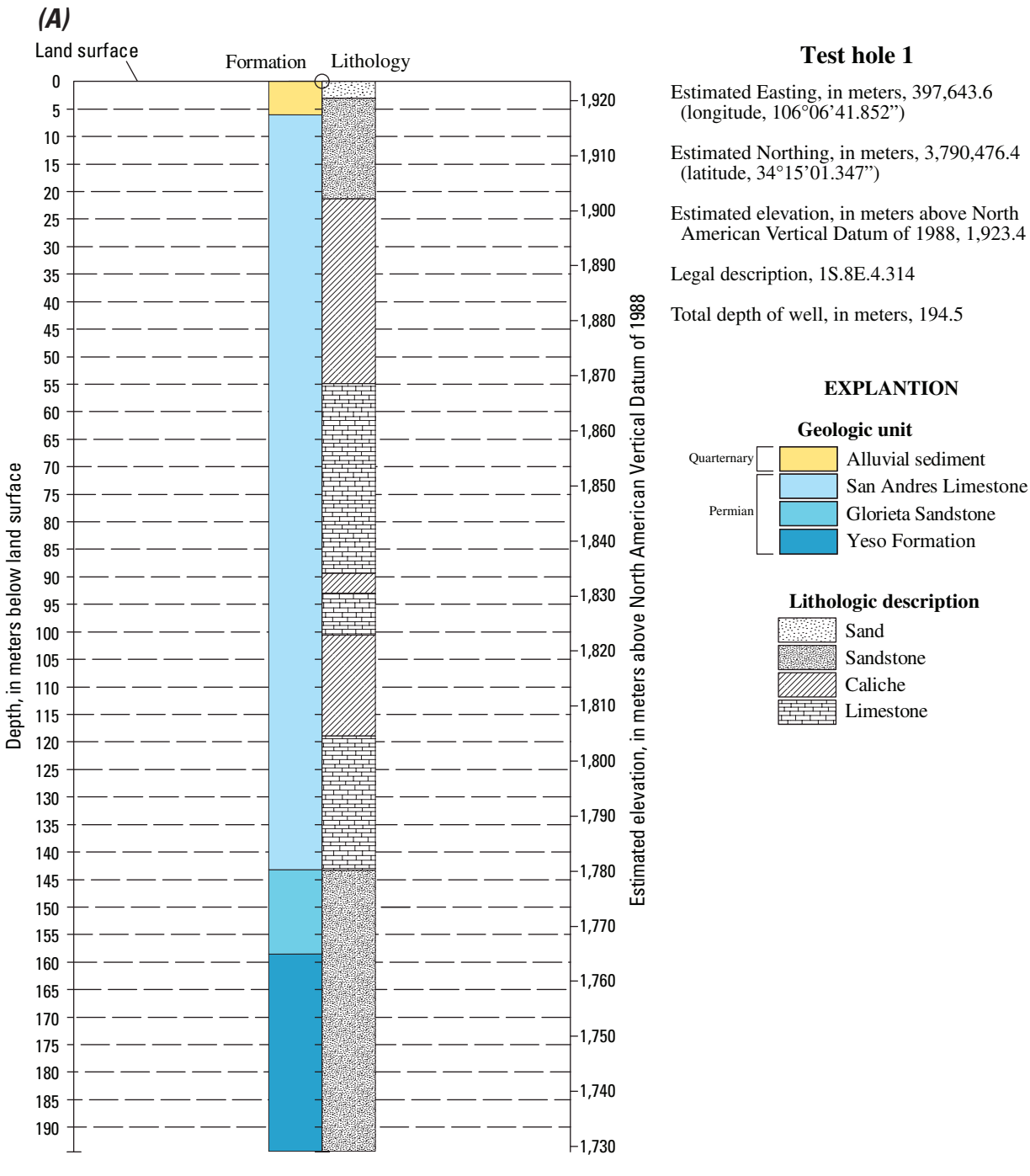

Figure 4*(A)*. Lithologic descriptions from test hole 1 (Marc LeFrancois, National Park Service, written commun., April 2005). Universal Transverse Mercator (UTM) zone 13 coordinates were estimated from the original legal descriptions and can only be assumed to be within 140 meters of the actual location.

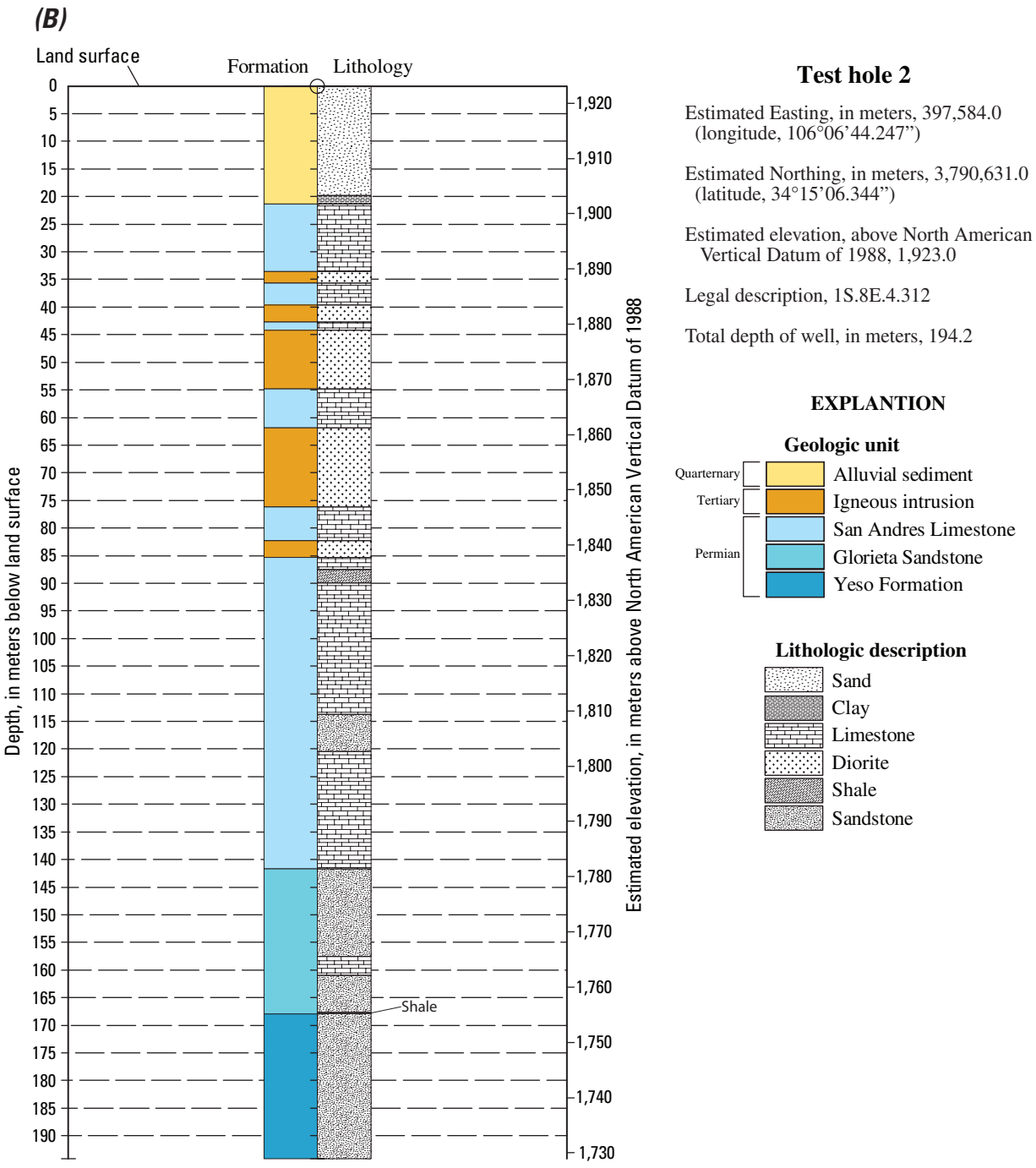

Figure 4*(B)*. Lithologic descriptions from test hole 2 (Titus, 1960. Universal Transverse Mercator (UTM) zone 13 coordinates were estimated from the original legal descriptions and can only be assumed to be within 140 meters of the actual location.

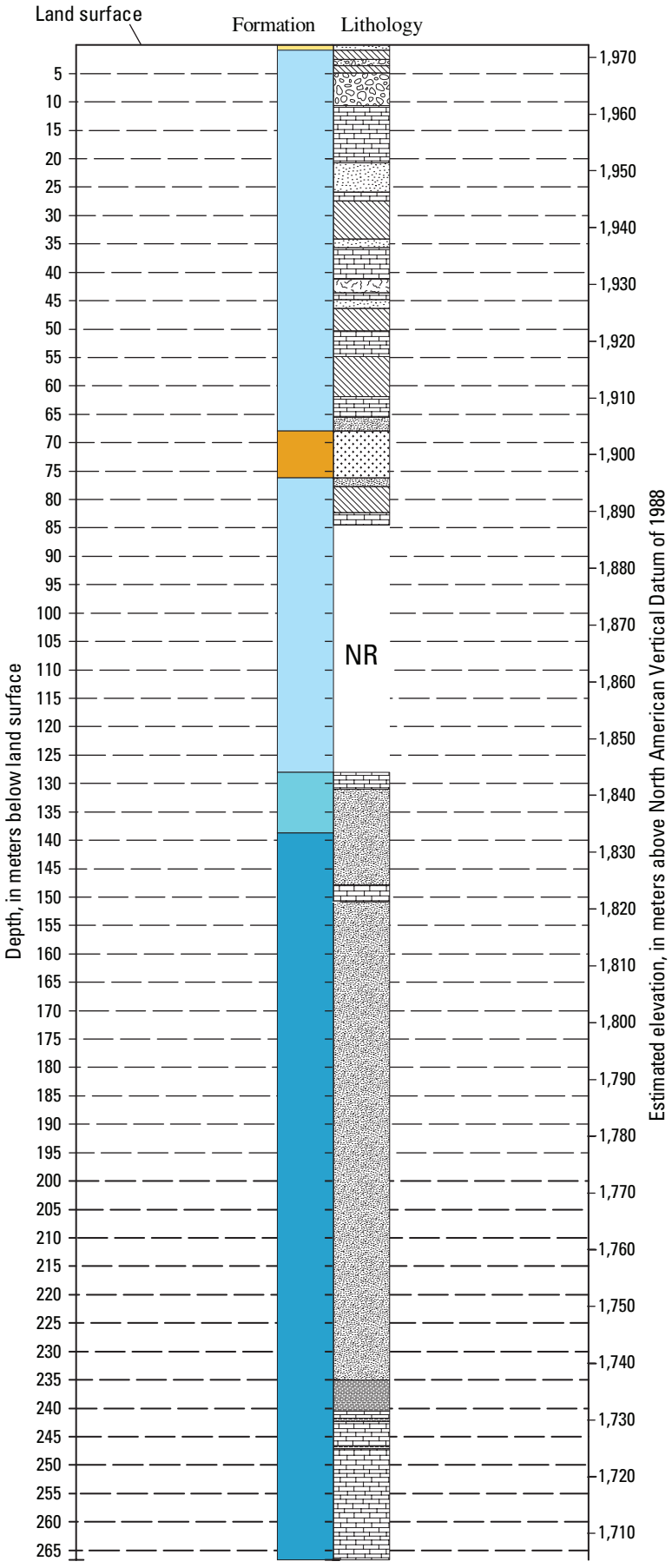

Test hole 3

Estimated Easting, in meters, 399,341.0 (longitude, 106°05'35.878")

Estimated Northing, in meters, 3,791,380.0 (latitude, 34°15'31.275")

Estimated elevation, in meters above North American Vertical Datum of 1988, 1,972.0

Legal description, 1S.8E.3.121

Total depth of well, in meters, 266.7

EXPLANTION

Geologic unit

- Quarternary: Alluvial sediment
- Tertiary: Igneous intrusion
- Permian: San Andres Limestone
- Permian: Glorieta Sandstone
- Permian: Yeso Formation

Lithologic description

- Sand
- Gypsum
- Boulders and Gravel
- Boulders
- Limestone
- Sandstone
- Quartz
- Diorite
- Clay
- NR: No record

Figure 4*(C)*. Lithologic descriptions from test hole 3 (Clebsch, 1957) near Gran Quivira Unit. Universal Transverse Mercator (UTM) zone 13 coordinates were estimated from the original legal descriptions and can only be assumed to be within 140 meters of the actual location.

Sincere appreciation is extended to Jared Abraham, Maria Deszcz-Pan, and Beth Burton, USGS Crustal Imaging and Characterization Team (Lakewood, Colo.), for lending their expertise and guidance in FDEM processing and inversion. The authors extend thanks to Wade Kress, USGS Texas Water Science Center (San Angelo, Tex.), for his support in the field and during interpretation. Thanks also are extended to Ted Asch, USGS Crustal Imaging and Characterization Team (Lakewood, Colo.), and Peter Joesten, USGS Branch of Geophysics (Storrs, Conn.), for providing technical review of data and interpretations in this report.

Approach and Methodology

General Approach

Lithologic descriptions from three historical test holes (circa 1930s and 1950s) were used to correlate electrical structures to geologic units (fig. 4; appendix 1). Universal Transverse Mercator (UTM) zone 13 map coordinates of test-hole locations were estimated from the original legal descriptions to the center of the 4-ha tract (appendix 1–1), and may be as far as about 140 m from the actual location. Elevations above the North American Vertical Datum of 1988 (NAVD 88) were sampled from the 10-m resolution USGS National Elevation Dataset (U.S. Geological Survey, 2005) at the estimated UTM coordinates.

Five TDEM soundings were collected in an approximate southwest-northeast trending line between TH 1 and the Gran Quivira Unit (fig. 1*A*). The TDEM soundings provided the general electrical structure from the known geology at TH 1 and TH 2, and attempted to detect the differences in electrical structure between these test holes and the study area.

DC resistivity and FDEM data were collected on the shoulder of Gran Quivira Road (fig. 1*A*). This location was selected because of the presence of a small gypsum cavern with an entrance about 20 cm wide and 10 cm high (fig. 5). This void was used to evaluate the effectiveness of both techniques to detect a known open void.

DC resistivity data were collected along six lines in the immediate area of the ruins (fig. 1*B*) to locate and resolve electrical anomalies that could be attributed to open subsurface voids, as well as to characterize the electrical structure of the local geology. Resistivity forward models were used to develop an understanding of the probable system response to several electrical scenarios, which were used as a tool in the interpretation of high-resistivity anomalies. FDEM data were collected over the same locations as the DC resistivity lines to evaluate the suitability of the FDEM method for karst investigations and to confirm the presence of electrical anomalies seen in the DC resistivity results. FDEM data also were collected in the immediate area of the Gran Quivira Unit in a predefined grid of north-south oriented lines. These data were gridded to create a map of the very near-surface EM response.

Time-Domain Electromagnetic Technique

TDEM soundings are used to infer the one-dimensional (1-D) electrical resistivity structure of the local subsurface geology. A constant DC current, passed through a square loop of insulated wire laying on the ground surface, produces a magnetic field about the loop. The current then is abruptly stopped, and the decaying magnetic field induces electric current in the subsurface under the loop, roughly in the shape of the loop. This eddy current diffuses into the subsurface causing progressively larger and deeper loops of energy. The current diffuses downward and outward as it interacts with the subsurface. Secondary magnetic fields are generated that

(A)

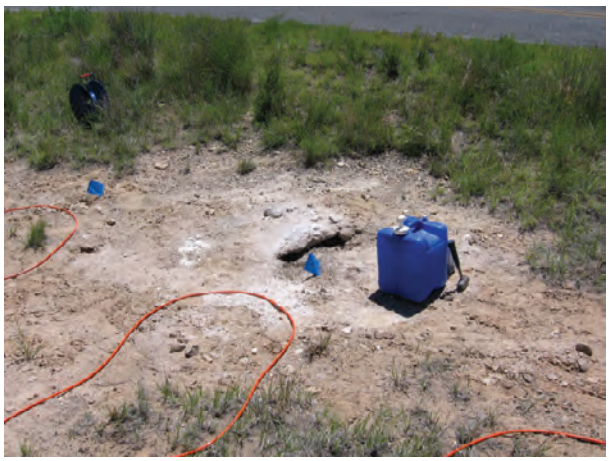

(B)

Figure 5. Photographs taken in June 2005 showing the small gypsum cavern along Gran Quivira Road near line 6.

induce a secondary current, and a voltage is recorded by a small receiving loop at the ground surface. This decaying voltage is measured at sequential time intervals, with later time intervals corresponding to deeper layers in the earth. The amplitude and rate of decay of the secondary magnetic field are related directly to the electrical structure of the geology. By using a numerical inversion process, a 1-D layered-earth model is created that represents the probable resistivity structure of the subsurface. TDEM methods are described in more detail by Fitterman and Stewart (1990).

Five TDEM soundings (TDEM 1–TDEM 5) were collected in a general southwest-northeast trending line from about 2 km southwest of the ruins at the Gran Quivira Unit to approximately 20 m north of San Buenaventura Mission to attempt to transfer the correlation between the electrical structure and a lithologic profile from TH 1 and TH 2 to the study area (fig. 1*A*). A Protem 47 TDEM sounding system (Geonics, Mississauga, Ontario, Canada) was used with a single-turn square transmitter (Tx) loop and a receiver (Rx) loop centered within the Tx loop, known as a central loop configuration. Current settings ranged from 1.3 to 2.5 amps. For TDEM 1, 2, and 3, a 60-m square Tx loop was used, although site restrictions caused by uneven topography and ruin walls only allowed 40-m square loops for TDEM 4 and 5. Coordinates and elevations of each sounding were derived using an Ashtech Z-Extreme (Thales Navigation, Santa Clara, Calif.) real-time kinematic (RTK) global positioning system (GPS). Data were inverted using TemixXL software (Interpex Limited, Golden, Colo.) to create a 1-D layered-earth inversion model of resistivity at each sounding location.

Direct-Current Resistivity Technique

Electrical resistivity measurements are made by transmitting current into the subsurface and measuring the resulting potential difference. The resistance, *R*, is then calculated by dividing the measured voltage by the transmitted current, as described by Ohm's Law (Zohdy and others, 1974):

$$R = \Delta V/I \qquad (1)$$

whereΔV represents the potential difference measured by the potential electrodes, and *I* represents the current applied through the current electrodes. The apparent resistivity of the subsurface is calculated by multiplying each resistance by a geometric factor determined by the geometry and the spacing of the electrode array (Zohdy and others, 1974). By increasing the distance between electrodes, deeper apparent-resistivity data can be obtained. The resistivity technique is described in detail by Grant and West (1965) and Zohdy and others (1974).

DC resistivity measurements were made along seven different lines at the Gran Quivira Unit (fig. 1) with a Syscal R1 Plus (IRIS Instruments, Orleans, France) resistivity meter. Electrode locations were georeferenced using an Ashtech Z-Extreme RTK GPS to derive geographic coordinates and elevations. Topographic corrections were made to the resistivity data using these GPS-derived elevations.

Line 6 had an electrode spacing of 2 m and was placed along the east side of Gran Quivira Road near the small cavern (fig. 5) about 800 m west of the study area (figs. 1*A* and 3). Gypsum was exposed over the majority of the surface, and a weathered igneous intrusion outcrops about 6 m east of the center of the line. Data from line 6 were used to aid in the interpretation of geophysical anomalies seen in other survey lines within the Gran Quivira Unit and to determine the ability of multiple arrays to detect the small void.

Six DC resistivity lines were placed in the immediate area of the Gran Quivira Unit to characterize the near-surface geology and to identify high-resistivity anomalies that could be associated with open subsurface voids (fig. 1*B*). Lines 3, 4, and 7 were placed around the perimeter of the Gran Quivira Unit in an intersecting triangle to define the major geologic units in the upper 50 m, as well as to identify high-resistivity features that could be associated with large open voids. An electrode spacing of 5 m was used for lines 3, 4, and 7. Lines 1 and 2 were placed on the west and east sides of Mound 7, respectively, and line 5 crossed through Mound 7 on the east side of Kiva C. Lines 1, 2, and 5 had an electrode spacing of 2 m to locate electrical anomalies that could be attributed to open voids in the upper 20 m below Mound 7.

Two arrays, the dipole-dipole and the hybrid Wenner-Schlumberger, were used to collect data along all DC resistivity lines. The dipole-dipole array is sensitive to horizontal changes in resistivity and is relatively insensitive to vertical changes. It has a shallow depth of investigation and low signal strength, making the signal more susceptible to environmental noise. The Wenner-Schlumberger array has moderate resolution in both the horizontal and vertical directions. It has a greater depth of investigation and higher signal strength than the dipole-dipole array, resulting in a higher signal-to-noise ratio (Loke, 2004b). Along lines 1, 2, 5, and 6, data also were collected with a high-resolution version of the Wenner-Schlumberger array, which was designed to maximize the number of data points in the upper 8 m without changing electrode spacing. By taking advantage of smaller dipole-separation factors (n), the high-resolution Wenner-Schlumberger array was used to attempt to detect smaller features that may be associated with voids immediately below Mound 7.

Two-Dimensional Inverse Modeling of Resistivity Data

The measured apparent resistivity, as determined from field measurements, is the electrical resistivity over an equivalent electrically homogeneous and isotropic subsurface and is used to represent the average resistivity of a more realistic, heterogeneous subsurface (Loke, 2000). To help determine the probable distribution of electrical resistivity, an inversion program develops a 2-D model consisting of rectangular blocks of individual resistivity values. The inversion program then

determines the calculated system response over that model, referred to as the calculated apparent resistivity, on the basis of the field data-collection parameters. These parameters include the type of array utilized, the distance between electrodes, and the number of measurements collected. The root-mean-square (RMS) difference between the measured and calculated apparent resistivities is used to determine the accuracy of the model. The inversion program then attempts to reduce the RMS difference by altering the model resistivity values and recalculating the apparent resistivity; this alteration is known as "iteration." When the RMS difference between the calculated and measured apparent resistivity no longer improves between iterations by more than 1 percent of the total RMS difference, a solution is reached. This final model represents a non-unique estimate of the probable distribution of electrical resistivity within the subsurface. This inversion process is described in detail by Loke (2004a).

All DC resistivity data were inverted using RES2DINV version 3.54.44 software (Geotomo Software, Penang, Malaysia), using the finite-element method with the least-squares approximation and robust model settings (appendix 4). The 2-D resistivity sections then were examined for anomalies that could be attributed to open subsurface voids as well as for general layers that could be associated with lithologic units. Forward models were developed for lines 1 through 7 to aid in the interpretation of high-resistivity anomalies.

Forward Modeling of Resistivity Data

Resistivity forward modeling is used to estimate the system response, or synthetic apparent resistivity, on the basis of an estimated "true" resistivity structure. Forward models have a grid of rectangular model blocks with user-assigned resistivity values representing one possible scenario of resistivity structure. Forward modeling was used to evaluate possible causes of high-resistivity anomalies, serving as an aid in the final interpretation of the inverted resistivity sections from the Gran Quivira Unit.

Basic forward models were developed for each DC resistivity line to provide a framework for the introduction of anomalous features. To estimate the general resistivity structure, 1-D resistivity soundings were extracted from the measured apparent resistivity data and inverted using IX1D version 3.25 software (Interpex Limited, Golden, Colo.). Following construction of the basic forward model, synthetic apparent-resistivity values were calculated using RES2DMOD version 3.02f beta plus software (Geotomo Software, Penang, Malaysia). These synthetic apparent-resistivity values were processed using the inverse modeling software RES2DINV version 3.54.44, following the same procedures used in processing the measured resistivity data. The basic forward models were refined until a close visual match was found between the measured and synthetic inverted resistivity sections.

High-resistivity features were introduced into the basic forward models to develop an understanding of possible sources of high-resistivity anomalies seen in the measured inverted resistivity section. Two forward-model scenarios were simulated on most of these anomalies—one with a 5,000 ohm-m feature representing an anomaly as a geologic layer, and the other with 40,000 or 100,000 ohm-m features representing an anomaly as an open void within a geologic layer (appendix 5). Because different structural scenarios can produce a similar system response, forward models were used as a learning tool, and these models do not provide independent interpretations of the geologic structure surrounding the Gran Quivira Unit.

Frequency-Domain Electromagnetic Technique

The FDEM technique uses EM induction at multiple frequencies to determine the electrical properties of the subsurface at varying depths. An alternating current energizes a Tx coil, producing a primary magnetic field that induces electrical current in the subsurface. This induced current creates a secondary magnetic field, the magnitude of which is dependent on the conductivity of the subsurface. An Rx coil measures the magnitude of the primary and secondary fields, and in-phase and quadrature responses are calculated. From these data, interpretations can be made about subsurface apparent resistivity and apparent magnetic susceptibility (Haung and Won, 2000).

The FDEM surveys were performed with the GEM-2, a broadband, multifrequency, fixed-coil EM induction instrument (Geophex, Ltd., Raleigh, N.C.). There are three small coils in the GEM-2—a Tx coil, an Rx coil, and a bucking coil that removes the primary field from the Rx signal. The instrument's software calculates the in-phase and quadrature response in units of parts per million (ppm), which represent the scaled ratio of the secondary magnetic field to the primary magnetic field at the Rx coil. More detailed information about the GEM-2 and its operating principle is discussed by Won and others (1996).

The GEM-2 was operated in vertical-dipole mode (horizontal, coplanar coils) with a fixed 1.67-m spacing between coils. Five frequencies were measured—1,170, 3,930, 13,590, 24,030, and 47,010 Hz (hertz). An environmental noise test was performed prior to the beginning of the FDEM survey to aid in the selection of frequencies that were not similar to ambient noise present on the site. Although no power-transmission lines were present in the immediate area, the 60 Hz frequency was monitored throughout the survey, and harmonic frequencies of 60 Hz were avoided.

At the beginning and end of each day on which FDEM data were collected, the GEM-2 was placed at a calibration point (fig. 1*B*), and approximately 3 to 5 minutes of data were collected three times—once with the sensor isolated, once with a ferrite rod placed on the Rx coil, and once with the operator standing next to the sensor. To monitor instrument drift throughout the day (temporal drift), the calibration point was reoccupied with the operator every time data were

downloaded or the GEM-2 required battery changes (typically four times a day).

FDEM data were collected in two phases for this study. In the first phase, a predetermined line grid was surveyed over the immediate area of the Gran Quivira Unit to create a basic map used in estimating the near-surface electrical properties. In the second phase, the GEM-2 was used to collect a series of individual depth soundings along DC resistivity lines to develop 2-D sections of apparent resistivity.

Areal Frequency-Domain Electromagnetic Survey

FDEM data were collected over 3 days using the GEM-2 in communication with a MiniMAX (CSI Wireless, Calgary, Alberta) differentially corrected GPS through an RS-232 wire connection. Continuous lines were collected bi-directionally in a north-south orientation at 5-m intervals over all open space, as well as inside San Buenaventura Mission and San Isidro Church, to optimize data coverage while minimizing the number of lines on the site. Tie lines were collected bi-directionally in an east-west orientation at 25-m intervals. Individual, stationary soundings were collected inside the majority of rooms in Mound 7 and House A while using the GPS to locate each sounding. Some small areas could not be surveyed, including rooms within Mound 7 and House A that were less than 2 m long and thus could not accommodate the GEM-2 sensor, as well as densely vegetated areas on the eastern side of the study area where the density of juniper and cactus prevented collection of reliable data.

Linear corrections for temporal drift were applied using Oasis montaj version 6.2 software (Geosoft, Toronto, Ontario). A 50-point low-pass filter was used to smooth the drift-corrected in-phase and quadrature responses. Linear levels were applied to the data to correct for value discrepancies at tie-line intersections. Data were gridded using the minimum-curvature interpolation method with a 2.5-m cell size. These grids were analyzed for general trends as well as for anomalies that could be attributed to open subsurface voids.

Profiled Frequency-Domain Electromagnetic Survey

Individual FDEM soundings were collected at 2-m intervals over lines 1, 2, 5, and 6 and at 2.5-m intervals over lines 3, 4, and 7 (fig. 1). Data were collected by occupying each station for approximately 15 seconds and recording approximately 100 observations at the five selected frequencies. The mean values for the in-phase and quadrature responses for the five frequencies measured were used to represent that station. Using the computer program GEM2COR (unpublished USGS software), the repeat measurements were averaged together and adjusted for temporal drift. The result was a single measurement at each frequency for each station. For each line, the measurements were "smoothed" using a three-point running average filter.

EM1DFM software (University of British Columbia's Geophysical Inversion Facility, Vancouver, British Columbia) was used to produce 1-D inversions of FDEM sounding data. This software was used to determine the best combination of the selected GEM-2 frequencies; the optimal number of model layers and overall depth; the best match of profiled, inverted FDEM sections to inverted resistivity sections produced from the DC resistivity measurements; and to determine the effectiveness and limits of the GEM-2 for locating open subsurface voids.

If the internal calibration file for the GEM-2 is appropriate, all observations should be no less than zero because the in-phase and quadrature responses in free space should be zero at all frequencies. However, many of the Gran Quivira observations were negative; in fact, nearly all the in-phase measurements were less than zero, possibly indicating that the sensor's free-air response had drifted since initial calibration and that the correction was no longer appropriate. The inverse modeling program EM1DFM could not model the data correctly because negative values are not permitted in the forward model. One solution was to adjust all the field observations so that the number of negative values was minimal while maintaining their relative value. For this study, a constant value of 2,900 ppm was added to the in-phase observation at all five frequencies. The quadrature data were not adjusted, and occasional negative values are still present. Both the in-phase and quadrature observations were used for the inverse modeling.

Characterization of Near-Surface Geology

Three surface-geophysical techniques were used to characterize the near-surface geology of the upper 50 m below the Gran Quivira Unit. Because of the reference to natural karst features in the study area and the proposed management activities of Mound 7 (Attwell, NPS, written commun., 1932, on record Salinas Pueblo Missions National Monument Headquarters Archive, Mountainair, N. Mex.; Steven DeVore, NPS, oral commun., 2005), higher resolution data were collected around Mound 7 to attempt to identify anomalies that could be attributed to open voids caused by natural caves or manmade tunnels.

Correlation Between Electrical and Geologic Structures

TDEM 1, 2, and 3 were located in the valley southwest of the Gran Quivira Unit. TDEM 4 was located on a side slope about 400 m southwest of the ruins, and TDEM 5 was placed slightly north of the San Buenaventura Mission. Substantial changes in land-surface elevation were found between the

different soundings, with TDEM 3 at 1,919.3 m and TDEM 5 at 1,985.5 m, a total vertical relief of 66.2 m (appendix 2–1). This change in elevation, as well as the lithologic variations described by Bates and others (1947) and Clebsch (1957), need to be considered when examining the results of the 1-D layered-earth inversion models.

TDEM 1 and 2 were used to develop 1-D inversion models containing three main layers (fig. 6, appendix 3–1, 3–2). The first layer, a low- to moderate-resistivity feature extending from the surface to an elevation of 1,914 m with a value of 130 ohm-m in TDEM 1 and an elevation of 1,911 m with a value of 240 ohm-m in TDEM 2, is most likely representative of the alluvial sediment and upper sandstone of the San Andres Limestone (figs. 4*A* and *B*). The second layer, a low-resistivity layer around 15 ohm-m, extends to a more variable lower elevation—1,875 m in TDEM 1 and 1,832 m in TDEM 2. In the lower third of the inversion model, the sensitivity becomes reduced, and although the TDEM system may be able to detect the presence of another electrical layer, it is difficult to resolve the elevation or resistivity value of this deeper feature. The lower extent of the second layer in TDEM 1 is within 10 m of the bottom of the caliche layer described in TH 1 (fig. 4*A*, appendix 1–1). The increased depth of this layer in TDEM 2 could possibly represent a thickening of the caliche layer, or a higher salt, clay, or water content at this location. The third layer is a moderate-resistivity feature, about 560 ohm-m, that extends below the depth of investigation and most likely represents the limestone described in TH 1 (fig. 4*A*, appendix 1–1).

A three-layer 1-D inversion model also was developed for TDEM 3 (fig. 6, appendix 3–3). Although the location of the contact between the first two layers was somewhat similar to those of TDEM 1 and 2, with an elevation of about 1,912 m, there was a decrease in the resistivity of the first layer to a resistivity value of 60 ohm-m, whereas the second layer remained very conductive at 25 ohm-m. The third layer showed an increase in resistivity to about 4,700 ohm-m, which is nearly an order of magnitude higher than that of the first two soundings. The top elevation (1,884 m) of this layer may indicate that it is representative of the same geologic layer seen in the third layer of TDEM 1 (fig. 6), and the increase in resistivity could be caused by an increase in grain size, pore space, or fracturing; a change in the chemical composition of the limestone, such as a decrease in salinity; or a reduction in water content. This third layer also may indicate a dipping geologic unit related to the high-resistivity layer seen in TDEM 4 and 5 that is below the depth of investigation in TDEM 1 and 2.

A four-layer 1-D inversion model was developed for TDEM 4 (fig. 6, appendix 3–4). The top layer had a low- to moderate-resistivity value of 150 ohm-m and a bottom elevation of 1,940 m and may be representative of the Quaternary sediments and limestone and gypsum layers described in TH 3 (fig. 4C, appendix 1–3). The second layer is a high-resistivity feature similar to that found in TDEM 3, with a resistivity value of 4,900 ohm-m and a lower elevation of about 1,895 m. The highly stratified nature of TH 3 makes it difficult to determine the geologic correlatives of this layer; TH 3 describes gypsum, limestone, sandstone, and diorite within this depth interval. The third and fourth layers occur in the deeper, less-sensitive part of the model, and although a contrast was detected, the resistivity values and elevations of these layers are difficult to determine. The relatively small third layer provides a "step" into the fourth layer, a moderate- to low-resistivity feature of 150 ohm-m. This lower layer may be indicative of the bottom contact of the diorite to the sandstone and gypsum. This layer also is closely aligned with an unrecorded section of the driller's log (described as "no record"), and the true lithology of this section is unknown. It is assumed that this interval is still part of the San Andres Limestone.

A two-layer 1-D inversion model was developed for TDEM 5 (fig. 6, appendix 3–5). The upper layer was a moderate-resistivity feature with a value of 350 ohm-m and, although substantially thicker than the surface layers at other locations with a total thickness of nearly 55 m, the bottom elevation of 1,930 m was within 10 m of a similar resistivity contrast in TDEM 4 (fig. 6). The second layer occurs in the less-sensitive part of the model, and the resistivity value and elevation are difficult to determine; however, modeling showed this layer to have a resistivity of about 4,400 ohm-m, similar to the second layer of TDEM 4.

Determination of Detection Limits

Data from line 6 were used to aid in the interpretation of geophysical anomalies seen in other lines within the study area and to determine the ability of the multiple arrays and instruments to detect the small void. Three 2-D inverted DC resistivity sections are shown in figures 7*A* through *C*. Figure 7*D* shows the results of the 1-D inversion of the FDEM soundings, which have been profiled and gridded into a section showing the changes in relative resistivity. Because of the adjustment of in-phase values required to make all values greater than zero, the resistivity values shown in the FDEM section are not intended to be directly compared to values shown in the DC resistivity sections but are used to identify resistivity contrasts. Therefore, DC resistivity and FDEM sections are shown using separate color scales.

Direct-Current Resistivity

The inverted DC resistivity sections show several features of low to moderate resistivity between 25 and 500 ohm-m extending from the surface to an elevation of about 1,935 m (figs. 7*A*, *B*, and *C*). Because of the surface occurrence of gypsum, it is possible that gypsum is represented by these features, although there also is a possibility that these features represent limestone or water- or clay-filled voids. Discrete moderate-resistivity features between 500 and 1,000 ohm-m were found throughout the sections. These features could possibly represent an increase in porosity in the gypsum

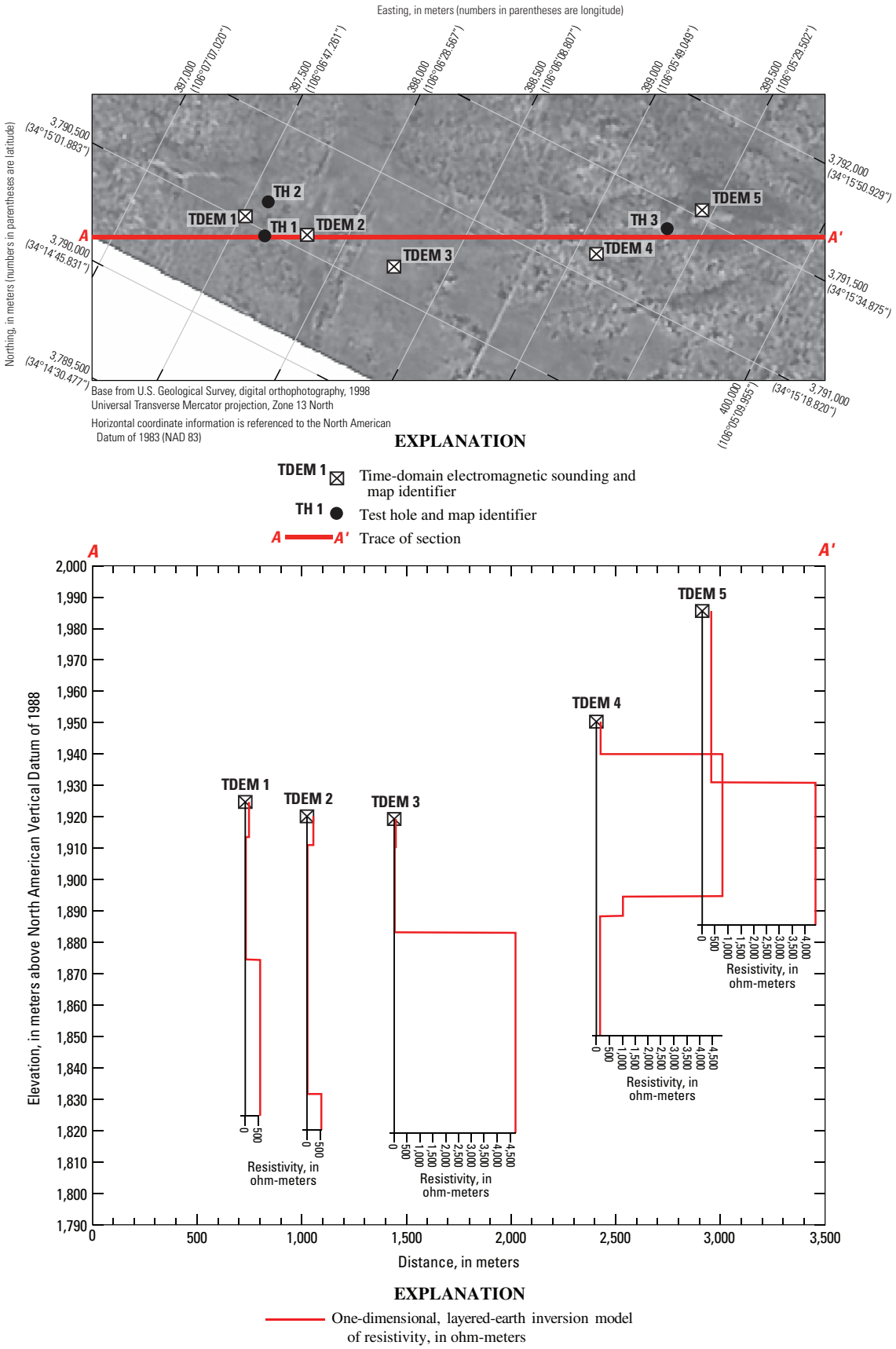

Figure 6. One-dimensional, layered-earth inversion models from time-domain electromagnetic sounding data (shown in profile along trace of section *A*–*A*').

(A) Two-dimensionally inverted direct-current resistivity section, from dipole-dipole array for line 6 (fig.1*A*)

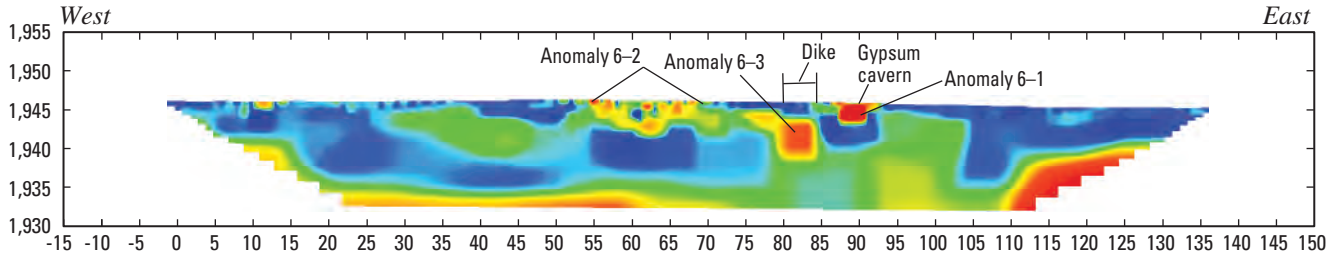

(B) Two-dimensionally inverted direct-current resistivity section, from Wenner-Schlumberger array for line 6 (fig.1*A*)

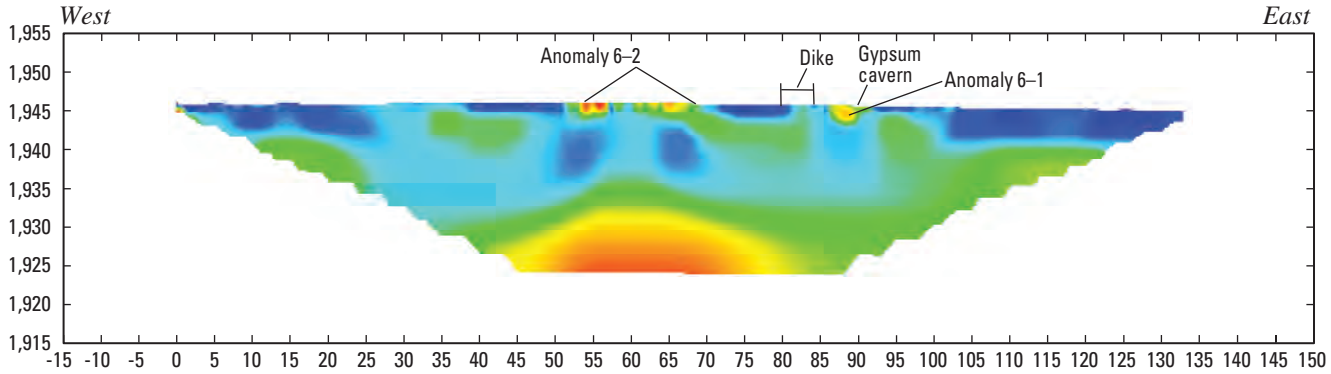

(C) Two-dimensionally inverted direct-current resistivity section, from high-resolution Wenner-Schlumberger array for line 6 (fig.1*A*)

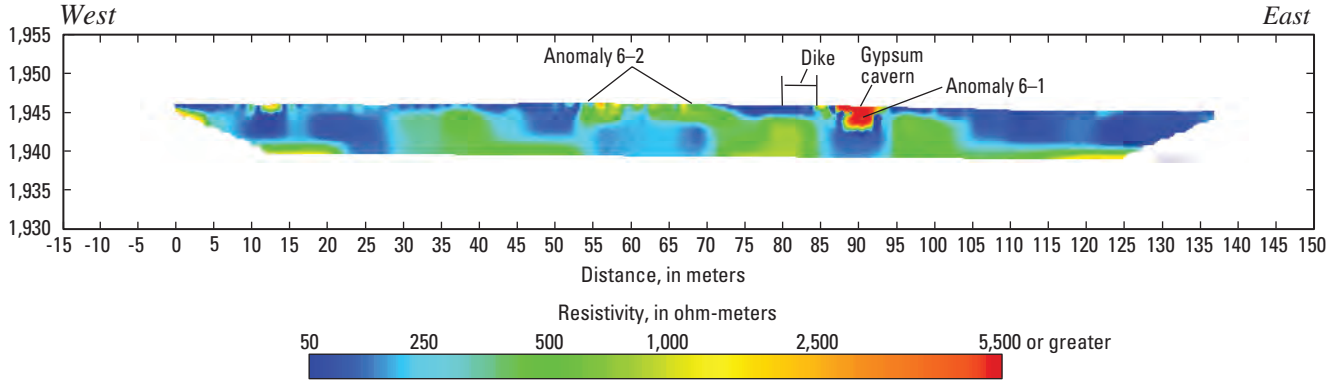

Elevation, in meters above North American Vertical Datum of 1988

(D) Profiled section of one-dimensionally, inverted frequency-domain electromagnetic soundings for line 6 (fig.1*A*)

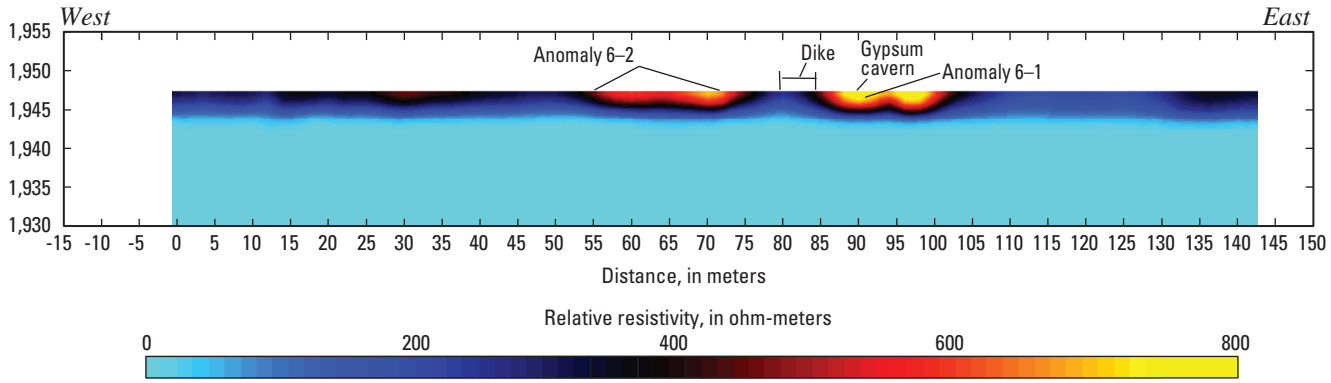

Figure 7. Profiles of surface-geophysical data from line 6 (fig. 1*A*) showing inverted direct-current resistivity sections from the *(A)* dipole-dipole, *(B)* Wenner-Schlumberger, and *(C)* high-resolution Wenner-Schlumberger arrays, as well as *(D)* profiled, inverted frequency-domain electromagnetic soundings.

deposit, gypsum interbedded with limestone, or a decrease in water content. A high-resistivity feature between 2,000 and 4,000 ohm-m was seen at the bottom of the section from the dipole-dipole and Wenner-Schlumberger arrays (figs. 7*A* and *B*). The bottom and edges of the inverted resistivity section are less sensitive to changing structures, and determining the source and dimensions of features found in these areas is difficult. This feature may represent the limestone, sandstone, or quartz layers indicated in TH 3 (fig. 4*C*). This high-resistivity feature may also indicate an increase in pore space, possibly resulting from dissolution of joints or bedding planes. This feature's resistivity did not exceed 4,000 ohm-m and has a relatively uniform extent across the bottom of the sections, making it more likely to be associated with a geologic layer than a large, open void, although there is a possibility for voids within this layer. Additional ground-truthing information, such as lithologic or borehole-geophysical logs in the vicinity of line 6, would substantially improve interpretations of the electrical structure and sources of anomalies shown throughout the section.

Three high-resistivity areas in the inverted resistivity sections for line 6 were designated as anomalies that may be attributed to open voids (fig. 7). It remains possible that the low-resistivity features also could represent voids filled with water or lined with clay. However, because a high-resistivity feature was found near the small gypsum cavern and the depth to the water table exceeds the depth of investigation, it is more likely that voids at this site are air-filled and appear as high-resistivity features.

Anomaly 6–1 is near the top of the inverted resistivity section between an elevation of 1,945 and 1,943 m. This anomaly intersects the surface at the same location as the surface expression of the small gypsum cavern. Anomaly 6–1 was clearly imaged in the results from the dipole-dipole and high-resolution Wenner-Schlumberger arrays (figs. 7*A* and *C*) with a resistivity value exceeding 12,000 ohm-m. This anomaly also appeared in the deeper Wenner-Schlumberger array; however, it did not express a very high resistivity value, only about 2,000 ohm-m (fig. 7*B*). The size of this feature is most likely near the resolution limit for the deeper array.

Anomaly 6–2 consists of a series of small, high-resistivity features in the upper 5 m. These features are displayed most prominently in results from the dipole-dipole array, although they are also clearly visible in results from both Wenner-Schlumberger arrays (figs. 7*A*, *B*, and *C*). These features may be caused by small voids that do not open to the surface.

Anomaly 6–3 is near the same location as the diorite dike that is exposed at the surface approximately 6 m east of line 6. This feature can be seen most clearly in results from the dipole-dipole array (fig. 7*A*) as having high resistivity, about 4,000 ohm-m, and located at an elevation of 1,943 to 1,939 m. Only moderate-resistivity features can be found at this location in results from both Wenner-Schlumberger arrays, making it unlikely that there is a void at this location. It is possible that this anomaly is caused by a lateral effect of the igneous intrusion.

Resistivity forward models were created for two scenarios—anomalies expressed as a moderate-resistivity unit (600 ohm-m) indicative of a geologic layer and anomalies expressed as a high-resistivity unit representing an air-filled void (40,000 ohm-m) (appendix 5–1). For anomalies 6–1 and 6–2, a better visual match between the inverted measured resistivity section and the inverted forward model section was achieved using the scenario with voids for all arrays, and particularly for the dipole-dipole and high-resolution Wenner-Schlumberger array results.

Results from line 6 illustrate the ability of the DC resistivity method to detect an open cavity close to the surface in a low-resistivity substrate. The gypsum provided a strong electrical contrast to the air in the cave, and forward models provided confident interpretations that anomaly 6–1 was caused by a highly resistive source, such as air in an open cavity.

Profiled Frequency-Domain Electromagnetic Inversion

The DC resistivity inversion models were used to determine the best settings for the FDEM inversion program EM1DFM. A total depth of 15 m was used for modeling; however, the total effective depth of investigation determined through EM1DFM was between 5 and 7 m. The EM1DFM final resistivity model (fig. 7*D*) was compared to the DC resistivity inversion results (fig. 7*A*, *B*, and *C*).

The inverted section of the profiled FDEM data along line 6 shows a moderate-resistivity layer about 2 m thick over a conductive layer (fig. 7*D*). The inverted FDEM section shows a strong relative resistivity contrast (greater than 600 ohm-m) between 85 and 95 m on the distance axis, which is the same location as anomaly 6–1 in the inverted DC resistivity section (fig. 7*A*, *B*, and *C*). This higher resistivity feature most likely corresponds to the small gypsum cavern found at the surface at this location, which illustrates the ability of the FDEM technique to detect high-resistivity features in the upper 5 m within a lower resistivity substrate.

Three additional resistivity contrasts also appear in the inverted FDEM section—a moderate contrast located between 25 and 35 m, a strong contrast between 55 and 75 m, and a strong contrast immediately east of anomaly 6–1 between 95 and 100 m. The remaining contrasts could be indicative of small voids in the near surface, especially between 55 and 75 m on the distance axis, which correlates to anomaly 6–2 in the inverted DC resistivity sections. The easternmost contrast is similar in strength to the features caused by the small cavern, which could indicate that the small cavern is still affecting the instrument at this location, resulting in a "false-positive," or that an additional smaller void is present in the upper 5 m that was not resolved in the DC resistivity data. The moderate contrast between 25 and 35 m may represent small voids or the moderate-resistivity feature approaching the surface in the same location in the inverted DC resistivity sections.

FDEM results suggest that this technique may be more capable of detecting small, near-surface voids than the DC resistivity technique at a 2-m electrode spacing. However, the FDEM technique is also more susceptible to environmental disturbances, potentially leading to anomalies that are not related to open voids. Additional DC resistivity data collection with a smaller electrode spacing or digging/coring near these additional contrasts may help determine the source of these features and the true detection limit of the technique.

Characterization of the Gran Quivira Unit

Correlations between the six DC resistivity lines (fig. 1*B*) placed in the immediate area of the Gran Quivira Unit are presented first in this section. Following that are the results for the areal FDEM data collected on a predetermined grid of the Gran Quivira Unit to define the near-surface electromagnetic response, as well as discussion of the correlations between the DC resistivity and areal FDEM results. Finally, high-resistivity anomalies that may be attributed to open voids are discussed in detail for each line.

Inverted DC resistivity sections were plotted as a fence diagram to compare the correlation of resistivity layers between the individual resistivity sections (fig. 8). Results from the Wenner-Schlumberger array were used to characterize the general resistivity structure because of the higher signal-to-noise ratio and greater investigation depth compared to the dipole-dipole array and the greater investigation depth compared to the high-resolution Wenner-Schlumberger array. Data from all arrays were used to identify anomalies that may be associated with open subsurface voids.

Comparison of the DC resistivity results shows that many major features were shared among the inverted resistivity sections, and correlation was excellent among the elevations of similar resistivity layers (fig. 8). Generally, two major electrical features were found to occur in the inverted resistivity sections. Low-resistivity features (25–150 ohm-m) commonly were seen as a layer extending from the surface to an elevation of around 1,975 m, although some variation in the lower elevation does occur. On the basis of results from line 6 and the lithologic log from TH 3 (fig. 4*C*; appendix 1–3), it is possible that this layer represents gypsum; however, reports from the excavation of adobe pits adjacent to Mound 7 document limestone bedrock occurring less than 1 m below the surface (Hayes and others, 1981; Howard, 1981). Given the proximity of lines 2 and 4 to these pits (fig. 1*B*), it is also likely that these low-resistivity features are associated with a limestone unit. High-resistivity features (1,000–5,000 ohm-m) commonly were seen as a layer below an elevation of around 1,975 m that may be associated with a different limestone unit, the boulder layer described in TH 3 (fig. 4*C*, appendix 1–3), an increase in pore space caused by dissolution of joints and bedding planes, or a series of larger voids. High-resistivity anomalies appeared in close proximity to one another along lines 1, 3, and 7 that may be indicative of a common source, possibly representative of the igneous intrusion found at the surface towards the middle of line 1, a limestone unit, or a series of larger voids detected in multiple lines. Moderate-resistivity features (200–1,000 ohm-m) also appeared throughout the inverted DC resistivity sections that could be associated with sand, gravel, boulder, or gypsum layers described in TH 3 (fig. 4*C*, appendix 1–3), or a transitional zone between the low- and high-resistivity features. Additional information, such as lithologic or borehole-geophysical logs, would substantially improve interpretations of the electrical structure.

Results from the areal FDEM survey were used to define the relative near-surface EM response, as well as to aid in interpretation of the DC resistivity data. Specifically, in-phase and quadrature responses at 47,010, 13,590, and 3,930 Hz (fig. 9) were examined for correlations to the DC resistivity data. Although the majority of the FDEM grid lines were straight and well-spaced, site restrictions such as ruin walls and vegetation required deviation from the planned grid lines (fig. 9). These deviations are most noticeable on the western side of the surveyed area where vegetation was more dense than on the remainder of the site.

It should be noted that EM induction sensors are very sensitive to the presence of metal. During the course of the survey, metal in the form of iron rebar and plates were found supporting the ruin walls, and it is likely that additional metal is present within the walls that is not visible (Lee Roy Nix, NPS, oral commun., June 2005). Very high in-phase and quadrature responses at all frequencies were seen around Mound 7, San Buenaventura Mission, San Isidro Church, and House A, which would be expected from the presence of metal, making it difficult to interpret geologic features below the structures. Several small areas of high in-phase response also can be attributed to metal near interpretive signs and benches found along trails throughout the study area.

Excluding the areas of metallic interference, strong correlation was found between the DC resistivity and areal FDEM results (figs. 8 and 9). The expansive area of low quadrature response west of Mound 7 and north of San Buenaventura Mission was found to intersect the high-resistivity layers seen in the DC resistivity results along lines 1, 3, and 7, supporting the interpretation that these DC resistivity features represent an extensive geologic layer. The high quadrature responses north and east of Mound 7 most likely can be attributed to the unexcavated ruins at those locations. There is a high in-phase and quadrature response located about 25 m west of Mound 7 that may be attributed to the igneous intrusion partially exposed at the surface. This igneous intrusion most likely would have a higher magnetic susceptibility than the surrounding limestone, and although there may not be a significant electrical contrast between these materials, the magnetic properties may vary enough to be a detectable contrast in the electromagnetic response.

(A) Looking east

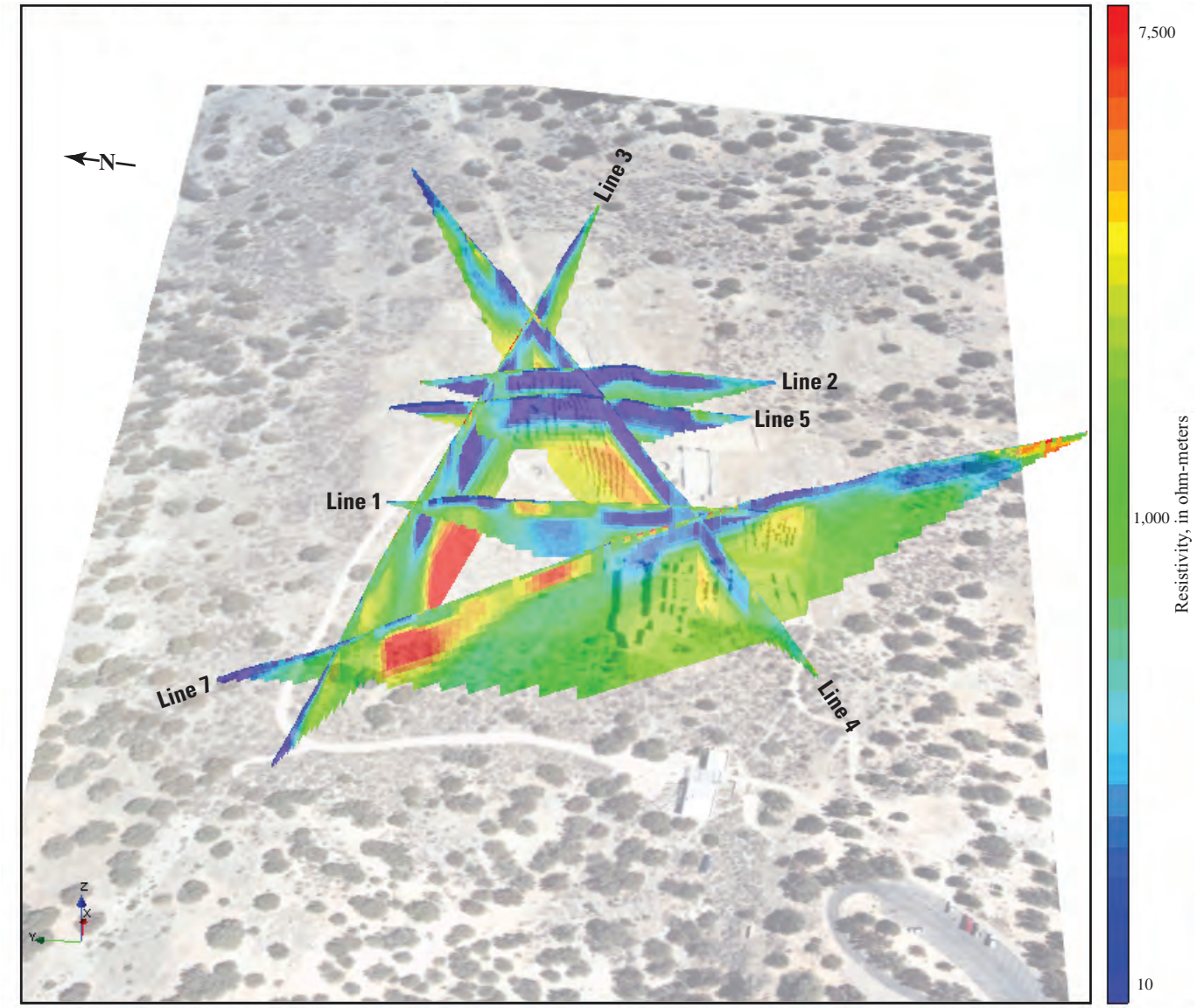

Base from Earth Data Analysis Center, digital orthophotography, 2003,
Western Mapping Company, digital elevation data, 2005

Figure 8. Inverted direct-current resistivity sections from Wenner-Schlumberger array near the Gran Quivira Unit, shown looking *(A)* east, *(B)* northwest, and *(C)* southwest.

Description of High-Resistivity Anomalies

DC resistivity features near or above 5,000 ohm-m were designated as anomalies that may be attributed to voids (figs. 10–15). In some geologic settings, voids can be lined with clay or filled with water, resulting in low-resistivity features. However, on the basis of the high-resistivity response of the small gypsum cavern seen along line 6 and the extent of low-resistivity features in most lines, it is more likely that voids in the study area are expressed as high-resistivity features, although the possibility of conductive voids cannot be dismissed completely. Additional ground truthing of both high- and low-resistivity features would substantially improve the delineation of possible open voids.

A series of high-resistivity anomalies commonly were found in the upper 1 m and often were too small to be detected in the deeper section produced by the Wenner-Schlumberger array (figs. 10–15). These anomalies most likely can be attributed to small voids in the unconsolidated masonry and other archeological features. Because of the frequency, shallow

(B) Looking northwest

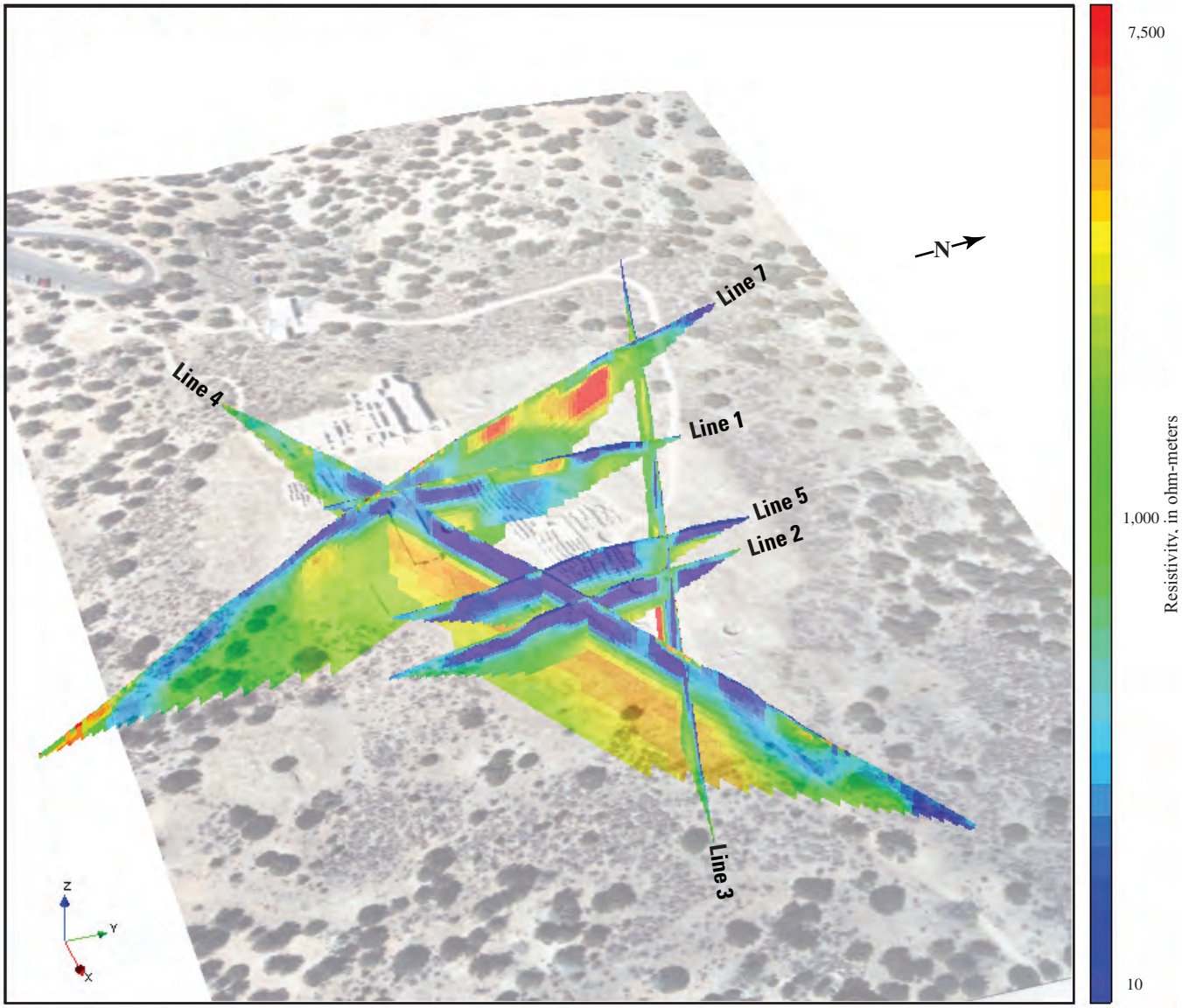

Base from Earth Data Analysis Center, digital orthophotography, 2003,
Western Mapping Company, digital elevation data, 2005

Figure 8. Inverted direct-current resistivity sections from Wenner-Schlumberger array near the Gran Quivira Unit, shown looking *(A)* east, *(B)* northwest, and *(C)* southwest.—Continued

extent, and small size of these features, they were not designated as anomalies for further discussion.

The inverted FDEM sections typically show two main layers—a resistive layer over a conductive layer (figs. 10*C*, 11*C*, 12*C*, 13*D*, 14*D*, 15*D*). The inverted FDEM sections show some correlation to the DC resistivity data in the upper 5 m. The characteristics of each DC resistivity line, as well as specific correlations between the DC resistivity and areal FDEM responses, are discussed in the following sections. Designated anomalies from each line also are described in detail. Designated anomalies from lines 3, 4, and 7 are summarized in table 1; designated anomalies from lines 1, 2, and 5 are summarized in table 2.

Line 3

Line 3 runs east-west on the north side of the study area and passes approximately 15 m north of Mound 7 (fig. 1*B*). The inverted DC resistivity sections show a combination of low- and moderate-resistivity features, possibly representative of gypsum or limestone, over a broken moderate- to high-resistivity feature that approaches the surface in the western

(C) Looking southwest

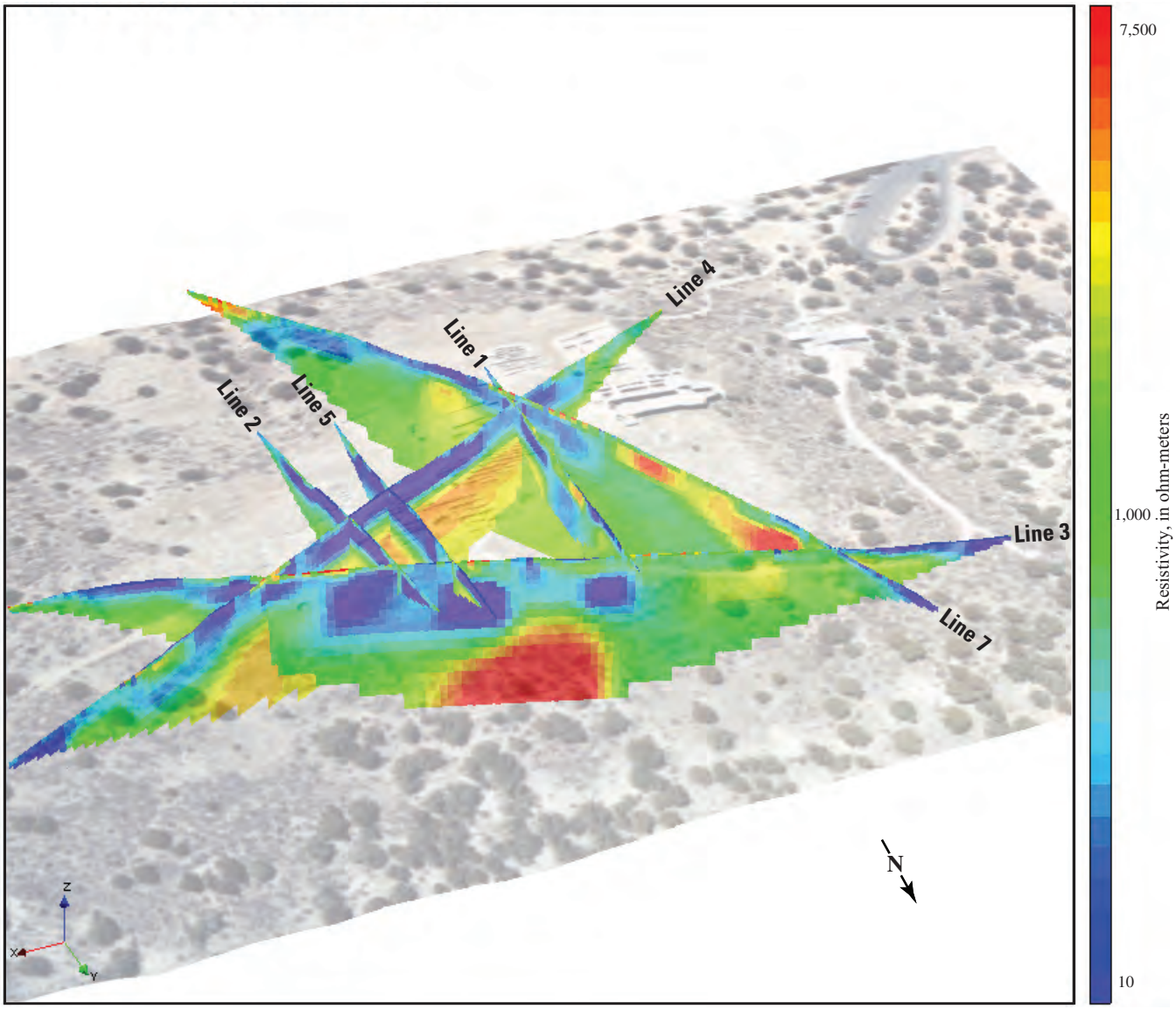

Base from Earth Data Analysis Center, digital orthophotography, 2003,
Western Mapping Company, digital elevation data, 2005

Figure 8. Inverted direct-current resistivity sections from Wenner-Schlumberger array near the Gran Quivira Unit, shown looking *(A)* east, *(B)* northwest, and *(C)* southwest.—Continued

part of the section (figs. 10*A* and *B*), designated as a series of anomalies. The inverted FDEM section shows high relative-resistivity contrasts in the upper 2 m that appear to correspond to the series of shallow DC resistivity anomalies that may be attributed to small voids near the surface, voids in the unconsolidated bricks, or other archeological features (fig. 10*C*).

Anomaly 3–1, in the western third of the resistivity section, visually appears as two groupings of resistive highs between 1,977 and 1,960 m in elevation. An elongated low in-phase response at all frequencies also appears at this location and extends northeast through line 7, and this low response could be associated with an open void; however, only the quadrature response at 3,930 Hz shows a complementary low response to support this interpretation (figs. 9 and 10). The inverted FDEM section does not show discrete high-resistivity responses (fig. 10*C*), as would be expected on the basis of the responses from line 6 (fig. 7*D*), particularly for the shallow, high-resistivity feature seen between 50 and 65 m on the distance axis (fig. 10*A* and *B*). Although the forward-model scenario representing the anomalies as voids was a slightly better match for results from the dipole-dipole array, forward models were unable to conclusively indicate if open voids occur within this layer because of the decreased sensitiv-

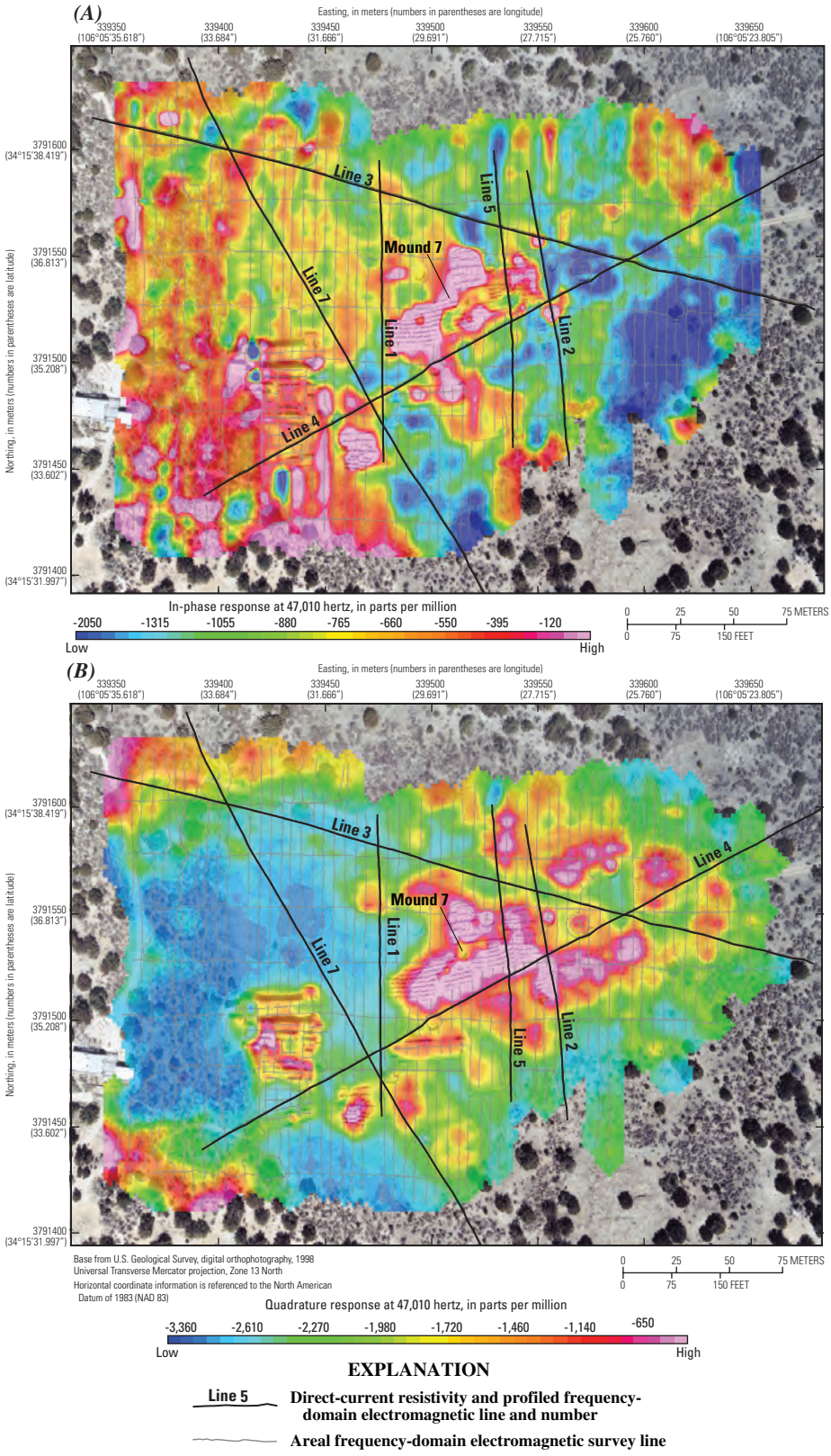

Figure 9. Results of the areal frequency-domain electromagnetic survey showing *(A)* in-phase and *(B)* quadrature response at 47,010 Hertz; *(C)* in-phase and *(D)* quadrature response at 13,590 Hertz, and *(E)* in-phase and *(F)* quadrature response at 3,930 Hertz.

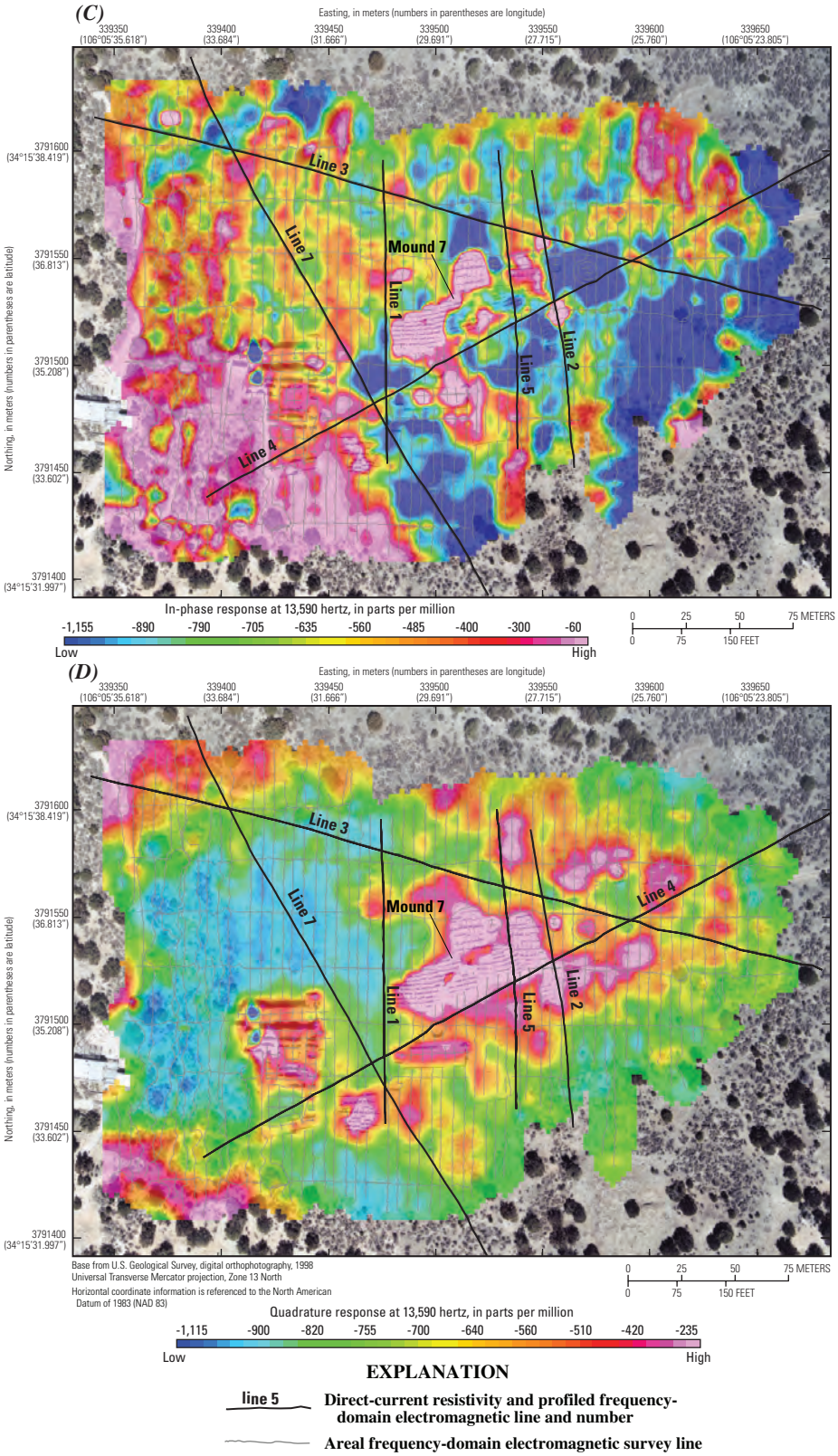

Figure 9. Results of the areal frequency-domain electromagnetic survey showing *(A)* in-phase and *(B)* quadrature response at 47,010 Hertz; *(C)* in-phase and *(D)* quadrature response at 13,590 Hertz, and *(E)* in-phase and *(F)* quadrature response at 3,930 Hertz.—Continued

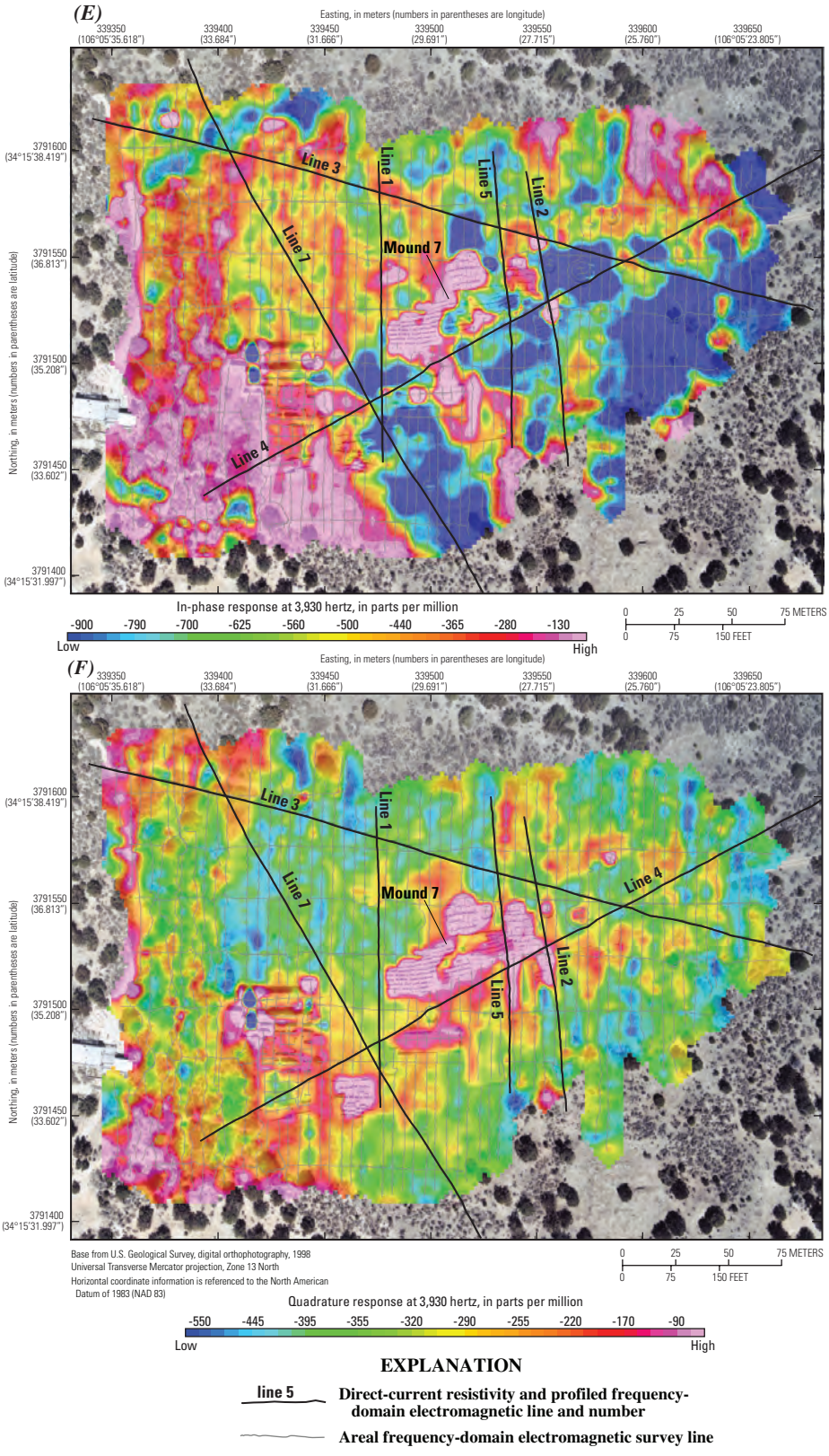

Figure 9. Results of the areal frequency-domain electromagnetic survey showing *(A)* in-phase and *(B)* quadrature response at 47,010 Hertz; *(C)* in-phase and *(D)* quadrature response at 13,590 Hertz, and *(E)* in-phase and *(F)* quadrature response at 3,930 Hertz.—Continued

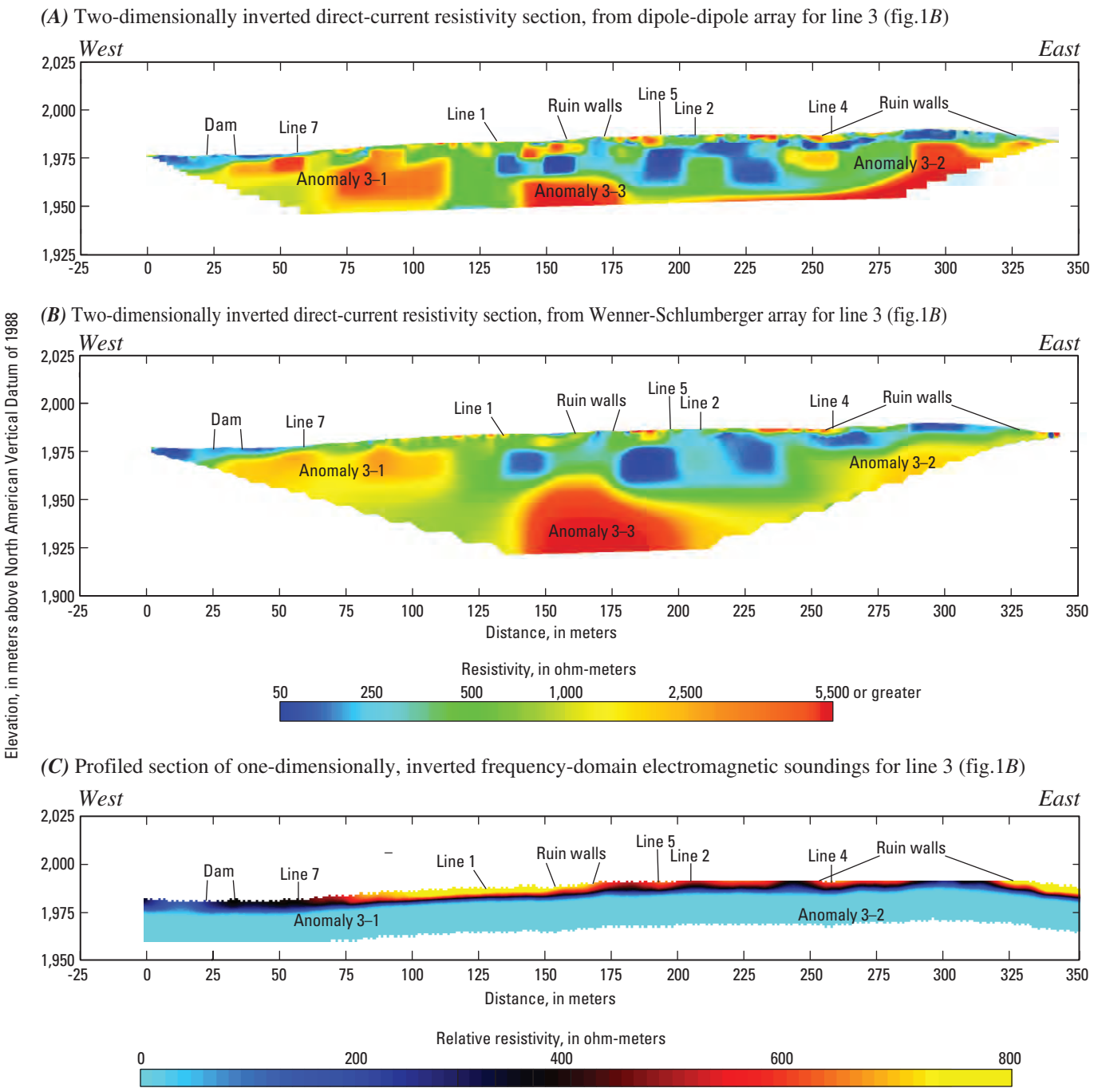

Figure 10. Surface-geophysical data showing inverted direct-current resistivity sections from *(A)* dipole-dipole and *(B)* Wenner-Schlumberger arrays, as well as *(C)* inverted frequency-domain electromagnetic data from line 3.

ity in highly resistive material (appendix 5–2). Although the inverted resistivity values of these features from the Wenner-Schlumberger array did not exceed 5,000 ohm-m (fig. 10*B*), the high-resistivity area seen between 50 and 65 m on the distance axis reached nearly 8,000 ohm-m in the results from the dipole-dipole array, leaving some possibility for the presence of a void. Anomaly 3–1 likely can be attributed to a geologic layer that could possibly contain open voids.

Anomaly 3–2 is on the east side of the bottom of the inverted model section and has a value of approximately 2,500 ohm-m in the results from the Wenner-Schlumberger array and 6,500 ohm-m in the results from the dipole-dipole array (figs. 10*A* and *B*). Forward-model results were similar to those for anomaly 3–1, where the scenario representing the anomaly as a void was a slightly better match for the results from the dipole-dipole array, but the final interpretation was inconclusive (appendix 5–2). The bottom and edges

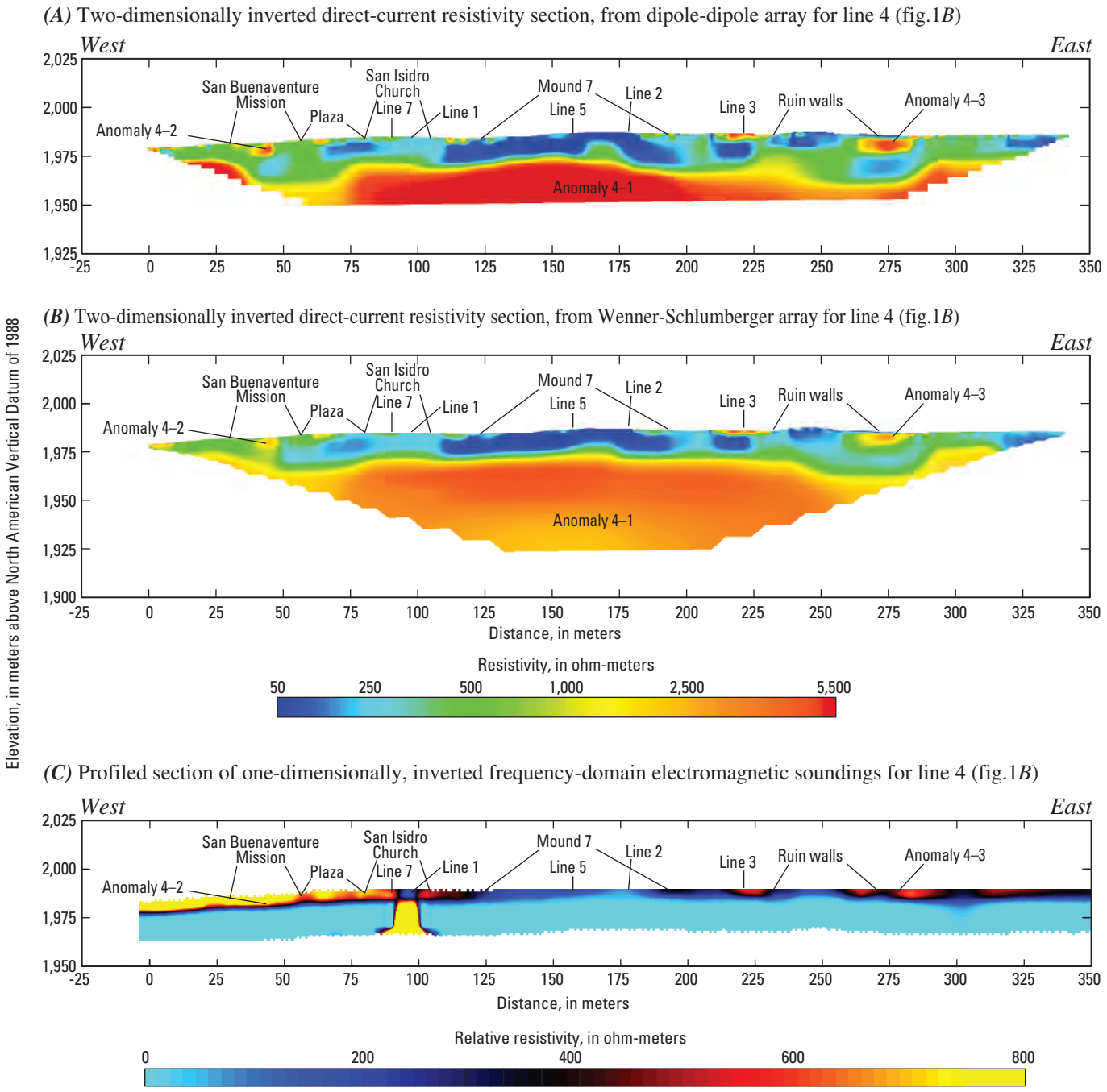

Figure 11. Surface-geophysical data showing inverted direct-current resistivity sections from *(A)* dipole-dipole and *(B)* Wenner-Schlumberger arrays, as well as *(C)* inverted frequency-domain electromagnetic data from line 4.

of the inverted resistivity section are somewhat insensitive to changing structures, and determination of the source of features found in these areas is difficult. The inverted FDEM section shows a high-resistivity contrast immediately east of the anomaly where the DC resistivity section becomes very shallow, supporting the interpretation of a void near this location. The quadrature response at 3,930 Hz also shows a small, discrete area of low response at this location. About 5 m south of line 3 at 300 m on the distance axis, a small land-surface depression was noted, possibly indicating the formation of a small sinkhole. Despite the generally lower resistivity values in the inverted resistivity sections, the FDEM response and evidence of a possible sinkhole make it possible that this anomaly represents a void.

Anomaly 3–3 is the highest resistivity feature along line 3 (greater than 10,000 ohm-m) and appears at the bottom of the DC resistivity sections. Because of the insensitivity at the bottom of inverted model sections, forward models were unable

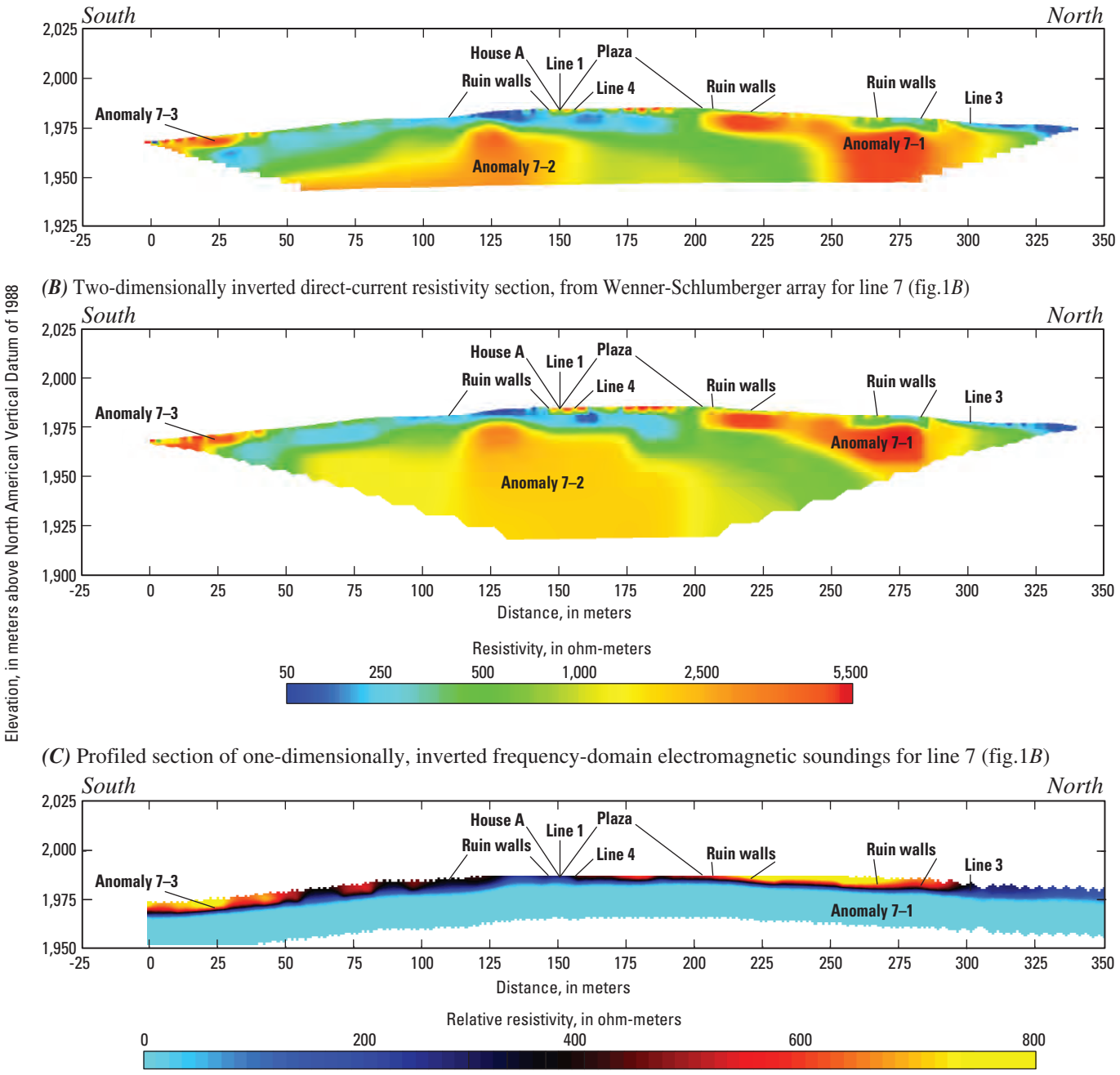

Figure 12. Surface-geophysical data showing inverted direct-current resistivity sections from *(A)* dipole-dipole and *(B)* Wenner-Schlumberger arrays, as well as *(C)* inverted frequency-domain electromagnetic data from line 7.

to conclusively indicate the source of this feature. The depth of the anomaly prevents detection by the FDEM technique. The high-resistivity value of this feature, especially in comparison to the lower resistivity values of the corresponding layers seen in lines 4 and 7 (figs. 11 and 12), indicates that anomaly 3–3 may be caused by an open void near the bottom of the section, although the size and exact location could not be determined because of the low sensitivity in this part of the model.

Line 4

Line 4 was located on the south side of Mound 7 and runs southwest to northeast. Two main electrical layers are present in the inverted DC resistivity sections—a low-resistivity layer over a high-resistivity layer, which was designated as anomaly 4–1 (fig. 11*A* and *B*). As limestone was documented during the excavation of an adobe pit near Kiva D (Howard, 1981), it is likely that the low-resistivity layer, seen

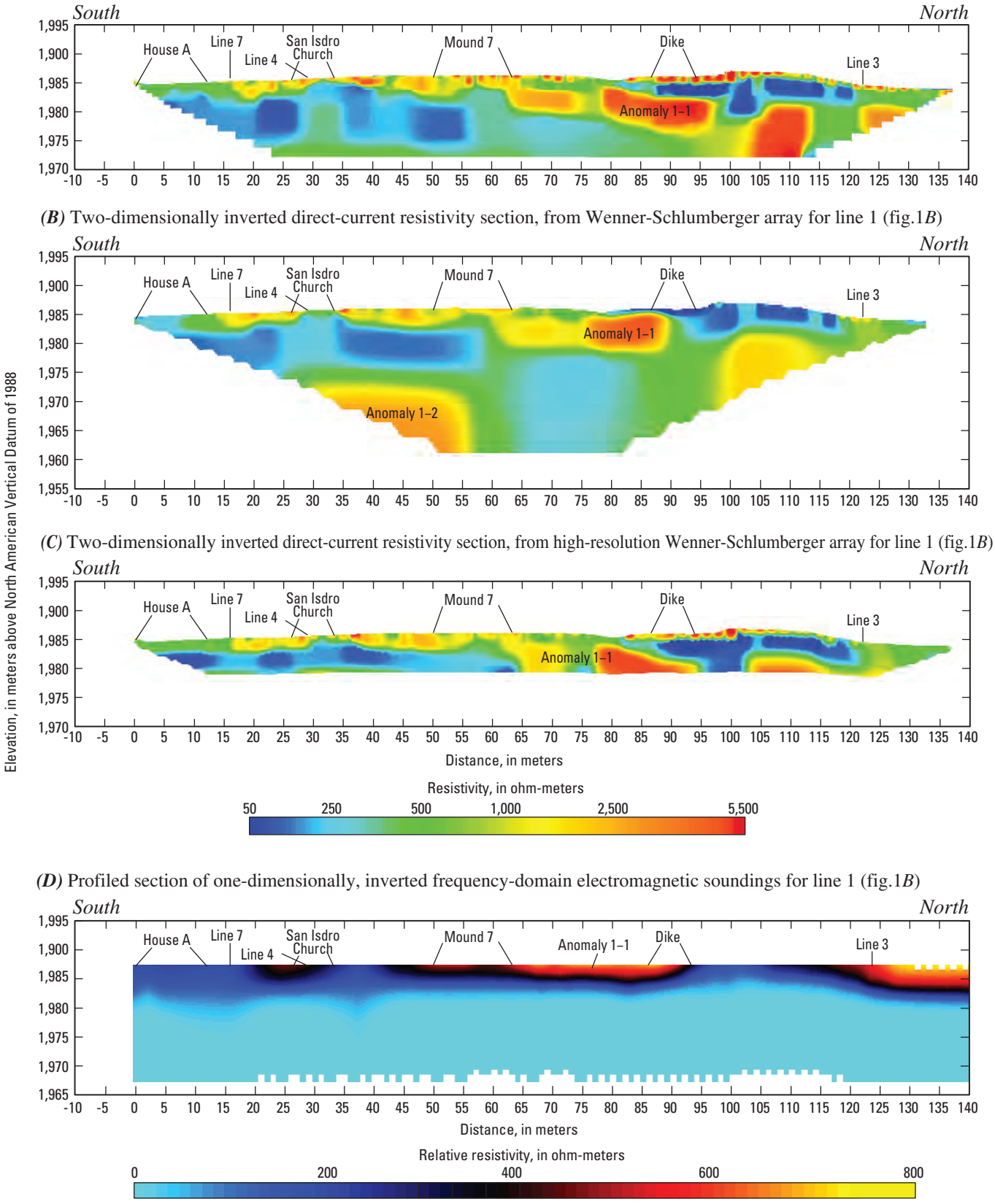

Figure 13. Surface-geophysical data showing inverted direct-current resistivity sections from *(A)* dipole-dipole and *(B)* Wenner-Schlumberger arrays, and *(C)* high-resolution Wenner-Schlumberger arrays, as well as *(D)* inverted frequency-domain electromagnetic data from line 1.

(A) Two-dimensionally inverted direct-current resistivity section, from dipole-dipole array for line 5 (fig.1*B*)

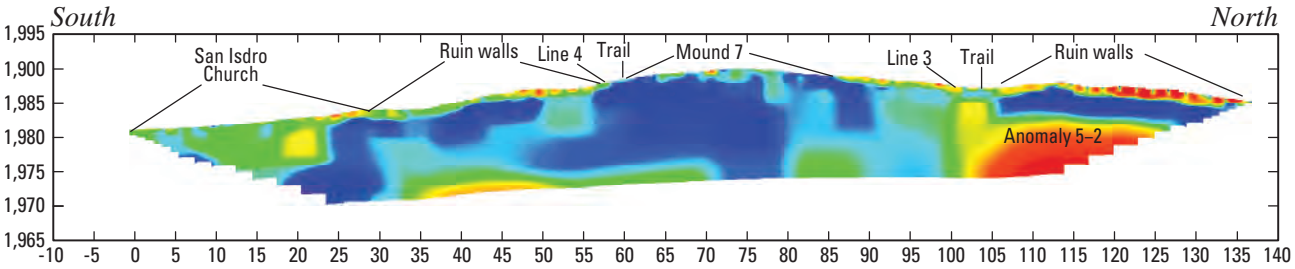

(B) Two-dimensionally inverted direct-current resistivity section, from Wenner-Schlumberger array for line 5 (fig.1*B*)

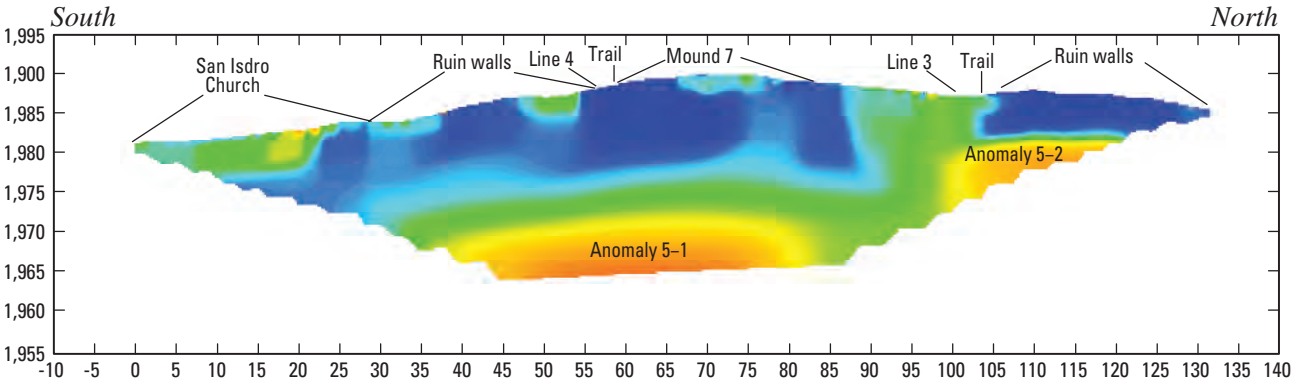

(C) Two-dimensionally inverted direct-current resistivity section, from high-resolution Wenner-Schlumberger array for line 5 (fig.1*B*)

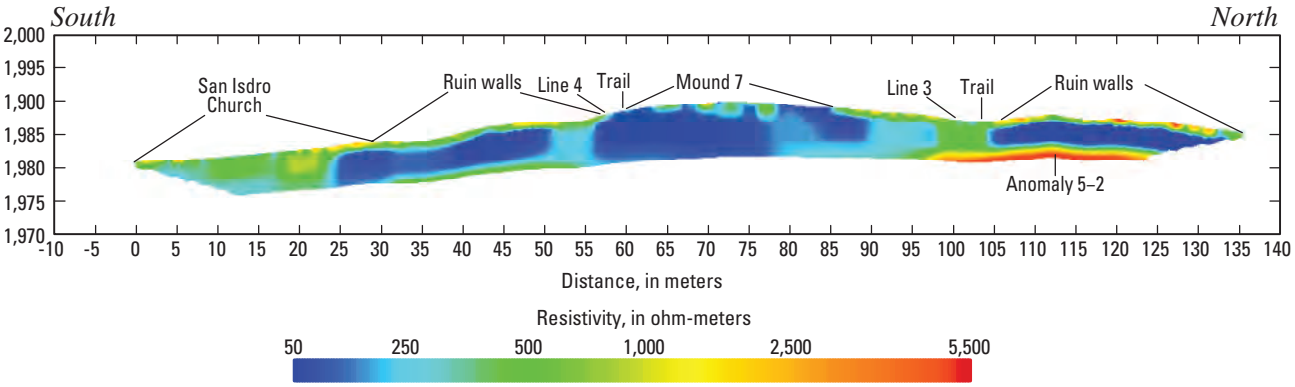

Elevation, in meters above North American Vertical Datum of 1988

(D) Profiled section of one-dimensionally, inverted frequency-domain electromagnetic soundings for line 5 (fig.1*B*)

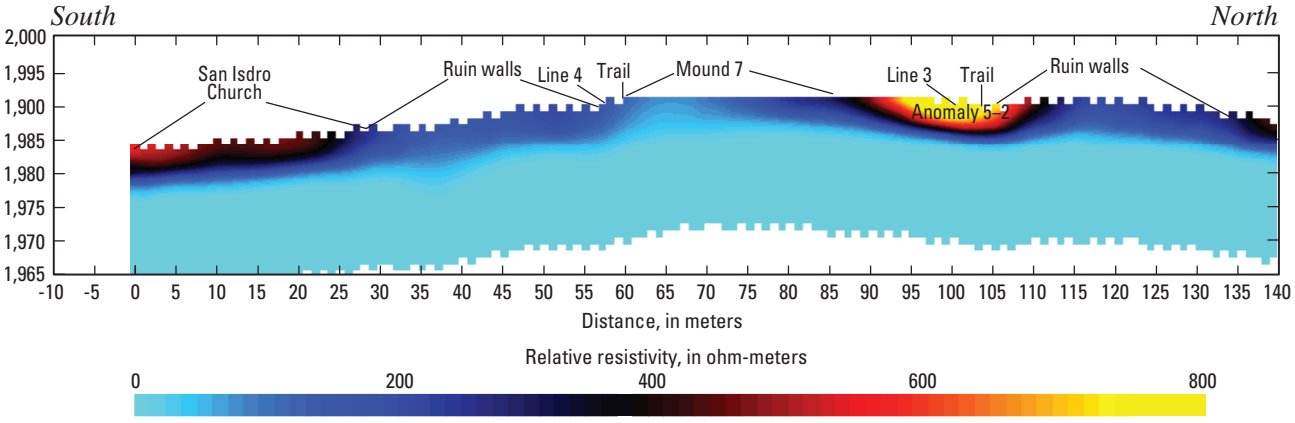

Figure 14. Surface-geophysical data showing inverted direct-current resistivity sections from *(A)* dipole-dipole, and *(B)* Wenner-Schlumberger arrays, and *(C)* high-resolution Wenner-Schlumberger arrays, as well as *(D)* inverted frequency-domain electromagnetic data from line 5.

(A) Two dimensionally inverted direct-current resistivity section, dipole-dipole array from resistivity line 2

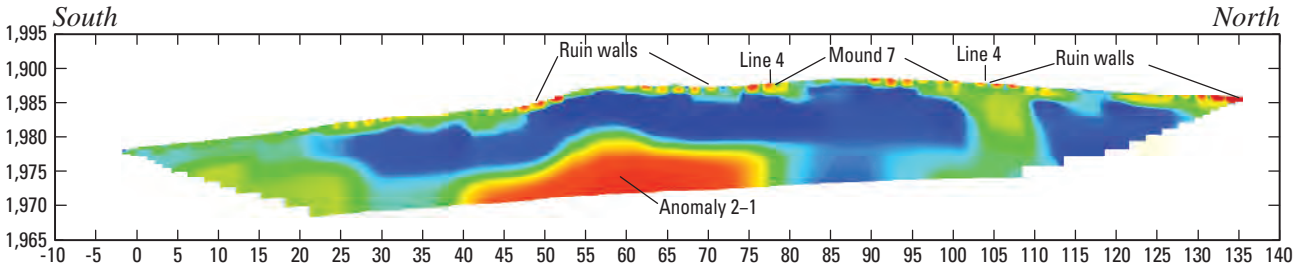

(B) Two-dimensionally inverted direct-current resistivity section, from Wenner-Schlumberger array for line 2 (fig.1*B*)

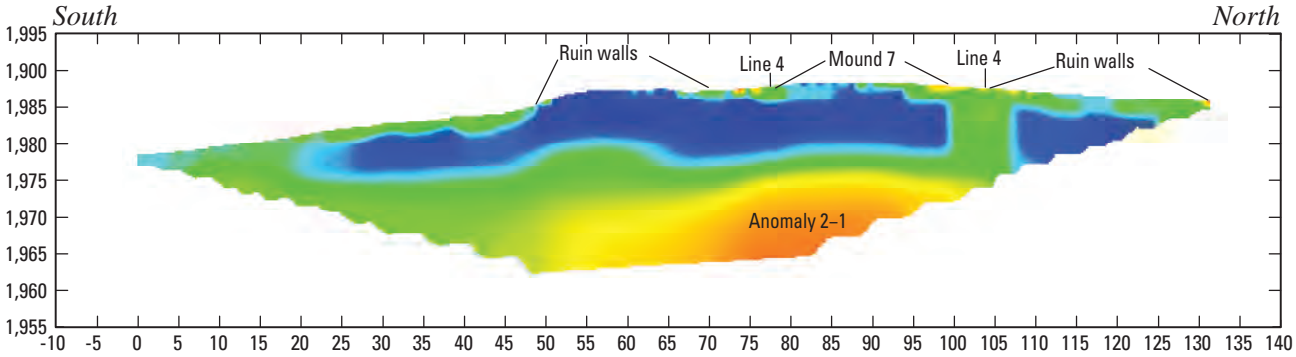

(C) Two-dimensionally inverted direct-current resistivity section, from high-resolution Wenner-Schlumberger array for line 2 (fig.1*B*)

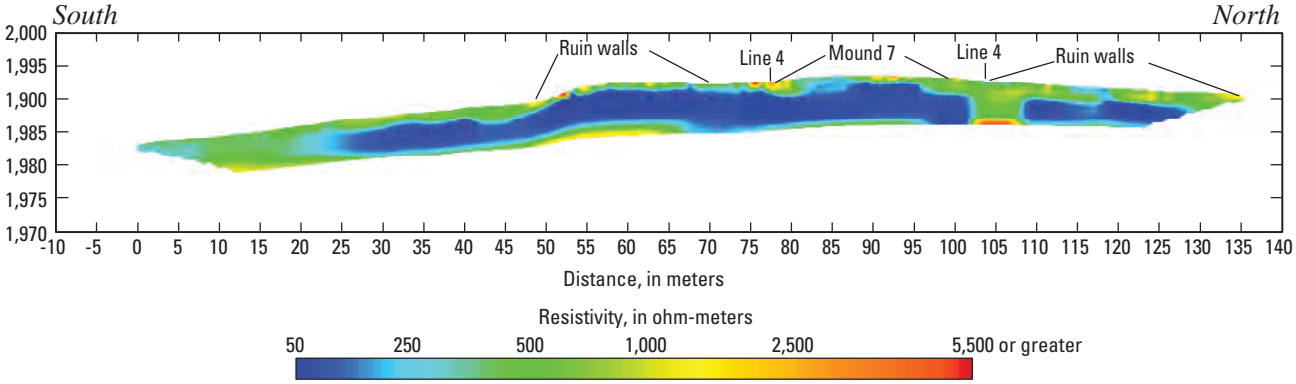

Elevation, in meters above North American Vertical Datum of 1988

(D) Profiled section of one-dimensionally, inverted frequency-domain electromagnetic soundings for line 2 (fig.1*B*)

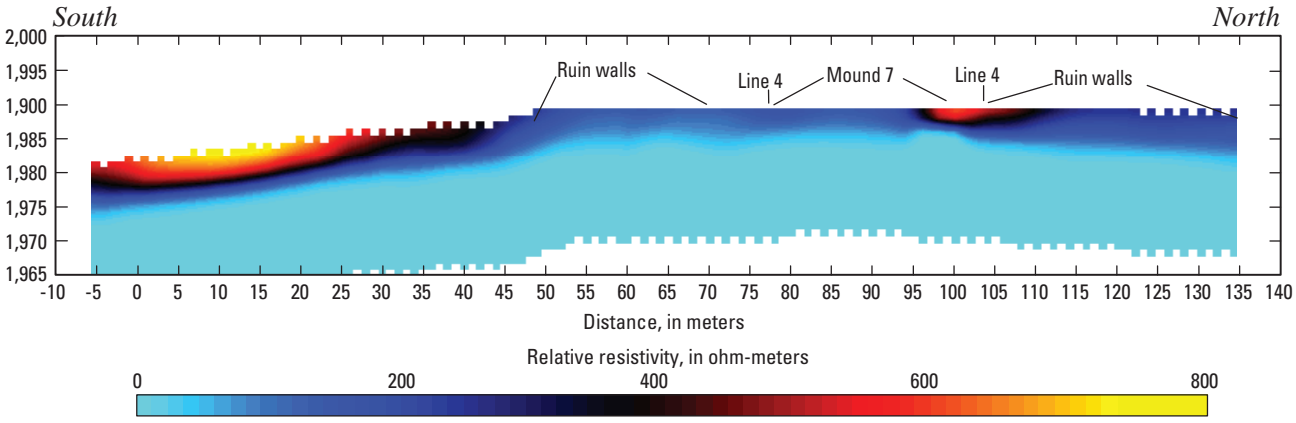

Figure 15. Surface-geophysical data showing inverted direct-current resistivity sections from *(A)* dipole-dipole, and *(B)* Wenner-Schlumberger arrays, and *(C)* high-resolution Wenner-Schlumberger arrays, as well as *(D)* inverted frequency-domain electromagnetic data from line 2.

Table 1. Center locations and possible sources of selected high-resistivity anomalies within the upper 50 meters of the study area, Gran Quivira Unit of Salinas Pueblo Missions National Monument, central New Mexico, June 2005.

[Horizontal coordinate information referenced to Universal Transverse Mercator projection, Zone 13 North, North American Datum of 1983; vertical coordinate information referenced to North American Vertical Datum of 1988]

Anomaly	Easting (meters)	Northing (meters)	Upper elevation (meters)	Lower elevation (meters)	Possible source
3–1	399,430	3,791,593	1,977	1,960	Geologic layer with possibility of small voids
	399,399	3,791,601	1,974	1,964	
3–2	399,621	3,791,540	1,972	?	Void of undetermined size, geologic layer
3–3	399,500	3,791,572	1,947	1,932?	Void of undetermined size, geologic layer
4–1	399,520	3,791,510	1,975	?	Geologic layer with a possibility of voids
4–2	399,436	3,791,462	1,981	1,975	Possible voids
4–3	399,636	3,791,572	1,984	1,977	Possible voids
7–1	399,416	3,791,577	1,975	1,960	Geologic layer with possible void
	399,444	3,791,530	1,982	1,975	Geologic layer with possible void
7–2	399,488	3,791,452	1,974	?	Geologic layer with possibility of small voids
7–3	399,540	3,791,365	1,971	?	Geologic layer with possibility of voids

Table 2. Center locations and possible sources of designated high-resistivity anomalies within the upper 20 meters near Mound 7, Gran Quivira Unit of Salinas Pueblo Missions National Monument, central New Mexico, June 2005. (Anomaly locations are based on data collected using the Wenner-Schlumberger array.)

[Horizontal coordinate information referenced to Universal Transverse Mercator projection, Zone 13 North, North American Datum of 1983; vertical coordinate information referenced to North American Vertical Datum of 1988]

Anomaly	Easting (meters)	Northing (meters)	Upper elevation (meters)	Lower elevation (meters)	Possible source
1–1	399,476	3,791,543	1,984	1,979	Possible small void within geologic layer
	399,476	3,791,563	1,981	?	Possible void within geologic layer
1–2	399,476	3,791,502	1,972	?	Geologic layer
5–1	399,535	3,791,535	1,972	?	Geologic layer
5–2	399,531	3,791,574	1,981	?	Possible void within geologic layer
2–1	399,558	3,791,515	1,975	?	Geologic layer with possibility of voids

extending from the surface to a lower elevation of 1,975 to 1,960 m, represents limestone, although there is also a possibility of gypsum in this layer as well. Two additional anomalies were identified near the surface, anomalies 4–2 and 4–3.

The most prominent contrast in the inverted FDEM section, near 100 m on the distance axis (fig. 11*C*), is at the same location as an interpretive sign in front of San Isidro Church, and the metal frame of the sign is the likely source of this feature. There is a correlation between the moderate DC resistivity features in the near-surface west of 125 m on the distance axis and the high relative-resistivity contrast at the same location in the inverted FDEM section, possibly indicating voids too small to be resolved by the DC resistivity technique at a 5-m electrode spacing. A high relative-resistivity contrast near 225 m appears to correspond to the shallow DC resistivity anomalies attributable to small voids in the unconsolidated bricks and other archeological features. Two additional contrasts can be seen near anomaly 4–3. The inverted resistivity section shows anomaly 4–3 centered near 270 m and rising eastward to the surface near 290 m. The increase in relative resistivity of the easternmost of these two contrasts in the inverted FDEM section may be caused by the reduction in depth of this feature.

Anomaly 4–1 is the large, level-surfaced layer that begins between an elevation of 1,975 and 1,960 m and extends below the depth of investigation. Forward models (appendix 5–3) and the correlation to anomalies 3–1 and 7–2 (figs. 8, 10, and 12) suggest that this is a geologic layer; however, there is a resistive high that exceeds 5,000 ohm-m in results from both arrays near 125 m on the distance axis at an elevation of 1,960 m. Forward modeling suggests that there may be a void in this location within a geologic layer, although the size of this potential void is difficult to determine because of the high resistivity of the surrounding material (appendix 5–3).

Anomaly 4–2 is a small feature seen on the southwestern side of the inverted DC resistivity section between elevations of 1,981 and 1,975 m, and anomaly 4–3 is on the northeastern side of the resistivity section at an elevation between 1,984 and 1,977 m. Both anomalies correlate to low quadrature responses (fig. 9). Although these features do not exceed 6,000 ohm-m in either array, forward model results suggest that there may be small voids at these locations.

Line 7

Line 7 runs southeast to northwest, and its center lies in the plaza of the Gran Quivira Unit (fig. 1*B*). The inverted DC resistivity sections have an anticlinal appearance (fig. 12), with a low- to moderate-resistivity layer, most likely associated with limestone or gypsum, intersecting the surface south of where the line passes by House A. Three major high-resistivity features appear in the section and have been classified as anomalies.

Anomaly 7–1 is contained within the northwestern high-resistivity layer, which also correlates to the locations of anomalies 3–1 and 1–1 (figs. 8, 10, 12, and 13). Forward model results from both the dipole-dipole and Wenner-Schlumberger arrays showed a better match to field data using the scenario with voids. Given that the resistivity values exceeded 5,000 ohm-m in both arrays, the presence of voids at the two resistive highs within the anomaly is possible (appendix 5–4). This high-resistivity feature also could be representative of the igneous intrusion seen at the surface near anomaly 1–1 (figs. 1*B* and 13). In the areal FDEM results, an elongated low in-phase response at all frequencies also appears near this location and extends southwest through anomaly 3–1 and could be associated with a void, although only the quadrature response at 3,930 Hz shows a correlative low response to support this interpretation (figs. 9 and 12). The inverted FDEM section shows strong-relative resistivity contrasts that correlate to anomaly 7–1, also supporting the interpretation of voids (fig. 12*C*).

Anomaly 7–2 represents the southeastern high-resistivity layer, which begins at an elevation of 1,974 m and extends below the depth of investigation. This feature does not exceed 5,000 ohm-m, and based on its correlation with the bottom high-resistivity layer in lines 3 and 4 (fig. 8), designated as anomalies 3–3 (fig. 10) and 4–1 (fig. 11), it is also most likely a geologic layer with the possibility of voids.

Anomaly 7–3 is located in the southern part of line 7 with DC resistivity values approaching 5,000 ohm-m. The inverted FDEM section shows strong relative-resistivity contrasts at the same location, supporting the interpretation of small voids (fig. 12*C*). Because this feature is south of the area of interest, no forward model scenarios were attempted for this feature.

Line 1

Line 1 was located along the west side of Mound 7, beginning to the south near House A and ending slightly north of a trail (fig. 1*B*). Evidence of an igneous intrusion is exposed at the surface between 80 and 95 m from the beginning of the line. The inverted DC resistivity section appears to have two moderate- to high-resistivity layers dipping to the north separated by a low-resistivity layer (fig. 13). The low-resistivity layer is most likely a geologic layer, such as limestone or gypsum. The high-resistivity layers were designated as two anomalies (table 2).

The inverted FDEM section shows a strong resistivity contrast that correlates to features seen in the inverted resistivity sections near anomaly 1–1 (fig. 13*D*). Another strong contrast can be seen north of 120 m on the distance axis, which appears to be related to the moderately high-resistivity feature at the surface in the same part of the inverted DC resistivity sections, seen most clearly in the results from the dipole-dipole array (fig. 13*A*) and again in line 3 just east of anomaly 3–1 (fig. 10). This contrast may indicate that voids may be present that are too small to be resolved clearly by the DC resistivity technique at a 2-m electrode spacing.

Anomaly 1–1 is the upper high-resistivity layer and is expressed across the majority of the section extending from near the surface to an elevation of 1,984 m to the south and dipping below the depth of investigation to the north. This layer may represent a series of voids or a high-resistivity geologic layer, such as a limestone unit or an igneous intrusion. Anomaly 1–1 also may correlate to the high-resistivity features seen in line 7 (fig. 8), designated as anomaly 7–1 (fig. 12). In the northern one-third of the resistivity sections, a low-resistivity feature appears above this anomaly. The areal grid from the FDEM survey of the quadrature response at 47,010 Hz shows a large low-parts-per-million feature that matches the surface occurrence of anomaly 1–1, and a high-parts-per-million feature appears where the low-resistivity surface unit begins in the DC resistivity section (fig. 9*B*). The extent of this low parts-per-million feature supports the concept that anomaly 1–1 and 7–1 are caused by the same source feature, possibly a geologic layer.

Multiple higher resistivity features are seen within the layer designated as anomaly 1–1. Forward-model scenarios using both voids and continuous layers were attempted but found to be inconclusive (appendix 5–5). The resistive high seen between 80 and 95 m and 100 and 115 m on the distance axis exceeded 7,000 ohm-m in the results from the dipole-dipole array and approached 5,000 ohm-m in the results from both Wenner-Schlumberger arrays (figs. 13*A*, *B*, and *C*),

indicating the possibility that the anomalies in this layer could be caused by open voids. The resistivity contrast seen in the inverted FDEM section also supports the possibility of voids.

Anomaly 1–2 is located at the bottom of the southern side of the DC resistivity section from the Wenner-Schlumberger array at an elevation of 1,972 m and extending below the depth of investigation (fig. 13*B*). The position of this feature at the side and bottom of the section makes it difficult to determine the source of the anomaly; however, the resistivity of this feature does not exceed 3,000 ohm-m and is not likely to be attributable to a substantial void under this exact location. The location of anomaly 1–2 (fig. 13) correlates to anomalies 7–2 (fig. 11) and 4–1 (fig. 12) and is possibly indicative of the same source, most likely a high-resistivity geologic layer with the possibility of voids.

Line 5

Line 5 crossed through Mound 7 on the east side of Kiva C. The inverted DC resistivity sections showed two main layers—a low-resistivity layer over a high-resistivity layer, seen most clearly in the results from the Wenner-Schlumberger array (fig. 14*B*). The high-resistivity layer is described as anomaly 5–1 (fig. 14*B*). At the southern end of the section near 20 m on the distance axis, another moderate- to high-resistivity feature appeared in the upper 8 m. Although there is a possibility that this feature indicates the presence of small voids, it also could be related to disturbed ground around San Isidro Cemetery. The resistivity value did not exceed 2,000 ohm-m in results from any array, and this feature was not classified as an anomaly.

The inverted FDEM section showed two major contrasts, with the highest relative resistivity values appearing between 95 and 105 m on the distance axis (fig. 14*D*). This feature appears in the same location as the narrow, moderate-resistivity feature in the inverted DC resistivity sections for line 5. This feature also appears in a very similar location to some of the small high-resistivity features seen in line 3 that were attributed to small voids in the unexcavated ruins. A weaker FDEM contrast is seen between 0 and 25 m on the distance axis and correlates to the moderate-resistivity feature in the inverted DC resistivity section. This contrast supports the possibility of small voids caused by disturbed ground or archeological features, although it also may be related to the presence of the San Isidro Cemetery.

Anomaly 5–1 is in the lower half of the DC resistivity section (fig. 14*B*) from an upper elevation of 1,972 to 1,970 m and may correlate to the high-resistivity layers designated as anomalies 3–3, 4–1, and 7–2. Forward-model scenarios were attempted both with and without voids, and the resistivity of this feature in the inverted resistivity sections of models expressing voids exceeded the values seen in the field data (appendix 5–6). This model result, in addition to the fact that the feature does not exceed 5,000 ohm-m in any inverted DC resistivity sections, supports the interpretation that this is a geologic layer, although there is a possibility for voids below the depth of investigation.

Anomaly 5–2 is at an upper elevation of 1,981 m and extends to the bottom edge of the northern side of the inverted resistivity section. Inverted DC resistivity sections from the Wenner-Schlumberger arrays show this feature as less than 2,500 ohm-m; however, the inverted resistivity section from the dipole-dipole array shows this feature as greater than 5,000 ohm-m. Forward-model results showed the scenario with voids as producing a less favorable visual match to the field data for the Wenner-Schlumberger arrays, but as a more favorable match to the dipole-dipole array. Because this is a low-sensitivity area of the resistivity sections, the cause of this resistive feature could not be determined. There is a possibility of an open void at this location.

Line 2

Line 2 was located on the east side of Mound 7. The inverted DC resistivity sections from this line (fig. 15) were quite similar to those of line 5 (fig. 14), which would be expected from their close proximity. A low-resistivity layer intersected the surface near the center of the inverted resistivity section, a moderate-resistivity layer appeared at the surface near the ends of the resistivity section, and a high-resistivity layer appeared at the bottom of the section and was designated as anomaly 2–1. Relative-resistivity contrasts in the inverted FDEM section (fig. 15*D*) showed correlations to moderate-resistivity surface features in the inverted DC resistivity sections, possibly indicating that there may be voids too small to be resolved by the DC resistivity technique at a 2-m electrode spacing.

Based on its elevation, anomaly 2–1 (fig. 15) could be a continuation of the same feature causing anomaly 5–1 (fig. 14). The feature extends below the depth of investigation from a top elevation of 1,978 m in results from the dipole-dipole array and 1,975 m in the results from the Wenner-Schlumberger array. The resistivity value of this layer did not exceed 5,000 ohm-m in the results from the Wenner-Schlumberger array; however, the results from the dipole-dipole array showed values exceeding 8,000 ohm-m (fig. 15*A*). Because this feature is located at the bottom of the section, lack of model sensitivity makes its source difficult to determine. Although there was a slightly better match using the forward-model scenario with voids for the dipole-dipole array, a conclusive source could not be identified (appendix 5–7). The lower resistivity values from the Wenner-Schlumberger array make it likely that this feature is a geologic layer, although there is a possibility of voids within the layer.

Summary and Conclusions

The near-surface geology in the immediate area of the Gran Quivira Unit of Salinas Pueblo Missions National Monu-

ment in central New Mexico is mostly composed of carbonates. Karst features such as sinkholes and caves have been found in the surrounding areas. Historic National Park Service records suggest that both natural caves and artificial tunnels may be present beneath and adjacent to Mound 7, a large excavated and partially reconstructed Native American pueblo. To improve the effectiveness of site preservation and resource management, especially near Mound 7, the U.S. Geological Survey, in cooperation with the National Park Service, used time-domain electromagnetic and frequency-domain electromagnetic (FDEM) techniques in conjunction with two-dimensional direct-current (DC) resistivity to characterize the electrical structure of the local subsurface geology, as well as to identify electrical anomalies that could be associated with open voids.

Time-domain electromagnetic soundings indicate three major subsurface electrical structures—a low-resistivity unit; a moderate- to high-resistivity unit; and a high-resistivity unit. The extreme variability in existing test-hole descriptions made correlation of geologic units to electrical layers difficult, and substantial variations were found between the resistivity values at different sounding locations.

Results from gridded lines and profiled, inverted soundings of FDEM data showed resistivity contrasts at locations that correlated to moderate- and high-resistivity features in the upper 5 m of the DC resistivity data. The inverted FDEM data also showed some contrasts not seen in inverted DC resistivity data that may indicate this technique is capable of detecting shallow voids too small to be detected by the DC resistivity technique at a 2-m electrode spacing.

Inverted resistivity data from six DC resistivity lines indicate that the geology in the upper 50 m below the study area is somewhat anticlinal in appearance. Typically, a low-resistivity layer, possibly indicative of limestone or gypsum, overlies a high-resistivity layer, possibly indicative of a different limestone unit, a gravel layer, an increase in pore space caused by dissolution of joints and bedding planes, or a series of larger voids. Moderate-resistivity features were found throughout the inverted DC resistivity sections that may be associated with sand, gravel, or gypsum layers, or a transitional zone between the low- and high-resistivity features.

Based on the high-resistivity response of a known cavern near the Gran Quivira Unit and the extent of low-resistivity features in most lines, it is likely that voids in the study area are expressed as high-resistivity features, although the possibility of electrically conductive voids cannot be dismissed completely. Several high-resistivity anomalies were identified in the data and explored through forward modeling to identify potential sources; however, this modeling was inconclusive in confirming the location of voids in most cases because of low model sensitivity or insufficient electrical contrast within the surrounding high-resistivity material. Nevertheless, the very high resistivity values found in some locations suggest the possibility of open voids in the upper 50 m along lines 3, 4, and 7. Below Mound 7, there is a possibility of larger voids extending between lines 3 and 4 below 20 m depth. However, the inverted resistivity sections from lines 1, 5, and 2 do not indicate the presence of voids larger than 3 m in diameter in the upper 20 m below Mound 7. Additional information, such as lithologic or borehole-geophysical logs and ground truthing of both high- and low-resistivity features, would substantially improve interpretations of the electrical structure and the delineation of possible voids.

References Cited

Bates, R.L., Wilpolt, R.H., MacAlpin, A.J., and Vorbe, Georges, 1947, Geology of the Gran Quivira quadrangle, New Mexico: New Mexico Bureau of Mines and Mineral Resources, Bulletin 26, 49 p.

Clebsch, Alfred, Jr., 1957, Availability of ground water at Gran Quivira National Monument, New Mexico: U.S. Geological Survey Open-File Report 57–19, 38 p.

Fitterman, D.V., and Stewart, M.T., 1990, Transient electromagnetic sounding for groundwater: Geophysics, v. 51, no. 4, p. 995–1005.

Grant, F.S., and West, G.F., 1965, Interpretation theory in applied geophysics—part 3, electrical conduction and electromagnetic induction methods: New York, McGraw-Hill, p. 384–572.

Hayes, A.C., Young, J.N., and Warren, A.H., 1981, Excavation of Mound 7, Gran Quivira National Monument, New Mexico: National Park Service, Publications in Archeology, no. 16, p. 1–12.

Howard, R.M., 1981, An adobe-lined pit, *in* Hayes, A.C., Contributions to Gran Quivira archeology, Gran Quivira National Monument, New Mexico: National Park Service, Publications in Archeology, no. 17, chap. 3, p. 13–14.

Huang, Haoping, and Won, I.J., 2000, Conductivity and susceptibility mapping using broadband electromagnetic sensors: Journal of Environmental and Engineering Geophysics, v. 5, no. 4, p. 31–41.

Lide, D.R., 2004, CRC handbook of chemistry and physics: Boca Raton, Fla., Taylor and Francis-CRC Press, p. 14–34.

Loke, M.H., 2000, Electrical imaging surveys for environmental and engineering studies—a practical guide to 2-D and 3-D surveys: Penang, Malaysia, M.H. Loke, 62 p., accessed August 2002 at *http://www.abem.com/files/res/2Dnotes.pdf*

Loke, M.H., 2004a, RES2DINV, version 3.54—Rapid 2D resistivity and IP inversion using the least-squares method—geoelectrical imaging 2-D and 3-D: Penang, Malaysia, Geotomo Software, 130 p., accessed September 12, 2005, at *http://www.geoelectrical.com/download.html*

Loke, M.H., 2004b, Tutorial — 2-D and 3-D electrical imaging surveys: Penang, Malaysia, Geotomo Software, 128 p., accessed July 23, 2004, at *http://www.geoelectrical.com*

Smith, R.E., 1957, Geology and ground-water resources of Torrance County, New Mexico: New Mexico Bureau of Mines and Mineral Resources Ground-Water Report 5, 186 p.

Titus, F.B., Jr., 1960, Summary of test drilling, Gran Quivira National Monument, New Mexico: U.S. Geological Survey Open-File Report 60–142, 12 p.

U.S. Geological Survey, 2005, National Elevation Dataset: Sioux Falls, S. Dak., U.S. Geological Survey data available on the Web, accessed June 19, 2006, at *http://ned.usgs.gov/*

Won, I.J., Keiswetter, D.A., Fields, G.R.A., Sutton, L.C., 1996, GEM-2—a new multifrequency electromagnetic sensor: Journal of Environmental and Engineering Geophysics, v. 1, no. 2, p. 129–137.

Zohdy, A.A.R, Eaton, G.P., and Mabey, D.R., 1974, Application of surface geophysics to ground-water investigations: U.S. Geological Survey Techniques of Water-Resources Investigations, book 2, chap. D1, 116 p.

Appendix 1. Lithologic logs for test holes.

Appendix 1–1. Lithologic log for test hole 1 (Marc LeFrancois, National Park Service, written commun., April 2005)

[Legal description: 1S.8E.4.314]

Depth (meters)	Lithology	Formation
0–3.0	loose sand	Quaternary alluvial sediment
3.0–6.1	loose sand and sandstone	
6.1–21.3	yellow sandstone	San Andres Limestone
21.3–54.9	caliche[1]	
54.9–57.9	grey limestone	
57.9–62.5	yellow limestone	
62.5–89.3	grey limestone	
89.3–93.0	yellow caliche[1]	
93.0–100.6	limestone[2]	
100.6–118.9	caliche[1]	
118.9–134.7	hard blue limestone	
134.7–143.3	grey limestone	
143.3–158.5	yellow sandstone	Glorieta Sandstone
158.5–169.2	sandstone	Yeso Formation
169.2–194.5	yellow sandstone[3]	

[1]Caliche possibly refers to gypsum.

[2]Seep at 97.5 meters.

[3]Water at 190.5 meters.

Appendix 1–2. Lithologic log for test hole 2 (adapted from Titus, 1960).

[Legal description: 1S.8E.4.312]

Depth (meters)	Lithology	Formation
0–19.8	sand	Quaternary alluvial sediment
19.8–21.3	clay	
21.3–27.4	limestone, slightly sandy	San Andres Limestone
27.4–33.5	limestone, small amounts of siltstone	
33.5–35.7	diorite, medium-gray to pale greenish-gray; contains mica, garnet, magnetite	Tertiary igneous intrusion
35.7–39.6	limestone; contains calcite veinlets	San Andres Limestone
39.6–42.7	diorite, light-gray to orangish-gray; contains mica, garnet, and magnetite	Tertiary igneous intrusion
42.7–44.2	limestone	San Andres Limestone
44.2–54.9	diorite	Tertiary igneous intrusion
54.9–61.9	limestone, interbedded with dolomite	San Andres Limestone
61.9–76.2	diorite	Tertiary igneous intrusion
76.2–82.3	limestone	San Andres Limestone
82.3–85.3	diorite	Tertiary igneous intrusion
85.3–87.5	limestone; contains calcite veins	San Andres Limestone
87.5–89.9	shale, very calcareous	
89.9–113.7	limestone, minor amounts of siltstone and gypsum[1]	
113.7–120.4	sandstone, very calcareous, coarse- to very fine-grained	
120.4–141.7	limestone, slightly fossiliferous	
141.7–157.6	sandstone, silty and calcareous	Glorieta Sandstone
157.6–160.9	limestone	
160.9–167.6	sandstone, silty and calcareous	
167.6–167.9	shale, gray	
167.9–194.2	sandstone, very fine- to medium-grained hard, tightly cemented[2]	Yeso Formation

[1]Seep at 97.5 meters.

[2]Water at 190.5 meters.

Appendix 1–3. Lithologic log for test hole 3 (adapted from Clebsch, 1957).

[Legal description: 1S.8E.3.121]

Depth (meters)	Lithology	Formation
0–0.9	sandy soil	Quaternary alluvial sediments
0.9–2.4	gypsum and limestone	San Andres Limestone
2.4–3.7	boulders and gravel	
3.7–4.9	gypsum	
4.9–10.7	boulders	
10.7–18.3	black limestone	
18.3–20.7	white limestone	
20.7–25.9	yellow sand	
25.9–27.4	limestone	
27.4–34.1	gypsum	
34.1-35.7	yellow sand	
35.7-41.1	limestone	
41.1–43.6	quartz	
43.6–44.8	limestone	
44.8–46.3	yellow sand	
46.3–50.3	gypsum	
50.3–54.9	limestone	
54.9–61.9	gypsum	
61.9–65.5	white limestone	
65.5–68.0	sandstone	
68.0–76.2	igneous dike rock	Malpais Basalt
76.2–77.7	broken sand	San Andres Limestone
77.7–82.3	gypsum	
82.3–84.4	limestone	
84.4–128	not record	
128–131.1	limestone	Glorieta Sandstone
131.1–138.7	yellow sandstone	
138.7–140.2	red sandstone	Yeso Formation
140.2–147.8	yellow sandstone	
147.8–150.9	sharp sandy limestone	
150.9–176.8	hard yellow sandstone	
176.8–182.9	soft white sandstone	
182.9–214	yellow sandstone	
214–235	red sandstone	
235–240.5	red clay	
240.5–241.7	limestone	
241.7–242.3	red clay	
242.3–243.8	limestone	
243.8–246.6	white limestone	
246.6–247.2	red clay	
247.2–256	white limestone	
256–266.7	black limestone[1]	

[1]Water at 256.0 meters.

Appendix 2. Location of time-domain electromagnetic soundings, electrodes along direct-resistivity lines, and additional surveyed features.

Appendix 2–1. Location of time-domain electromagnetic (TDEM) soundings near the Gran Quivira Unit of Salinas Pueblo Missions National Monument.

[Coordinate system: Universal Transverse Mercator Zone 13, North American Datum of 1983; elevation is in meters above the North American Vertical Datum of 1988; TDEM, time-domain electromagnetic]

Sounding identifier (fig.1)	Easting (meters)	Northing (meters)	Elevation (meters)
TDEM 1	397,519.27	3,790,519.85	1,924.7
TDEM 2	397,823.11	3,790,573.58	1,920.2
TDEM 3	398,261.40	3,790,629.06	1,919.3
TDEM 4	399,095.36	3,791,121.32	1,950.3
TDEM 5	399,450.69	3,791,535.46	1,985.5

Appendix 2–2. Location of each direct-current resistivity electrode along line 1 within the Gran Quivira Unit of Salinas Pueblo Missions National Monument.

[Coordinate system: Universe Transverse Mercator Zone 13, North American Datum of 1983; elevation is in meters above the North American Vertical Datum of 1988]

Electrode identifier	Easting (meters)	Northing (meters)	Elevation (meters)
Electrode 1	399,477.19	3,791,453.55	1,985.0
Electrode 2	399,477.22	3,791,455.45	1,985.8
Electrode 3	399,477.24	3,791,457.47	1,984.9
Electrode 4	399,477.11	3,791,459.45	1,984.9
Electrode 5	399,477.09	3,791,461.44	1,985.0
Electrode 6	399,477.08	3,791,463.41	1,985.2
Electrode 7	399,477.00	3,791,465.40	1,985.2
Electrode 8	399,477.03	3,791,467.39	1,985.3
Electrode 9	399,476.98	3,791,469.46	1,985.4
Electrode 10	399,476.95	3,791,471.41	1,985.5
Electrode 11	399,476.99	3,791,473.40	1,985.5
Electrode 12	399,476.96	3,791,475.41	1,985.6
Electrode 13	399,476.91	3,791,477.39	1,985.6
Electrode 14	399,476.86	3,791,479.37	1,985.6
Electrode 15	399,476.84	3,791,481.42	1,985.7
Electrode 16	399,476.85	3,791,483.38	1,985.8
Electrode 17	399,476.80	3,791,485.38	1,985.9
Electrode 18	399,476.75	3,791,487.37	1,986.0
Electrode 19	399,476.80	3,791,489.38	1,986.1
Electrode 20	399,476.70	3,791,491.35	1,986.2
Electrode 21	399,476.67	3,791,493.35	1,986.3
Electrode 22	399,476.67	3,791,495.38	1,986.4
Electrode 23	399,476.64	3,791,497.39	1,986.4
Electrode 24	399,476.62	3,791,499.39	1,986.5
Electrode 25	399,476.63	3,791,501.37	1,986.5
Electrode 26	399,476.63	3,791,503.39	1,986.4
Electrode 27	399,476.62	3,791,505.37	1,986.4
Electrode 28	399,476.62	3,791,507.38	1,986.4
Electrode 29	399,476.64	3,791,509.37	1,986.5
Electrode 30	399,476.65	3,791,511.42	1,986.5

Appendix 2–2. Location of each direct-current resistivity electrode along line 1 within the Gran Quivira Unit of Salinas Pueblo Missions National Monument.—Continued

[Coordinate system: Universe Transverse Mercator Zone 13, North American Datum of 1983; elevation is in meters above the North American Vertical Datum of 1988]

Electrode identifier	Easting (meters)	Northing (meters)	Elevation (meters)
Electrode 31	399,476.62	3,791,513.37	1,986.5
Electrode 32	399,476.57	3,791,515.36	1,986.5
Electrode 33	399,476.58	3,791,517.39	1,986.5
Electrode 34	399,476.58	3,791,519.38	1,986.5
Electrode 35	399,476.61	3,791,521.37	1,986.5
Electrode 36	399,476.55	3,791,523.40	1,986.6
Electrode 37	399,476.37	3,791,525.37	1,986.5
Electrode 38	399,476.42	3,791,527.44	1,986.4
Electrode 39	399,476.52	3,791,529.33	1,986.4
Electrode 41	399,476.47	3,791,533.34	1,986.1
Electrode 42	399,476.50	3,791,535.29	1,985.7
Electrode 43	399,476.49	3,791,537.27	1,985.7
Electrode 44	399,476.37	3,791,539.27	1,986.2
Electrode 45	399,476.46	3,791,541.26	1,986.3
Electrode 46	399,476.47	3,791,543.25	1,986.3
Electrode 47	399,476.43	3,791,545.26	1,986.4
Electrode 48	399,476.42	3,791,547.32	1,986.3
Electrode 49	399,476.47	3,791,549.35	1,986.2
Electrode 50	399,476.55	3,791,551.27	1,986.5
Electrode 51	399,476.65	3,791,553.15	1,986.4
Electrode 52	399,476.53	3,791,555.27	1,987.4
Electrode 53	399,476.52	3,791,557.23	1,987.3
Electrode 54	399,476.52	3,791,559.16	1,987.2
Electrode 55	399,476.39	3,791,561.20	1,987.1
Electrode 56	399,476.37	3,791,563.10	1,987.2
Electrode 57	399,476.32	3,791,565.18	1,987.0
Electrode 58	399,476.17	3,791,567.16	1,986.7
Electrode 59	399,476.13	3,791,569.26	1,986.7
Electrode 60	399,476.04	3,791,571.12	1,986.2
Electrode 61	399,475.91	3,791,573.07	1,985.7

Appendix 2–2. Location of each direct-current resistivity electrode along line 1 within the Gran Quivira Unit of Salinas Pueblo Missions National Monument.—Continued

[Coordinate system: Universe Transverse Mercator Zone 13, North American Datum of 1983; elevation is in meters above the North American Vertical Datum of 1988]

Electrode identifier	Easting (meters)	Northing (meters)	Elevation (meters)
Electrode 62	399,475.82	3,791,575.15	1,985.4
Electrode 63	399,475.66	3,791,577.00	1,984.8
Electrode 64	399,475.51	3,791,579.07	1,984.7
Electrode 65	399,475.52	3,791,581.07	1,984.6
Electrode 66	399,475.56	3,791,583.03	1,984.4
Electrode 67	399,475.38	3,791,585.07	1,984.3
Electrode 68	399,475.40	3,791,587.03	1,984.2
Electrode 69	399,475.35	3,791,589.08	1,984.2
Electrode 70	399,475.28	3,791,591.05	1,984.2
Electrode 71	399,475.25	3,791,593.03	1,984.0
Electrode 72	399,475.23	3,791,595.04	1,983.8

Appendix 2–3. Location of each direct-current resistivity electrode along line 2 within the Gran Quivira Unit of Salinas Pueblo Missions National Monument.

[Coordinate system: Universal Transverse Mercator Zone 13, North American Datum of 1983; elevation is in meters above the North American Vertical Datum of 1988]

Electrode identifier	Easting (meters)	Northing (meters)	Elevation (meters)
Electrode 1	399,564.46	3,791,451.70	1978.1
Electrode 2	399,564.27	3,791,453.76	1978.2
Electrode 3	399,564.25	3,791,455.60	1978.6
Electrode 4	399,564.05	3,791,457.69	1978.9
Electrode 5	399,563.84	3,791,459.55	1979.1
Electrode 6	399,563.41	3,791,461.47	1979.3
Electrode 7	399,563.14	3,791,463.46	1979.5
Electrode 8	399,562.91	3,791,465.35	1979.8
Electrode 9	399,562.81	3,791,467.32	1980.1
Electrode 10	399,562.67	3,791,469.36	1980.3
Electrode 11	399,562.38	3,791,471.32	1980.7
Electrode 12	399,562.23	3,791,473.04	1981.0
Electrode 13	399,562.22	3,791,475.07	1981.4
Electrode 14	399,562.09	3,791,477.20	1981.7
Electrode 15	399,562.07	3,791,478.96	1982.1
Electrode 16	399,561.90	3,791,480.94	1982.3
Electrode 17	399,561.77	3,791,482.95	1982.6
Electrode 18	399,561.68	3,791,485.02	1982.8
Electrode 19	399,561.37	3,791,486.88	1983.2
Electrode 20	399,561.33	3,791,489.07	1983.2
Electrode 21	399,561.16	3,791,490.80	1983.4
Electrode 22	399,561.00	3,791,492.83	1983.7
Electrode 23	399,560.87	3,791,494.78	1984.1
Electrode 24	399,560.67	3,791,496.75	1984.2
Electrode 25	399,560.42	3,791,498.77	1984.3
Electrode 26	399,560.17	3,791,500.68	1984.4
Electrode 27	399,560.01	3,791,502.63	1984.9
Electrode 28	399,559.76	3,791,504.59	1985.5
Electrode 29	399,559.67	3,791,506.20	1986.4
Electrode 30	399,559.46	3,791,508.04	1987.2

Appendix 2–3. Location of each direct-current resistivity electrode along line 2 within the Gran Quivira Unit of Salinas Pueblo Missions National Monument.—Continued

[Coordinate system: Universal Transverse Mercator Zone 13, North American Datum of 1983; elevation is in meters above the North American Vertical Datum of 1988]

Electrode identifier	Easting (meters)	Northing (meters)	Elevation (meters)
Electrode 31	399,559.14	3,791,510.05	1987.4
Electrode 32	399,558.73	3,791,511.96	1987.8
Electrode 33	399,558.31	3,791,513.89	1987.7
Electrode 34	399,557.97	3,791,515.88	1987.8
Electrode 35	399,557.51	3,791,517.78	1987.6
Electrode 36	399,557.06	3,791,519.74	1988.0
Electrode 37	399,556.68	3,791,521.60	1987.5
Electrode 38	399,556.35	3,791,523.56	1987.5
Electrode 39	399,555.92	3,791,525.51	1987.6
Electrode 40	399,555.49	3,791,527.44	1987.7
Electrode 41	399,555.13	3,791,529.40	1987.8
Electrode 42	399,554.84	3,791,531.35	1988.1
Electrode 43	399,554.55	3,791,533.32	1988.3
Electrode 44	399,554.24	3,791,535.27	1988.6
Electrode 45	399,553.83	3,791,537.20	1988.7
Electrode 46	399,553.45	3,791,539.14	1988.8
Electrode 47	399,553.07	3,791,541.11	1988.8
Electrode 48	399,552.76	3,791,543.10	1988.8
Electrode 49	399,552.44	3,791,545.07	1988.7
Electrode 50	399,552.13	3,791,547.03	1988.7
Electrode 51	399,551.77	3,791,548.98	1988.6
Electrode 52	399,551.48	3,791,550.96	1988.5
Electrode 53	399,551.14	3,791,552.96	1988.5
Electrode 54	399,550.82	3,791,554.87	1988.1
Electrode 55	399,550.46	3,791,556.84	1988.0
Electrode 56	399,550.10	3,791,558.84	1987.9
Electrode 57	399,549.80	3,791,560.77	1987.8
Electrode 58	399,549.46	3,791,562.74	1987.6
Electrode 59	399,549.09	3,791,564.67	1987.4
Electrode 60	399,548.75	3,791,566.62	1987.2

Appendix 2–3. Location of each direct-current resistivity electrode along line 2 within the Gran Quivira Unit of Salinas Pueblo Missions National Monument.—Continued

[Coordinate system: Universal Transverse Mercator Zone 13, North American Datum of 1983; elevation is in meters above the North American Vertical Datum of 1988]

Electrode identifier	Easting (meters)	Northing (meters)	Elevation (meters)
Electrode 61	399,548.42	3,791,568.57	1987.1
Electrode 62	399,548.00	3,791,570.55	1987.0
Electrode 63	399,547.69	3,791,572.53	1986.8
Electrode 64	399,547.33	3,791,574.44	1986.6
Electrode 65	399,547.00	3,791,576.41	1986.5
Electrode 66	399,546.65	3,791,578.40	1986.3
Electrode 67	399,546.31	3,791,580.38	1986.3
Electrode 68	399,545.97	3,791,582.33	1986.3
Electrode 69	399,545.66	3,791,584.31	1986.2
Electrode 70	399,545.31	3,791,586.29	1986.0
Electrode 71	399,545.02	3,791,588.24	1985.8
Electrode 72	399,544.72	3,791,590.19	1985.6

Appendix 2–4. Location of each direct-current resistivity electrode along line 3 within the Gran Quivira Unit of Salinas Pueblo Missions National Monument.

[Coordinate system: Universal Transverse Mercator Zone 13, North American Datum of 1983; elevation is in meters above the North American Vertical Datum of 1988]

Electrode identifier	Easting (meters)	Northing (meters)	Elevation (meters)
Electrode 1	399,340.41	3,791,615.02	1,977.8
Electrode 2	399,344.76	3,791,613.75	1,977.8
Electrode 3	399,349.71	3,791,612.51	1,977.5
Electrode 4	399,354.44	3,791,611.42	1,977.1
Electrode 5	399,359.33	3,791,610.45	1,976.9
Electrode 6	399,364.19	3,791,609.40	1,976.9
Electrode 7	399,369.02	3,791,608.34	1,977.5
Electrode 8	399,373.91	3,791,607.20	1,977.7
Electrode 9	399,378.74	3,791,606.08	1,977.3
Electrode 10	399,383.62	3,791,604.99	1,977.2
Electrode 11	399,388.46	3,791,603.85	1,977.5
Electrode 12	399,393.28	3,791,602.66	1,977.6
Electrode 13	399,398.13	3,791,601.42	1,978.0
Electrode 14	399,402.94	3,791,600.29	1,978.9
Electrode 15	399,407.70	3,791,599.10	1,979.6
Electrode 16	399,412.60	3,791,597.91	1,980.0
Electrode 17	399,417.34	3,791,596.77	1,980.3
Electrode 18	399,422.21	3,791,595.55	1,980.8
Electrode 19	399,427.00	3,791,594.33	1,981.5
Electrode 20	399,431.82	3,791,593.08	1,982.0
Electrode 21	399,436.64	3,791,591.80	1,982.2
Electrode 22	399,441.74	3,791,590.42	1,982.8
Electrode 23	399,446.55	3,791,589.01	1,983.1
Electrode 24	399,451.27	3,791,587.48	1,983.4
Electrode 25	399,456.04	3,791,585.97	1,983.8
Electrode 26	399,460.88	3,791,584.42	1,984.1
Electrode 27	399,465.50	3,791,583.09	1,984.4
Electrode 28	399,470.34	3,791,581.65	1,984.2
Electrode 29	399,475.12	3,791,580.38	1,984.5
Electrode 30	399,479.87	3,791,579.07	1,984.6

Appendix 2–4. Location of each direct-current resistivity electrode along line 3 within the Gran Quivira Unit of Salinas Pueblo Missions National Monument.—Continued

[Coordinate system: Universal Transverse Mercator Zone 13, North American Datum of 1983; elevation is in meters above the North American Vertical Datum of 1988]

Electrode identifier	Easting (meters)	Northing (meters)	Elevation (meters)
Electrode 31	399,484.71	3,791,577.87	1,984.4
Electrode 32	399,489.42	3,791,576.41	1,984.5
Electrode 33	399,494.13	3,791,574.84	1,984.9
Electrode 34	399,498.84	3,791,573.01	1,985.6
Electrode 35	399,503.67	3,791,571.74	1,986.2
Electrode 36	399,508.22	3,791,570.31	1,987.2
Electrode 37	399,512.96	3,791,568.83	1,986.7
Electrode 38	399,517.70	3,791,567.48	1,986.6
Electrode 39	399,522.50	3,791,566.13	1,987.1
Electrode 40	399,527.32	3,791,564.98	1,987.3
Electrode 41	399,532.16	3,791,563.69	1,987.5
Electrode 42	399,537.14	3,791,562.30	1,987.6
Electrode 43	399,541.94	3,791,561.08	1,987.7
Electrode 44	399,546.79	3,791,559.84	1,987.7
Electrode 45	399,551.62	3,791,558.58	1,987.9
Electrode 46	399,556.42	3,791,557.51	1,988.3
Electrode 47	399,561.34	3,791,556.27	1,987.8
Electrode 48	399,566.09	3,791,554.64	1,987.8
Electrode 49	399,570.84	3,791,553.27	1,987.7
Electrode 50	399,575.64	3,791,552.06	1,987.7
Electrode 51	399,580.55	3,791,550.66	1,987.8
Electrode 52	399,585.25	3,791,549.40	1,987.5
Electrode 53	399,590.20	3,791,548.29	1,987.3
Electrode 54	399,595.06	3,791,547.23	1,987.9
Electrode 55	399,599.37	3,791,545.33	1,989.1
Electrode 56	399,603.92	3,791,543.71	1,988.9
Electrode 57	399,608.90	3,791,542.90	1,988.5
Electrode 58	399,613.78	3,791,542.12	1,989.0
Electrode 59	399,618.66	3,791,541.11	1,990.3
Electrode 60	399,623.08	3,791,539.84	1,990.4

Appendix 2–4. Location of each direct-current resistivity electrode along line 3 within the Gran Quivira Unit of Salinas Pueblo Missions National Monument.—Continued

[Coordinate system: Universal Transverse Mercator Zone 13, North American Datum of 1983; elevation is in meters above the North American Vertical Datum of 1988]

Electrode identifier	Easting (meters)	Northing (meters)	Elevation (meters)
Electrode 61	399,627.91	3,791,538.75	1,990.6
Electrode 62	399,632.87	3,791,537.31	1,990.3
Electrode 63	399,637.56	3,791,535.91	1,990.2
Electrode 64	399,642.26	3,791,534.24	1,989.6
Electrode 65	399,646.96	3,791,533.32	1,989.1
Electrode 66	399,651.84	3,791,532.26	1,988.9
Electrode 67	399,656.73	3,791,531.35	1,988.2
Electrode 68	399,661.46	3,791,529.89	1,987.4
Electrode 69	399,666.28	3,791,528.68	1,986.1
Electrode 70	399,671.14	3,791,527.44	1,985.5
Electrode 71	399,675.66	3,791,527.13	1,984.8
Electrode 72	399,680.03	3,791,525.04	1,983.9

Appendix 2–5. Location of each direct-current resistivity electrode on line 4 within the Gran Quivira Unit of Salinas Pueblo Missions National Monument.

[Coordinate system: Universal Transverse Mercator Zone 13, North American Datum of 1983; elevation is in meters above the North American Vertical Datum of 1988]

Electrode identifier	Easting (meters)	Northing (meters)	Elevation (meters)
Electrode 1	399,392.70	3,791,437.96	1,979.4
Electrode 2	399,396.55	3,791,440.42	1,979.6
Electrode 3	399,400.79	3,791,442.92	1,980.0
Electrode 4	399,405.12	3,791,445.55	1,980.5
Electrode 5	399,409.44	3,791,447.88	1,980.9
Electrode 6	399,413.86	3,791,450.03	1,981.7
Electrode 7	399,417.93	3,791,452.48	1,982.1
Electrode 8	399,422.61	3,791,455.07	1,982.4
Electrode 9	399,426.68	3,791,457.41	1,982.4
Electrode 10	399,431.07	3,791,459.78	1,982.4
Electrode 11	399,435.46	3,791,462.10	1,982.8
Electrode 12	399,439.83	3,791,464.51	1,983.1
Electrode 13	399,444.04	3,791,467.16	1,983.8
Electrode 14	399,448.38	3,791,469.19	1,984.5
Electrode 15	399,452.75	3,791,471.49	1,984.8
Electrode 16	399,457.03	3,791,474.06	1,985.1
Electrode 17	399,461.50	3,791,476.18	1,985.3
Electrode 18	399,465.82	3,791,478.73	1,985.4
Electrode 19	399,470.15	3,791,481.15	1,985.7
Electrode 20	399,474.41	3,791,483.73	1,985.9
Electrode 21	399,478.97	3,791,485.72	1,985.9
Electrode 22	399,483.29	3,791,488.26	1,985.9
Electrode 23	399,487.67	3,791,490.80	1,985.5
Electrode 24	399,491.89	3,791,493.23	1,985.3
Electrode 25	399,496.07	3,791,496.04	1,985.1
Electrode 26	399,499.68	3,791,499.51	1,985.1
Electrode 27	399,504.38	3,791,501.49	1,985.0
Electrode 28	399,508.72	3,791,503.86	1,985.6
Electrode 29	399,513.08	3,791,506.34	1,985.9
Electrode 30	399,517.50	3,791,508.62	1,985.9

Appendix 2–5. Location of each direct-current resistivity electrode on line 4 within the Gran Quivira Unit of Salinas Pueblo Missions National Monument.—Continued

[Coordinate system: Universal Transverse Mercator Zone 13, North American Datum of 1983; elevation is in meters above the North American Vertical Datum of 1988]

Electrode identifier	Easting (meters)	Northing (meters)	Elevation (meters)
Electrode 31	399,521.88	3,791,511.07	1,986.1
Electrode 32	399,526.25	3,791,513.44	1,987.3
Electrode 33	399,530.51	3,791,515.89	1,987.5
Electrode 34	399,534.91	3,791,518.25	1,987.9
Electrode 35	399,539.30	3,791,520.56	1,988.5
Electrode 36	399,543.82	3,791,522.75	1,988.2
Electrode 37	399,548.11	3,791,525.28	1,988.1
Electrode 38	399,552.44	3,791,527.93	1,988.2
Electrode 39	399,556.76	3,791,530.15	1,987.7
Electrode 40	399,561.10	3,791,532.46	1,987.7
Electrode 41	399,565.55	3,791,534.61	1,987.8
Electrode 42	399,569.95	3,791,537.10	1,987.1
Electrode 43	399,574.68	3,791,538.60	1,987.0
Electrode 44	399,578.79	3,791,541.70	1,987.5
Electrode 45	399,583.14	3,791,544.12	1,987.5
Electrode 46	399,587.63	3,791,546.37	1,987.3
Electrode 47	399,592.09	3,791,548.51	1,987.3
Electrode 48	399,596.68	3,791,550.66	1,986.7
Electrode 49	399,601.03	3,791,553.06	1,986.9
Electrode 50	399,605.20	3,791,555.46	1,988.3
Electrode 51	399,609.36	3,791,557.93	1,988.5
Electrode 52	399,613.86	3,791,560.27	1,988.5
Electrode 53	399,618.28	3,791,562.65	1,988.4
Electrode 54	399,622.47	3,791,564.68	1,986.7
Electrode 55	399,626.85	3,791,567.13	1,987.0
Electrode 56	399,631.28	3,791,569.31	1,987.0
Electrode 57	399,635.28	3,791,571.68	1,986.2
Electrode 58	399,639.61	3,791,574.13	1,986.2
Electrode 59	399,644.09	3,791,576.48	1,986.0
Electrode 60	399,648.54	3,791,578.72	1,985.9

Appendix 2–5. Location of each direct-current resistivity electrode on line 4 within the Gran Quivira Unit of Salinas Pueblo Missions National Monument.—Continued

[Coordinate system: Universal Transverse Mercator Zone 13, North American Datum of 1983; elevation is in meters above the North American Vertical Datum of 1988]

Electrode identifier	Easting (meters)	Northing (meters)	Elevation (meters)
Electrode 61	399,652.97	3,791,580.94	1,986.2
Electrode 62	399,657.33	3,791,583.28	1,986.1
Electrode 63	399,661.60	3,791,585.72	1,986.3
Electrode 64	399,665.80	3,791,588.22	1,986.5
Electrode 65	399,670.24	3,791,590.43	1,986.4
Electrode 66	399,674.87	3,791,592.82	1,986.5
Electrode 67	399,679.28	3,791,594.85	1,986.6
Electrode 68	399,683.50	3,791,597.55	1,986.6
Electrode 69	399,687.77	3,791,599.87	1,986.6
Electrode 70	399,692.31	3,791,602.32	1,986.5
Electrode 71	399,696.40	3,791,604.95	1,986.5
Electrode 72	399,700.77	3,791,607.13	1,986.6

Appendix 2–6. Location of each direct-current resistivity electrode of line 5 within the Gran Quivira Unit of Salinas Pueblo Missions National Monument.

[Coordinate system: Universal Transverse Mercator Zone 13, North American Datum of 1983; elevation is in meters above the North American Vertical Datum of 1988]

Electrode identifier	Easting (meters)	Northing (meters)	Elevation (meters)
Electrode 1	399,537.98	3,791,460.44	1,980.8
Electrode 2	399,538.00	3,791,462.33	1,981.1
Electrode 3	399,537.93	3,791,464.29	1,981.4
Electrode 4	399,538.04	3,791,466.36	1,981.5
Electrode 5	399,537.94	3,791,468.42	1,981.5
Electrode 6	399,537.91	3,791,470.38	1,981.7
Electrode 7	399,537.85	3,791,472.32	1,981.8
Electrode 8	399,537.87	3,791,474.21	1,982.0
Electrode 9	399,537.86	3,791,476.30	1,982.2
Electrode 10	399,537.85	3,791,478.27	1,982.4
Electrode 11	399,537.77	3,791,480.34	1,982.7
Electrode 12	399,537.83	3,791,482.20	1,982.9
Electrode 13	399,537.80	3,791,484.22	1,983.1
Electrode 14	399,537.88	3,791,486.16	1,983.3
Electrode 15	399,538.02	3,791,488.07	1,983.7
Electrode 16	399,538.08	3,791,490.13	1,984.1
Electrode 17	399,537.95	3,791,492.24	1,984.1
Electrode 18	399,537.95	3,791,494.00	1,984.2
Electrode 19	399,537.74	3,791,495.96	1,984.1
Electrode 20	399,537.85	3,791,497.97	1,984.3
Electrode 21	399,537.86	3,791,499.96	1,984.7
Electrode 22	399,537.82	3,791,502.05	1,985.3
Electrode 23	399,537.96	3,791,503.72	1,985.9
Electrode 24	399,537.77	3,791,505.91	1,986.5
Electrode 25	399,537.93	3,791,507.68	1,986.6
Electrode 26	399,537.95	3,791,509.70	1,987.1
Electrode 27	399,537.77	3,791,511.71	1,987.3
Electrode 28	399,537.35	3,791,513.76	1,987.3
Electrode 29	399,537.10	3,791,515.63	1,987.3
Electrode 30	399,537.13	3,791,517.75	1,987.5

Appendix 2–6. Location of each direct-current resistivity electrode of line 5 within the Gran Quivira Unit of Salinas Pueblo Missions National Monument.—Continued

[Coordinate system: Universal Transverse Mercator Zone 13, North American Datum of 1983; elevation is in meters above the North American Vertical Datum of 1988]

Electrode identifier	Easting (meters)	Northing (meters)	Elevation (meters)
Electrode 31	399,537.24	3,791,519.44	1,988.2
Electrode 32	399,537.32	3,791,521.47	1,988.6
Electrode 33	399,536.75	3,791,523.17	1,989.0
Electrode 34	399,536.82	3,791,525.08	1,989.4
Electrode 35	399,536.55	3,791,527.02	1,989.6
Electrode 36	399,536.32	3,791,529.12	1,989.8
Electrode 37	399,536.04	3,791,530.52	1,989.8
Electrode 38	399,535.74	3,791,532.93	1,990.2
Electrode 39	399,535.72	3,791,534.45	1,990.3
Electrode 41	399,534.85	3,791,538.54	1,990.1
Electrode 42	399,534.74	3,791,540.47	1,990.1
Electrode 43	399,534.34	3,791,542.43	1,989.7
Electrode 44	399,534.13	3,791,544.41	1,989.4
Electrode 45	399,534.21	3,791,546.47	1,989.3
Electrode 46	399,533.92	3,791,548.45	1,989.2
Electrode 47	399,533.58	3,791,550.35	1,989.1
Electrode 48	399,533.36	3,791,552.33	1,988.8
Electrode 49	399,533.24	3,791,554.30	1,988.6
Electrode 50	399,533.05	3,791,556.31	1,988.5
Electrode 51	399,532.79	3,791,558.25	1,988.3
Electrode 52	399,532.59	3,791,560.15	1,987.9
Electrode 53	399,532.39	3,791,562.16	1,987.5
Electrode 54	399,532.11	3,791,564.18	1,987.4
Electrode 55	399,531.89	3,791,566.14	1,987.3
Electrode 56	399,531.66	3,791,568.09	1,987.5
Electrode 57	399,531.48	3,791,569.93	1,987.8
Electrode 58	399,531.24	3,791,572.02	1,987.9
Electrode 59	399,531.13	3,791,573.88	1,988.4
Electrode 60	399,530.93	3,791,576.06	1,987.9
Electrode 61	399,530.85	3,791,577.84	1,987.5

Appendix 2–6. Location of each direct-current resistivity electrode of line 5 within the Gran Quivira Unit of Salinas Pueblo Missions National Monument.—Continued

[Coordinate system: Universal Transverse Mercator Zone 13, North American Datum of 1983; elevation is in meters above the North American Vertical Datum of 1988]

Electrode identifier	Easting (meters)	Northing (meters)	Elevation (meters)
Electrode 62	399,530.74	3,791,579.82	1,987.5
Electrode 63	399,530.49	3,791,581.81	1,987.7
Electrode 64	399,530.43	3,791,583.96	1,987.4
Electrode 65	399,530.21	3,791,585.77	1,987.1
Electrode 66	399,530.02	3,791,587.85	1,987.2
Electrode 67	399,529.89	3,791,589.76	1,986.7
Electrode 68	399,529.87	3,791,591.85	1,986.4
Electrode 69	399,529.47	3,791,593.76	1,986.0
Electrode 70	399,529.21	3,791,595.69	1,985.8
Electrode 71	399,529.29	3,791,597.67	1,985.5
Electrode 72	399,529.10	3,791,599.70	1,985.5

Appendix 2–7. Location of each direct-current resistivity electrode on line 6 near the Gran Quivira Unit of Salinas Pueblo Missions National Monument.

[Coordinate system: Universal Transverse Mercator Zone 13, North American Datum of 1983; elevation is in meters above the North American Vertical Datum of 1988]

Electrode identifier	Easting (meters)	Northing (meters)	Elevation (meters)
Electrode 1	398,552.92	3,791,600.53	1,946.3
Electrode 2	398,553.41	3,791,598.58	1,946.2
Electrode 3	398,553.81	3,791,596.68	1,946.2
Electrode 4	398,554.21	3,791,594.71	1,946.2
Electrode 5	398,554.67	3,791,592.64	1,946.2
Electrode 6	398,555.14	3,791,590.82	1,946.2
Electrode 7	398,555.52	3,791,588.86	1,946.2
Electrode 8	398,555.84	3,791,586.92	1,946.1
Electrode 9	398,556.15	3,791,584.80	1,946.2
Electrode 10	398,556.56	3,791,582.76	1,946.2
Electrode 11	398,556.94	3,791,580.97	1,946.2
Electrode 12	398,557.38	3,791,578.97	1,946.2
Electrode 13	398,557.83	3,791,577.02	1,946.2
Electrode 14	398,558.20	3,791,575.12	1,946.2
Electrode 15	398,558.70	3,791,573.17	1,946.2
Electrode 16	398,559.16	3,791,571.21	1,946.1
Electrode 17	398,559.63	3,791,569.28	1,946.3
Electrode 18	398,560.00	3,791,567.48	1,946.2
Electrode 19	398,560.45	3,791,565.54	1,946.2
Electrode 20	398,560.76	3,791,563.56	1,946.3
Electrode 21	398,561.16	3,791,561.64	1,946.4
Electrode 22	398,561.60	3,791,559.68	1,946.3
Electrode 23	398,562.17	3,791,557.65	1,946.3
Electrode 24	398,562.61	3,791,555.70	1,946.3
Electrode 25	398,563.02	3,791,553.76	1,946.4
Electrode 26	398,563.44	3,791,551.79	1,946.4
Electrode 27	398,563.90	3,791,549.84	1,946.6
Electrode 28	398,564.28	3,791,547.87	1,946.5
Electrode 29	398,564.74	3,791,545.99	1,946.5
Electrode 30	398,565.19	3,791,543.98	1,946.5

Appendix 2–7. Location of each direct-current resistivity electrode on line 6 near the Gran Quivira Unit of Salinas Pueblo Missions National Monument—Continued

[Coordinate system: Universal Transverse Mercator Zone 13, North American Datum of 1983; elevation is in meters above the North American Vertical Datum of 1988]

Electrode identifier	Easting (meters)	Northing (meters)	Elevation (meters)
Electrode 31	398,565.56	3,791,542.10	1,946.5
Electrode 32	398,565.94	3,791,540.10	1,946.4
Electrode 33	398,566.40	3,791,538.17	1,946.3
Electrode 34	398,566.71	3,791,536.15	1,946.3
Electrode 35	398,567.17	3,791,534.25	1,946.3
Electrode 36	398,567.63	3,791,532.35	1,946.3
Electrode 37	398,568.05	3,791,530.37	1,946.3
Electrode 38	398,568.46	3,791,528.43	1,946.3
Electrode 39	398,568.88	3,791,526.49	1,946.3
Electrode 41	398,569.67	3,791,522.58	1,946.3
Electrode 42	398,570.02	3,791,520.65	1,946.2
Electrode 43	398,570.48	3,791,518.72	1,946.2
Electrode 44	398,570.78	3,791,516.64	1,946.1
Electrode 45	398,571.22	3,791,514.73	1,946.1
Electrode 46	398,571.62	3,791,512.77	1,946.1
Electrode 47	398,572.00	3,791,510.81	1,946.1
Electrode 48	398,572.37	3,791,508.85	1,946.0
Electrode 49	398,572.90	3,791,506.97	1,946.0
Electrode 50	398,573.34	3,791,504.99	1,946.0
Electrode 51	398,573.75	3,791,503.07	1,945.9
Electrode 52	398,574.13	3,791,501.13	1,945.8
Electrode 53	398,574.59	3,791,499.13	1,945.7
Electrode 54	398,575.00	3,791,497.24	1,945.7
Electrode 55	398,575.36	3,791,495.22	1,945.8
Electrode 56	398,575.80	3,791,493.24	1,945.6
Electrode 57	398,576.18	3,791,491.27	1,945.6
Electrode 58	398,576.58	3,791,489.32	1,945.6
Electrode 59	398,577.07	3,791,487.44	1,945.5
Electrode 60	398,577.55	3,791,485.48	1,945.5
Electrode 61	398,577.96	3,791,483.58	1,945.5

Appendix 2–7. Location of each direct-current resistivity electrode on line 6 near the Gran Quivira Unit of Salinas Pueblo Missions National Monument.—Continued

[Coordinate system: Universal Transverse Mercator Zone 13, North American Datum of 1983; elevation is in meters above the North American Vertical Datum of 1988]

Electrode identifier	Easting (meters)	Northing (meters)	Elevation (meters)
Electrode 62	398,578.27	3,791,481.53	1,945.5
Electrode 63	398,578.76	3,791,479.66	1,945.5
Electrode 64	398,579.10	3,791,477.60	1,945.5
Electrode 65	398,579.73	3,791,475.86	1,945.4
Electrode 66	398,580.22	3,791,473.91	1,945.5
Electrode 67	398,580.75	3,791,471.93	1,945.4
Electrode 68	398,581.23	3,791,470.06	1,945.4
Electrode 69	398,581.66	3,791,468.05	1,945.4
Electrode 70	398,581.90	3,791,466.03	1,945.4
Electrode 71	398,582.19	3,791,464.08	1,945.5
Electrode 72	398,582.55	3,791,462.08	1,945.5

Appendix 2–8. Location of each direct-current resistivity electrode on line 7 within the Gran Quivira Unit of Salinas Pueblo Missions National Monument.

[Coordinate system: Universal Transverse Mercator Zone 13, North American Datum of 1983; elevation is in meters above the North American Vertical Datum of 1988]

Electrode identifier	Easting (meters)	Northing (meters)	Elevation (meters)
Electrode 1	399,557.26	3,791,336.40	1,969.0
Electrode 2	399,554.79	3,791,340.74	1,969.0
Electrode 3	399,552.24	3,791,345.12	1,969.2
Electrode 4	399,550.03	3,791,349.41	1,969.7
Electrode 5	399,547.52	3,791,353.74	1,970.4
Electrode 6	399,545.06	3,791,357.96	1,971.1
Electrode 7	399,542.36	3,791,362.20	1,971.4
Electrode 8	399,539.82	3,791,366.57	1,972.1
Electrode 9	399,537.65	3,791,370.90	1,972.9
Electrode 10	399,534.80	3,791,374.94	1,973.6
Electrode 11	399,532.22	3,791,378.97	1,974.3
Electrode 12	399,529.39	3,791,383.47	1,975.0
Electrode 13	399,526.94	3,791,387.43	1,975.6
Electrode 14	399,524.57	3,791,392.02	1,976.4
Electrode 15	399,522.29	3,791,396.40	1,977.2
Electrode 16	399,520.04	3,791,400.80	1,978.0
Electrode 17	399,517.40	3,791,404.90	1,978.8
Electrode 18	399,515.55	3,791,409.50	1,979.7
Electrode 19	399,513.04	3,791,413.78	1,980.3
Electrode 20	399,510.63	3,791,417.90	1,980.4
Electrode 21	399,507.84	3,791,422.07	1,980.4
Electrode 22	399,505.17	3,791,426.14	1,980.5
Electrode 23	399,502.46	3,791,430.44	1,980.7
Electrode 24	399,499.83	3,791,434.73	1,981.1
Electrode 25	399,497.20	3,791,438.68	1,981.8
Electrode 26	399,494.54	3,791,442.98	1,982.7
Electrode 27	399,491.59	3,791,446.78	1,983.8
Electrode 28	399,488.87	3,791,450.89	1,984.6
Electrode 29	399,486.16	3,791,454.99	1,985.1
Electrode 30	399,483.83	3,791,459.27	1,985.0

Appendix 2–8. Location of each direct-current resistivity electrode on line 7 within the Gran Quivira Unit of Salinas Pueblo Missions National Monument.—Continued

[Coordinate system: Universal Transverse Mercator Zone 13, North American Datum of 1983; elevation is in meters above the North American Vertical Datum of 1988]

Electrode identifier	Easting (meters)	Northing (meters)	Elevation (meters)
Electrode 31	399,481.50	3,791,463.74	1,986.0
Electrode 32	399,478.90	3,791,467.80	1,985.4
Electrode 33	399,476.27	3,791,471.98	1,985.5
Electrode 34	399,473.91	3,791,476.48	1,985.6
Electrode 35	399,471.52	3,791,480.89	1,985.6
Electrode 36	399,469.16	3,791,485.26	1,985.8
Electrode 37	399,466.98	3,791,489.71	1,985.8
Electrode 38	399,464.70	3,791,494.23	1,986.1
Electrode 39	399,462.23	3,791,498.59	1,986.2
Electrode 40	399,459.91	3,791,503.01	1,986.2
Electrode 41	399,457.41	3,791,507.31	1,986.2
Electrode 42	399,454.85	3,791,511.54	1,986.2
Electrode 43	399,452.36	3,791,515.92	1,986.0
Electrode 44	399,449.83	3,791,520.22	1,985.9
Electrode 45	399,447.50	3,791,524.58	1,985.1
Electrode 46	399,445.00	3,791,528.91	1,984.5
Electrode 47	399,442.62	3,791,533.11	1,984.1
Electrode 48	399,440.06	3,791,537.51	1,983.9
Electrode 49	399,437.41	3,791,541.70	1,983.8
Electrode 50	399,434.97	3,791,546.08	1,983.5
Electrode 51	399,432.50	3,791,550.38	1,983.2
Electrode 52	399,429.90	3,791,554.78	1,982.7
Electrode 53	399,427.40	3,791,558.94	1,982.3
Electrode 54	399,424.91	3,791,563.45	1,981.8
Electrode 55	399,422.18	3,791,567.72	1,981.5
Electrode 56	399,419.63	3,791,571.97	1,981.1
Electrode 57	399,416.91	3,791,576.10	1,981.3
Electrode 58	399,414.52	3,791,580.40	1,981.3
Electrode 59	399,412.57	3,791,584.94	1,980.6
Electrode 60	399,411.33	3,791,587.10	1,980.3

Appendix 2–8. Location of each direct-current resistivity electrode on line 7 within the Gran Quivira Unit of Salinas Pueblo Missions National Monument.—Continued

[Coordinate system: Universal Transverse Mercator Zone 13, North American Datum of 1983; elevation is in meters above the North American Vertical Datum of 1988]

Electrode identifier	Easting (meters)	Northing (meters)	Elevation (meters)
Electrode 61	399,410.08	3,791,589.27	1,980.0
Electrode 62	399,407.93	3,791,593.67	1,979.0
Electrode 63	399,405.68	3,791,598.13	1,978.5
Electrode 64	399,403.38	3,791,602.41	1,978.0
Electrode 65	399,399.22	3,791,611.34	1,977.4
Electrode 66	399,396.80	3,791,615.71	1,977.3
Electrode 67	399,394.40	3,791,620.14	1,977.4
Electrode 68	399,392.43	3,791,624.48	1,977.4
Electrode 69	399,390.64	3,791,629.29	1,977.2
Electrode 70	399,389.27	3,791,633.87	1,976.6
Electrode 71	399,387.03	3,791,638.42	1,975.9
Electrode 72	399,385.39	3,791,642.96	1,975.6

Appendix 2–9. Additional surveyed features within the Gran Quivira Unit of Salinas Pueblo Missions National Monument.

[Coordinate system: Universal Transverse Mercator Zone 13, North American Datum of 1983; elevation is in meters above the North American Vertical Datum of 1988]

Location description	Easting (meters)	Northing (meters)	Elevation (meters)
Approximate center of gypsum cave located on line 6	398,571.63	3,791,510.42	1,946.1
Benchmark: GM03-17	399,579.49	3,791,551.77	1,987.7
Benchmark: GM03-18	399,480.95	3,791,538.15	1,987.3
Benchmark: GM03-19	399,478.77	3,791,489.86	1,987.1
Center of pueblo room number 98	399,517.24	3,791,529.43	1,987.4
GEM-2 calibration point	399,351.93	3,791,621.95	1,976.2

Appendix 3. One-dimensional, layered-earth inversion models from time-domain electromagnetic data.

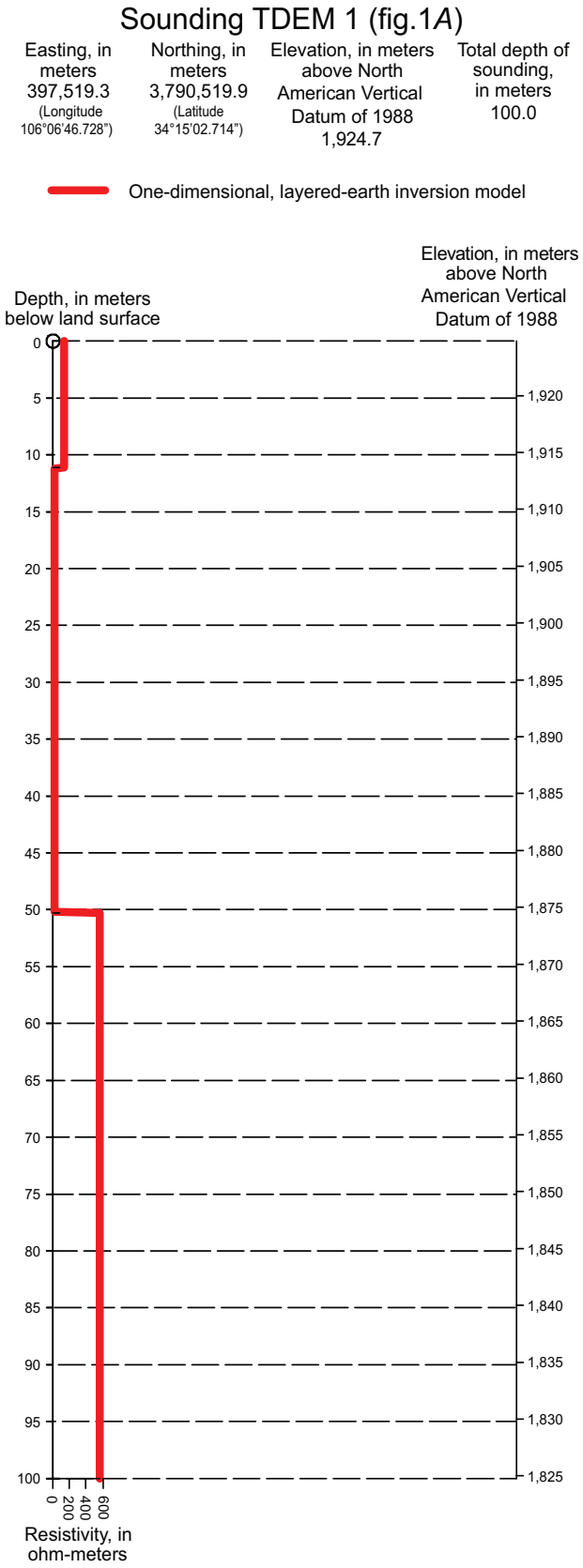

Sounding TDEM 2 (fig. 1*A*)

Easting, in meters	Northing, in meters	Elevation, in meters above North American Vertical Datum of 1988	Total depth of sounding, in meters
397,823.1 (Longitude 106°06'34.876")	3,790,573.6 (Latitude 34°15'04.565")	1,920.2	100.0

One-dimensional, layered-earth inversion model

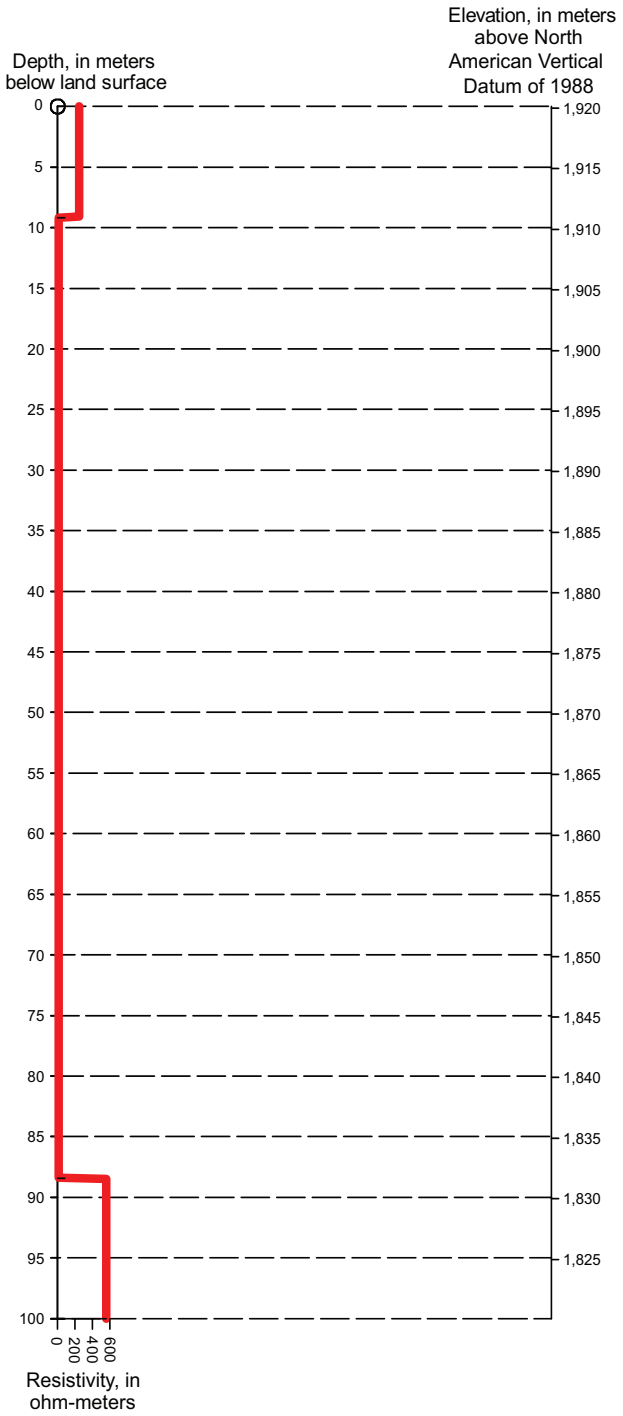

Sounding TDEM 3 (fig.1*A*)

Easting, in meters	Northing, in meters	Elevation, in meters above North American Vertical Datum of 1988	Total depth of sounding, in meters
398,261.4 (Longitude 106°06'17.766")	3,790,629.1 (Latitude 34°15'06.522")	1,919.3	100.0

One-dimensional, layered-earth inversion model

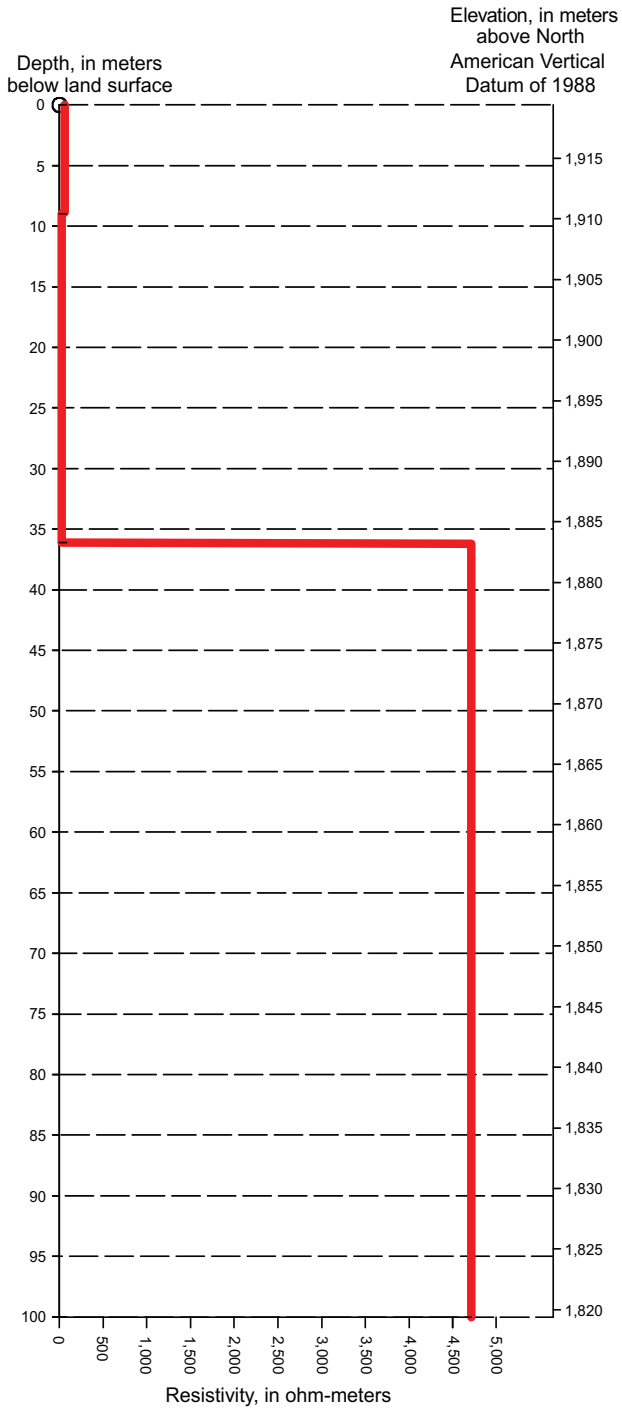

Sounding TDEM 4 (fig.1*A*)

Easting, in meters	Northing, in meters	Elevation, in meters above North American Vertical Datum of 1988	Total depth of sounding, in meters
399,095.4 (Longitude 106°05'45.371")	3,791,121.3 (Latitude 34°15'22.792")	1,950.3	100.0

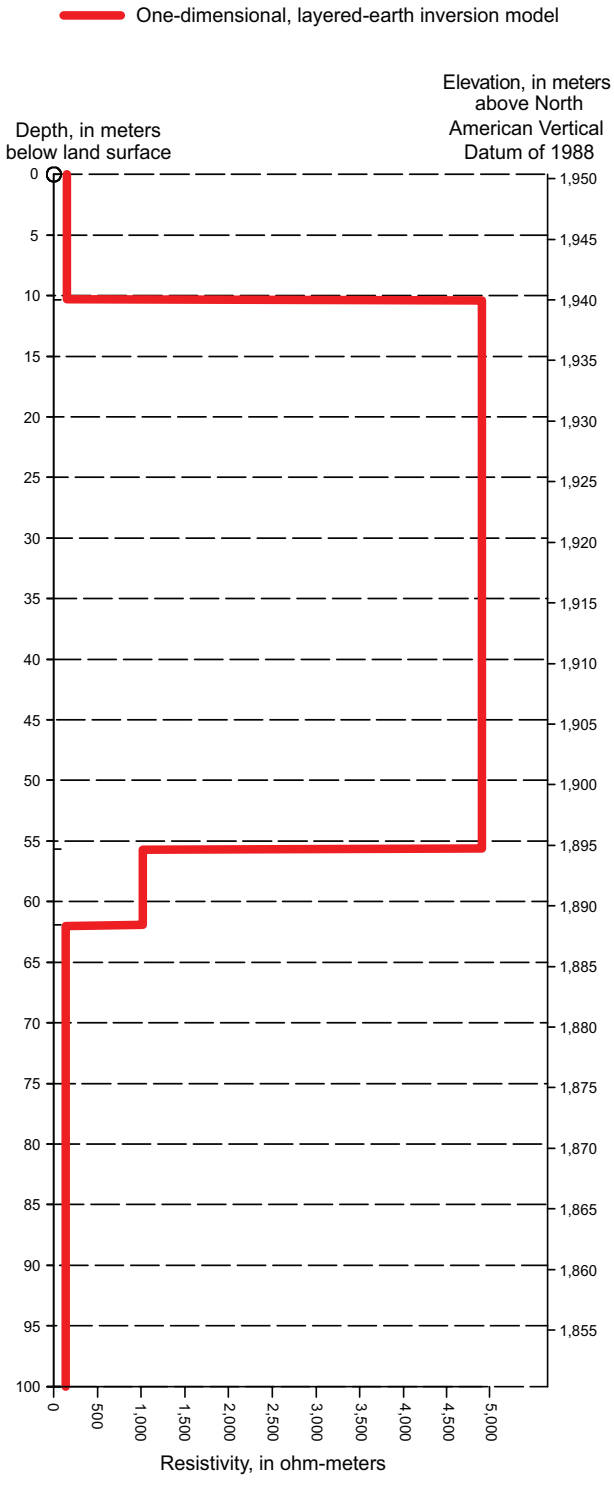

Sounding TDEM 5 (fig.1*A*)

Easting, in meters	Northing, in meters	Elevation, in meters above North American Vertical Datum of 1988	Total depth of sounding, in meters
399,450.7 (Longitude 106°05'31.654")	3,791,535.5 (Latitude 34°15'36.361")	1,985.5	100.0

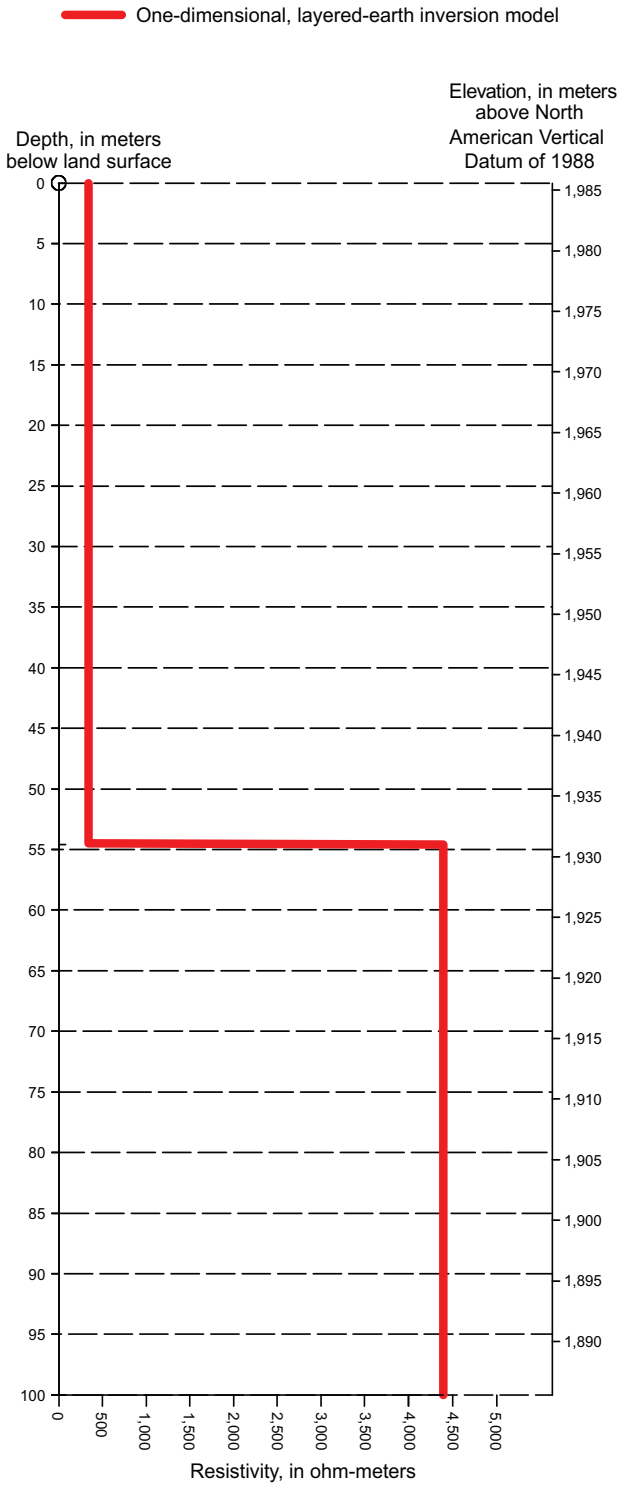

Appendix 4. Inversion parameters used for inversion of direct-current resistivity data and forward-model scenarios.

FINITE ELEMENT METHOD
LOGARITHM OF APPARENT RESISTIVITY
Half-cell model refinement
Combined Marquardt and Occam inversion used
Gauss-Newton optimization method
Initial damping factor is 0.1600
Minimum damping factor is 0.0150
Increase of damping factor with depth by a factor of 1.05
Vertical to horizontal flatness filter ratio is 1.0000
Number of nodes between adjacent electrodes is 2
Flatness filter type, include smoothing of model resistivity
Topographic modeling used
Full Jacobian matrix calculation
Robust data constraint used
    Cutoff factor for data constraint is 0.0500
Robust model constraint used
    Cutoff factor for model constraint is 0.0050
Reduce effect of side blocks - yes
Thickness of first model layer is 0.6920
Factor to increase model layer thickness with depth is 1.1000
Root mean square error convergence limit is 1.000 percent between iterations
Minimum change in root mean square error is 0.400
Root mean square error convergence limit is 1.000 percent overall
Total number of iterations is 5

Appendix 5–1.1. Sections from line 6 showing inversion results of the *(A)* field data and *(B)* synthetic forward-model data for the dipole-dipole array, as well as *(C)* the forward model itself for the scenario with voids.

(A)

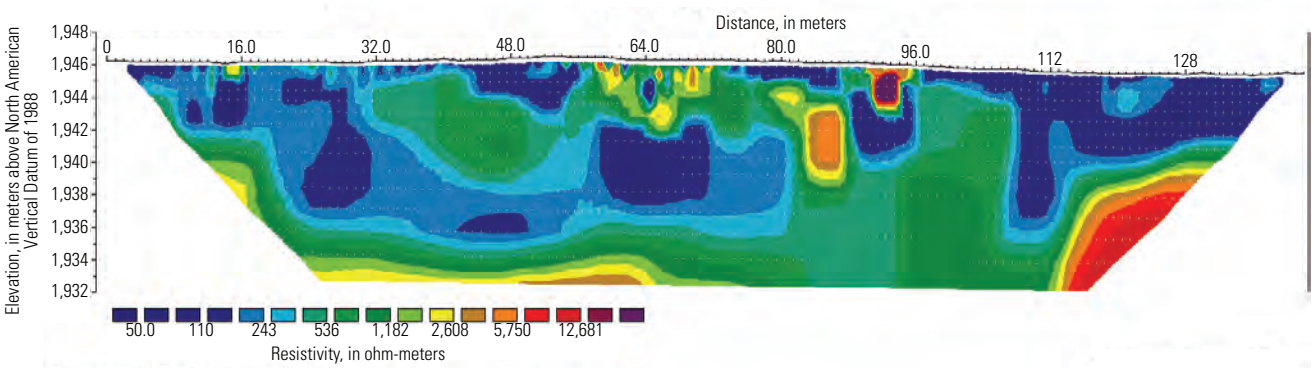

(B)

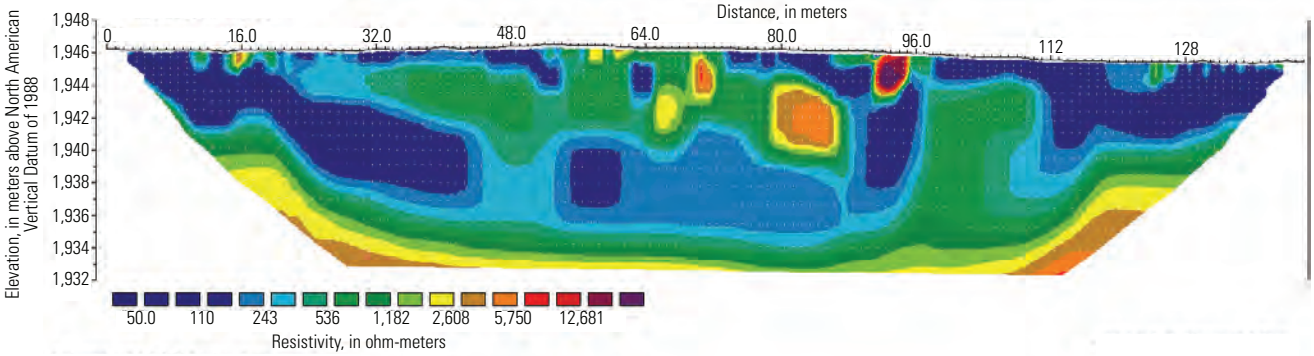

(C)

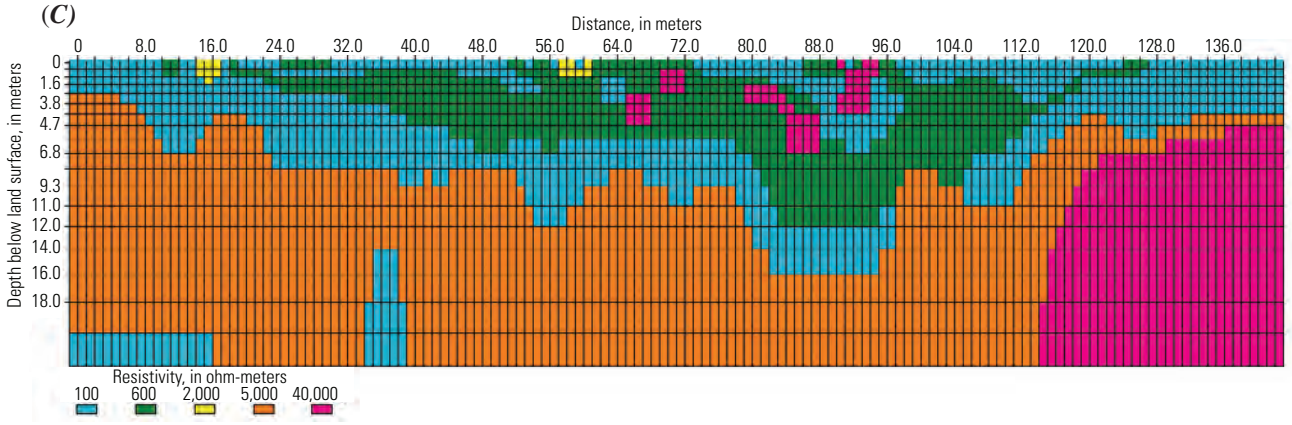

Appendix 5–1.2. Sections from line 6 showing inversion results of the *(A)* field data and *(B)* synthetic forward-model data for the dipole-dipole array, as well as *(C)* the forward model itself for the scenario without voids.

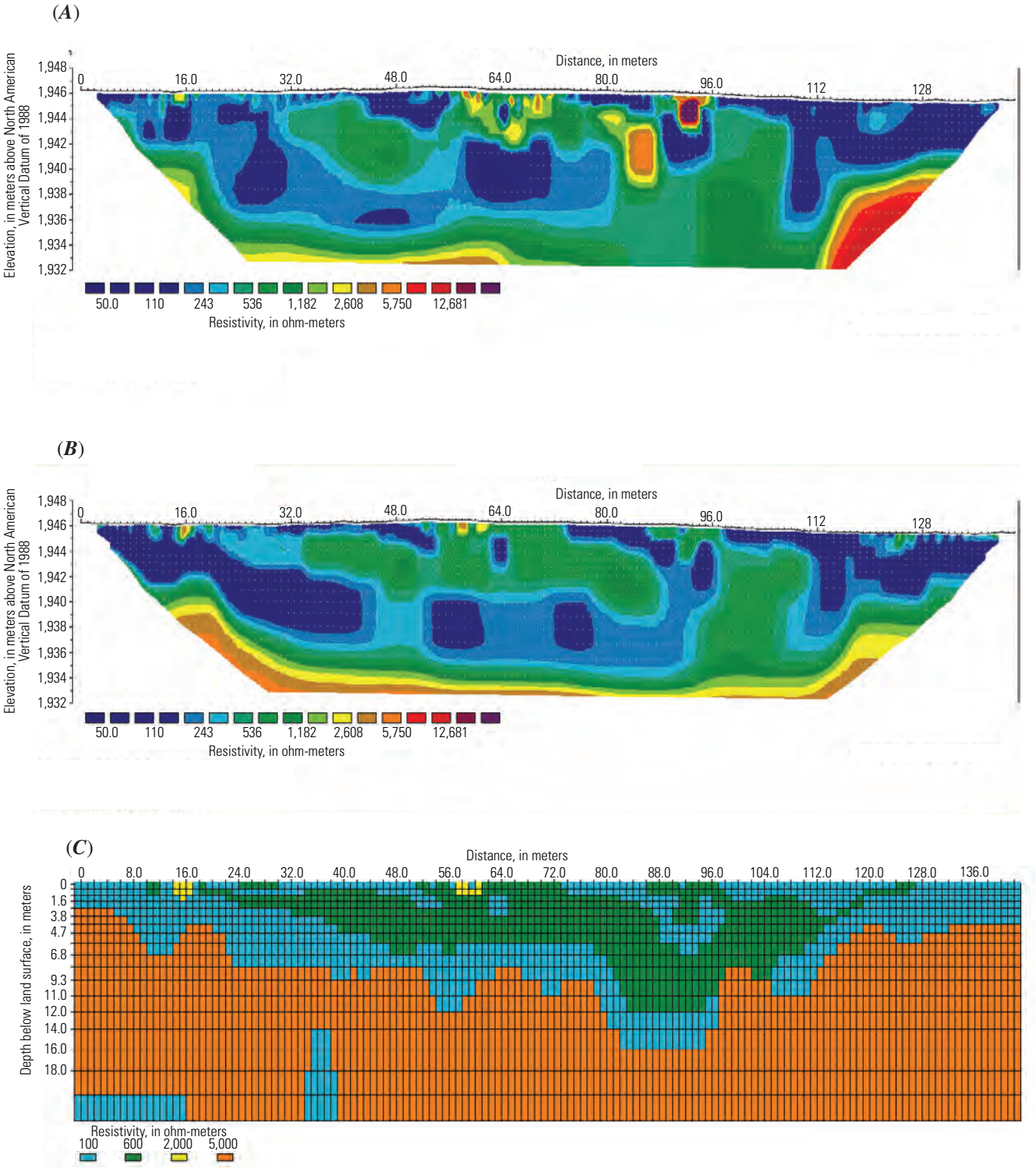

Appendix 5–1.3. Sections from line 6 showing inversion results of the *(A)* field data and *(B)* synthetic forward-model data for the Wenner-Schlumberger array, as well as *(C)* the forward model itself for the scenario with voids.

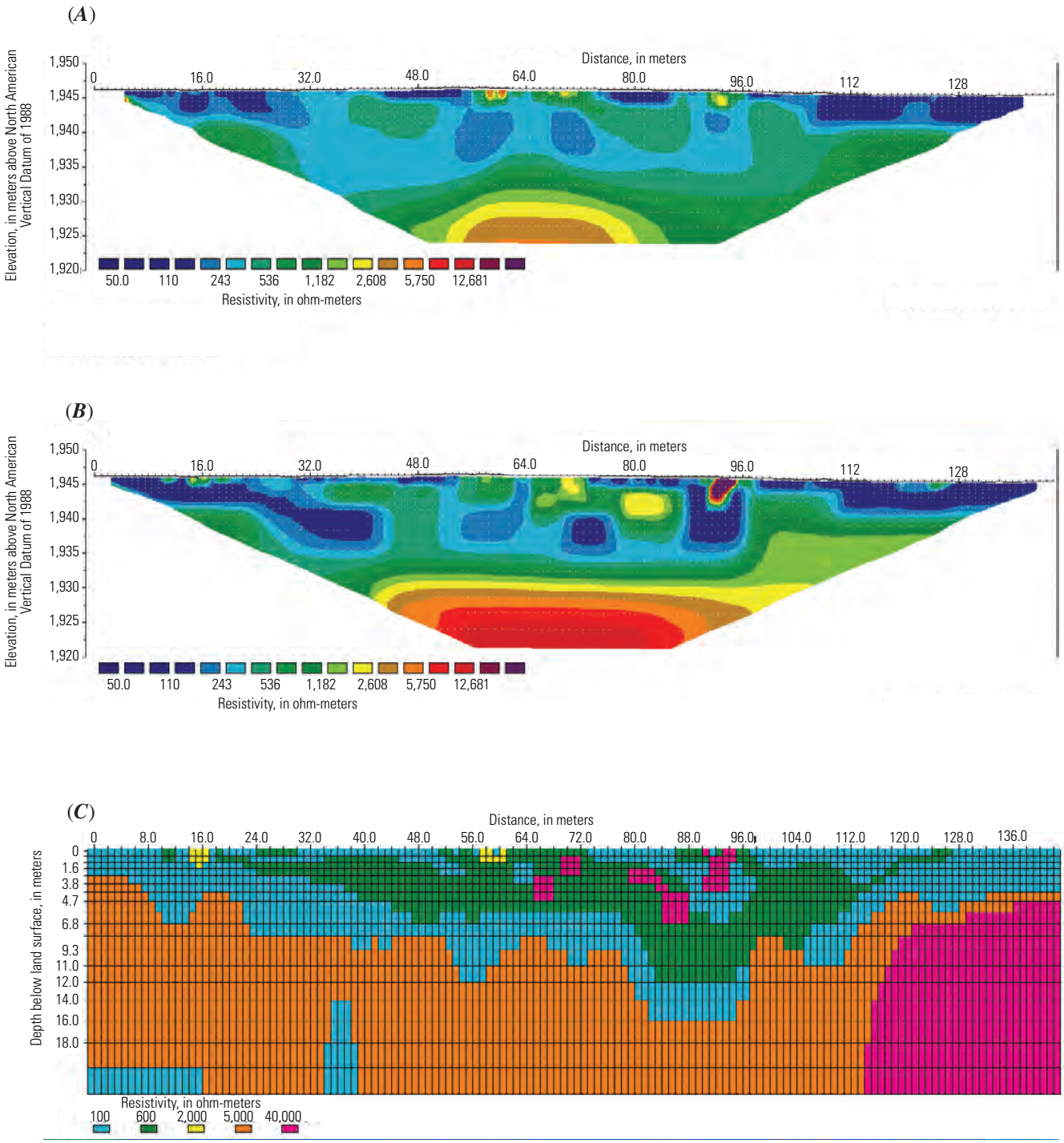

Appendix 5–1.4. Sections from line 6 showing inversion results of the *(A)* field data and *(B)* synthetic forward-model data for the Wenner-Schlumberger array, as well as *(C)* the forward model itself for the scenario without voids.

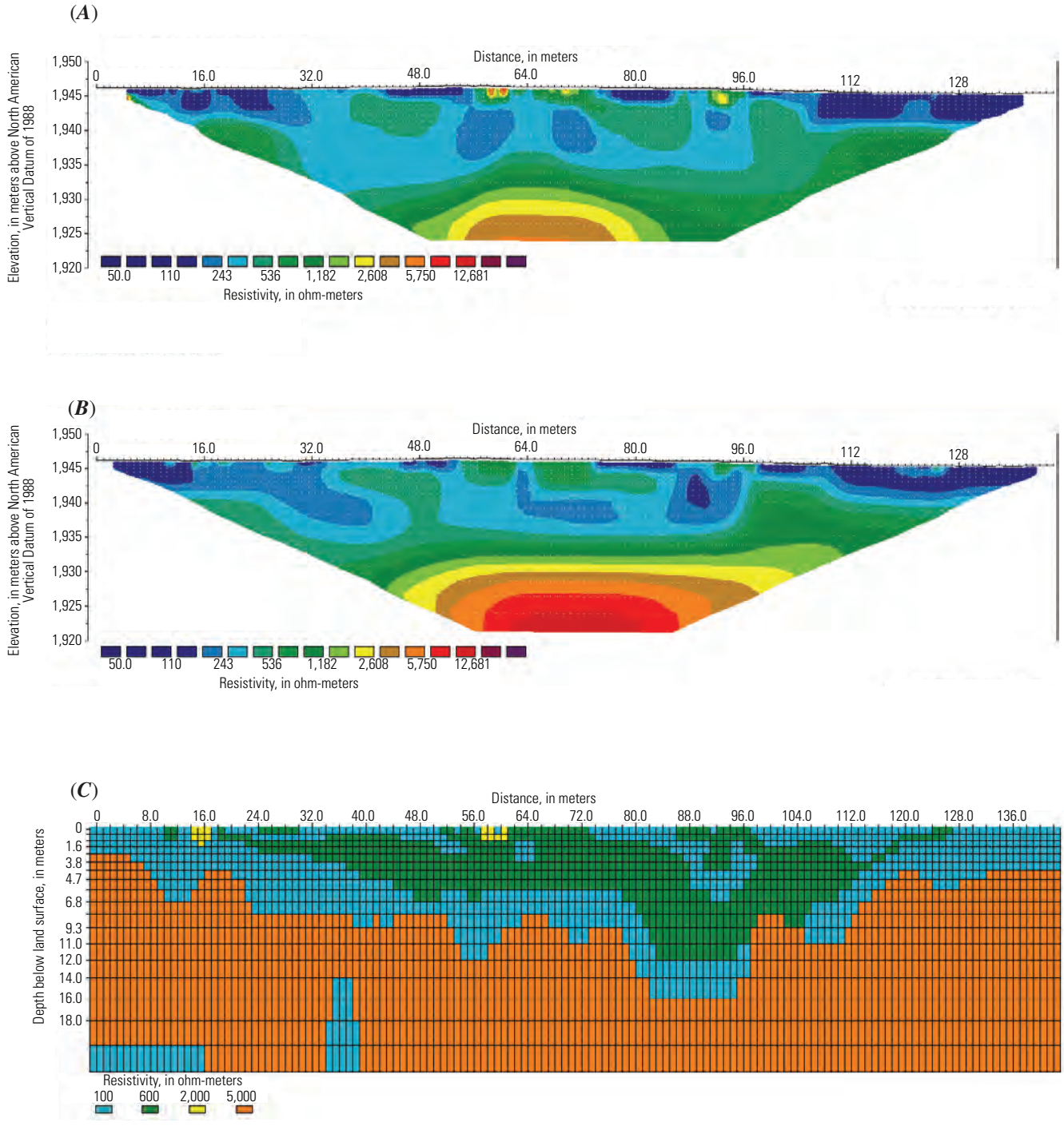

Appendix 5–1.5. Sections from line 6 showing inversion results of the *(A)* field data and *(B)* synthetic forward-model data for the high-resolution Wenner-Schlumberger array, as well as *(C)* the forward model itself for the scenario with voids.

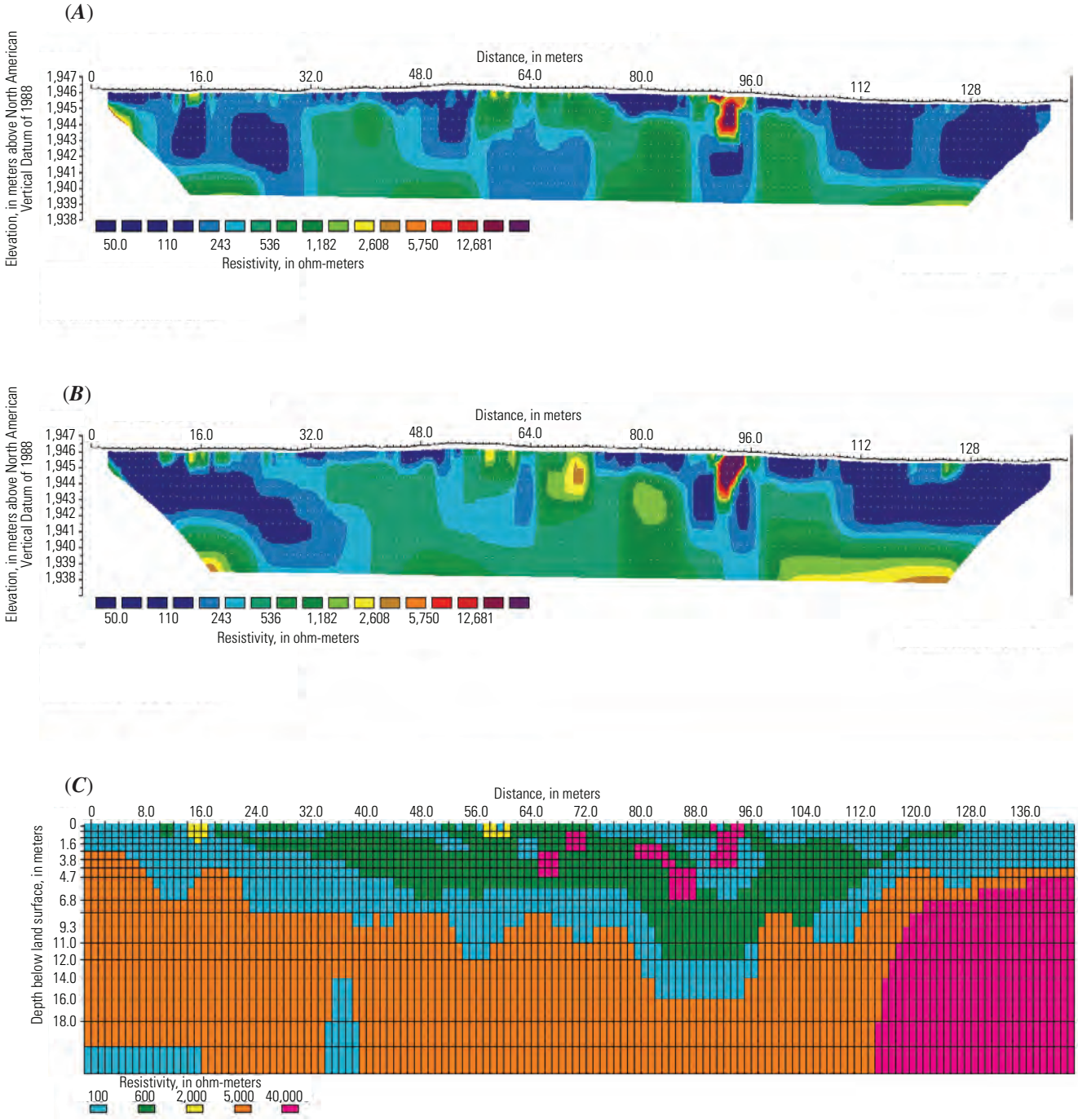

Appendix 5–1.6. Sections from line 6 showing inversion results of the *(A)* field data and *(B)* synthetic forward-model data for the high-resolution Wenner-Schlumberger array, as well as *(C)* the forward model itself for the scenario without voids.

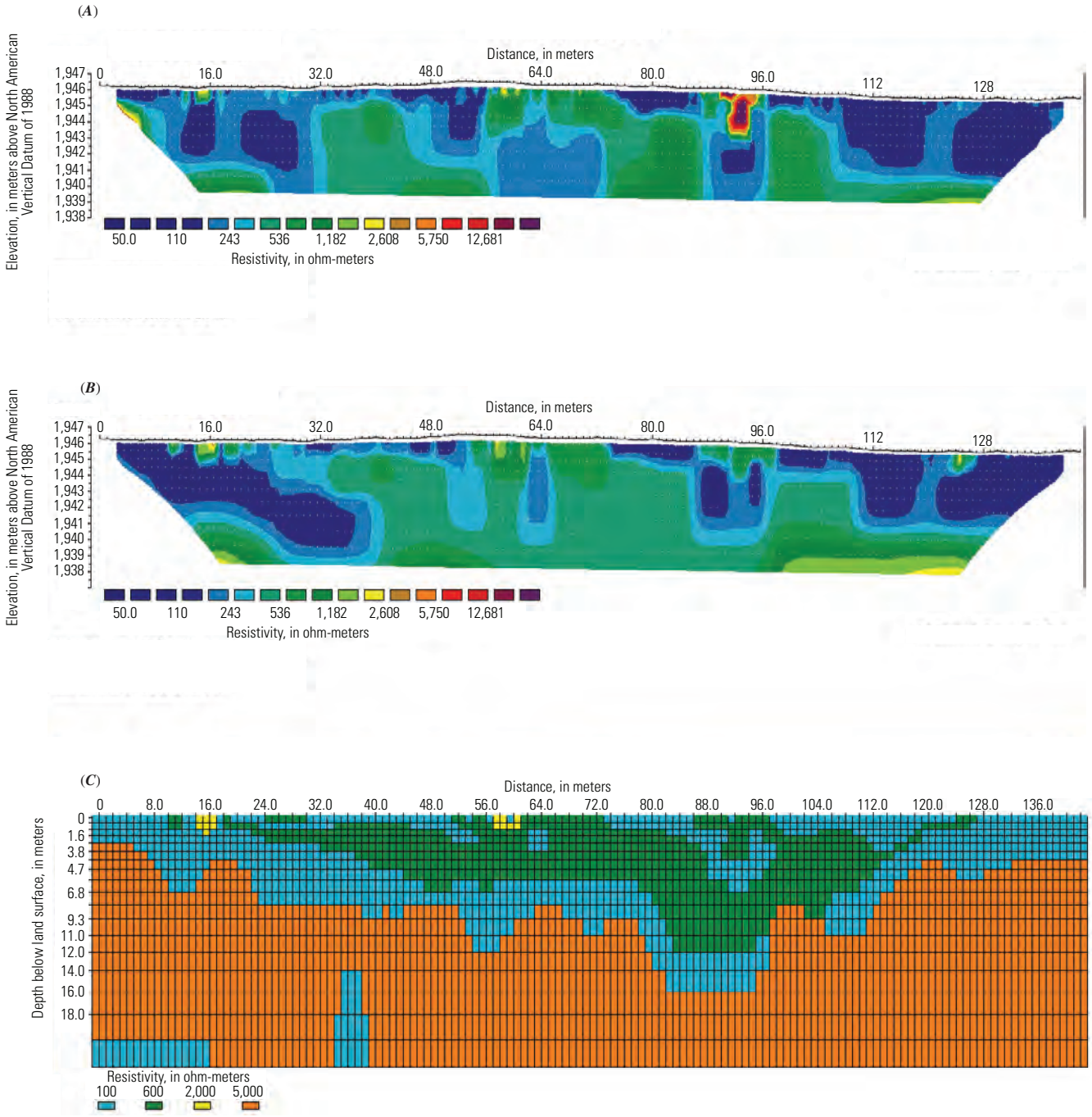

Appendix 5–2.1. Sections from line 3 showing inversion results of the *(A)* field data and *(B)* synthetic forward-model data for the dipole-dipole array, as well as *(C)* the forward model itself for the scenario with voids.

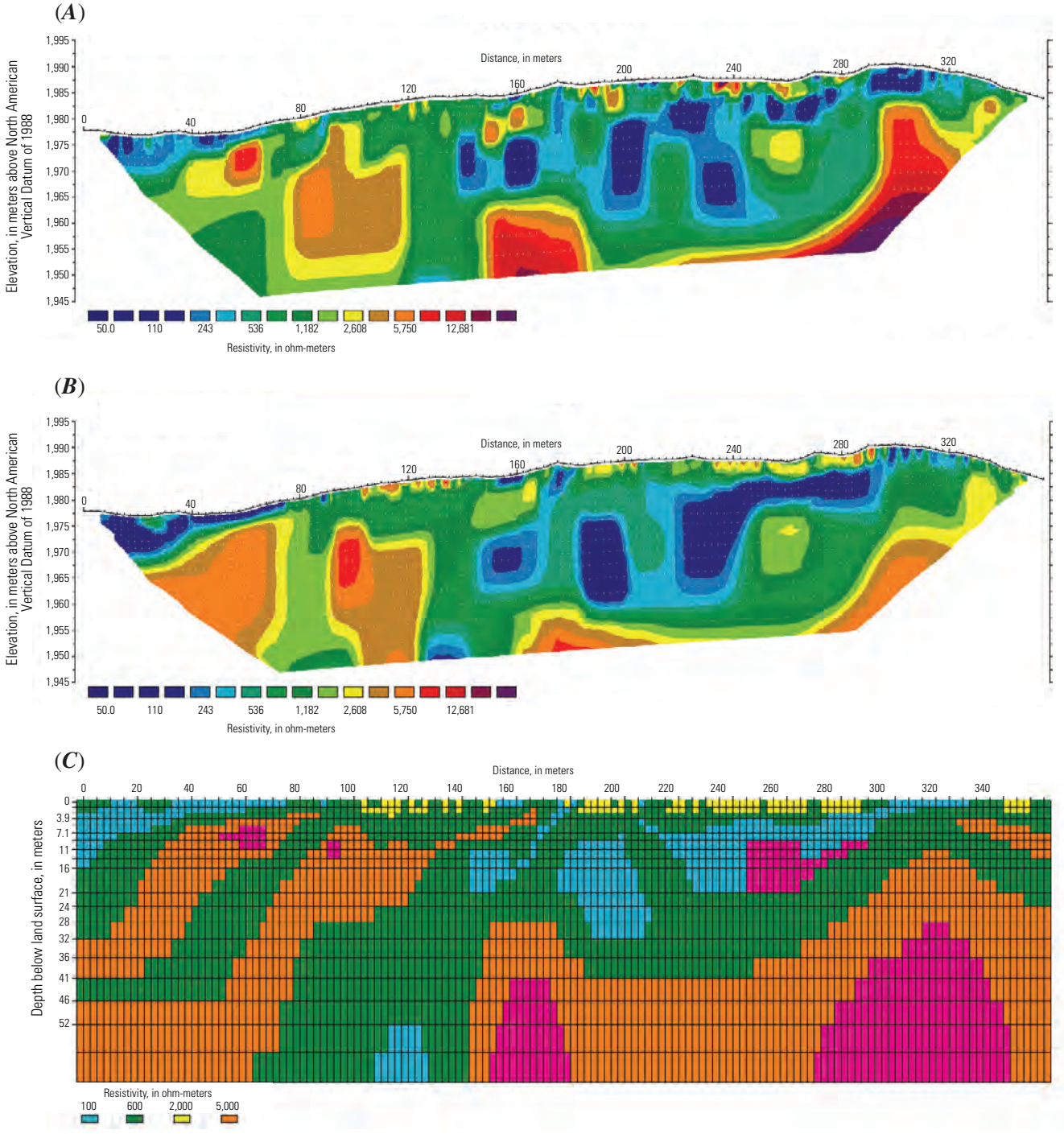

Appendix 5–2.2. Sections from line 3 showing inversion results of the *(A)* field data and *(B)* synthetic forward-model data for the dipole-dipole array, as well as *(C)* the forward model itself for the scenario without voids.

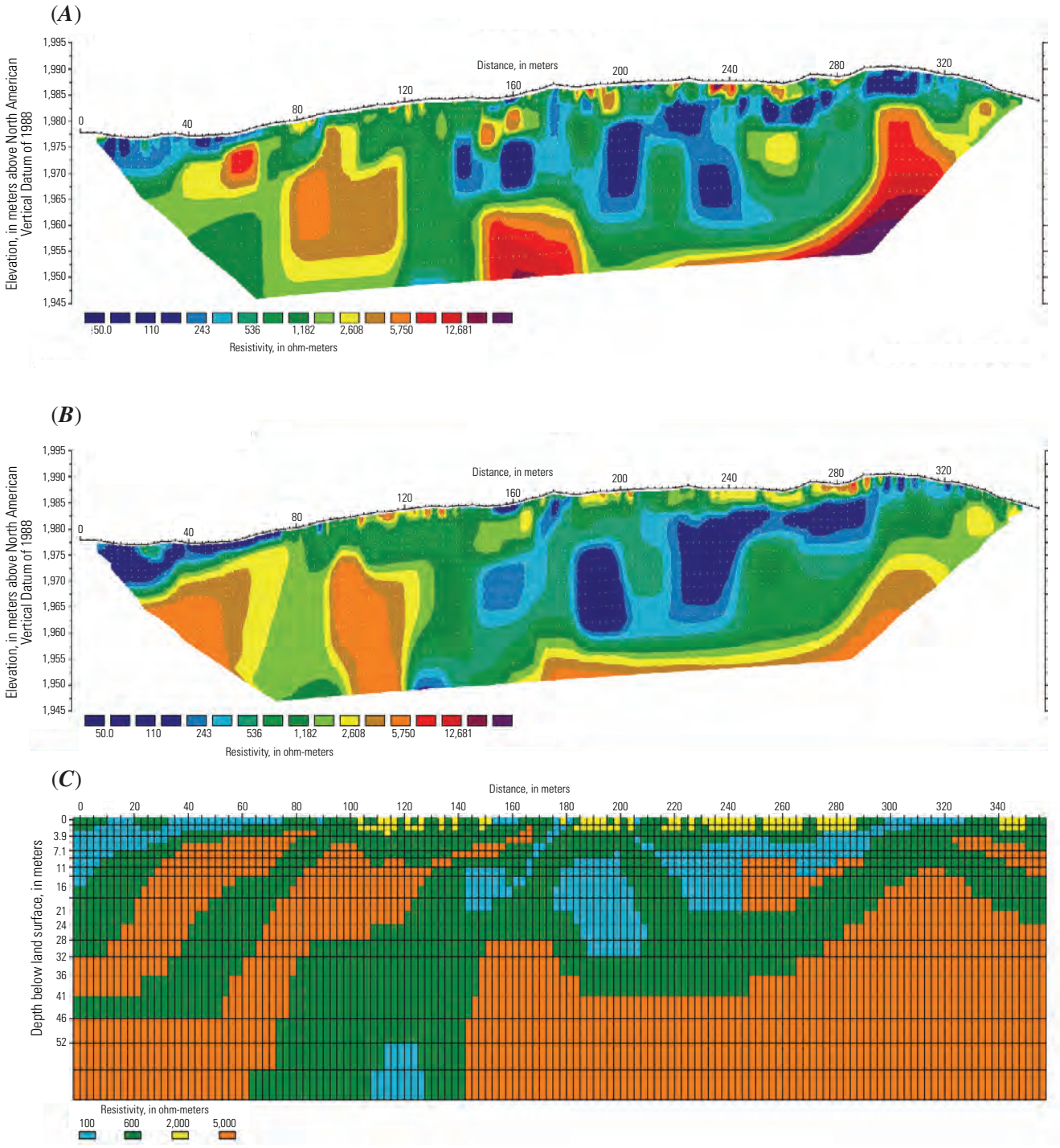

Appendix 5–2.3. Sections from line 3 showing inversion results of the *(A)* field data and *(B)* synthetic forward-model data for the Wenner-Schlumberger array, as well as *(C)* the forward model itself for the scenario with voids.

(*A*)

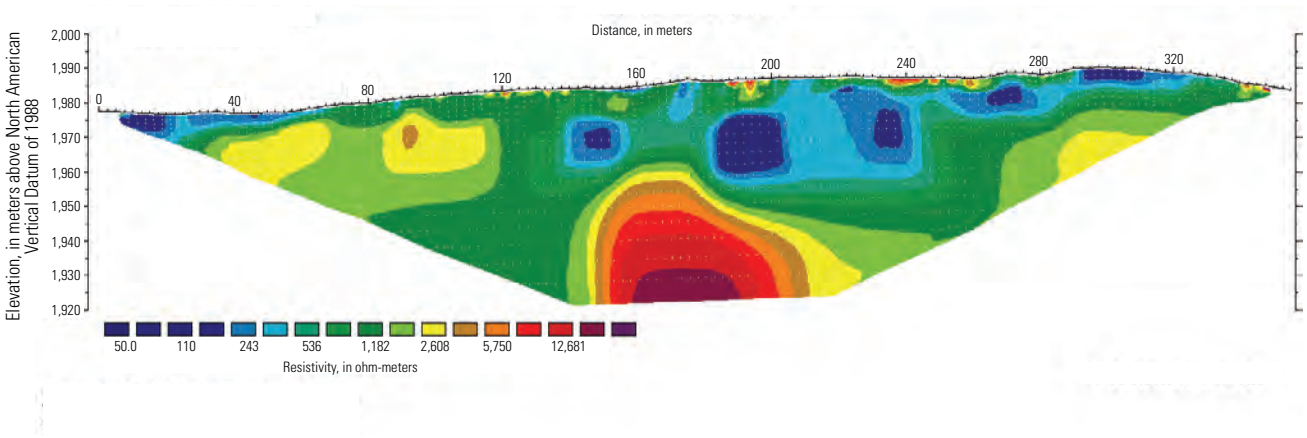

(*B*)

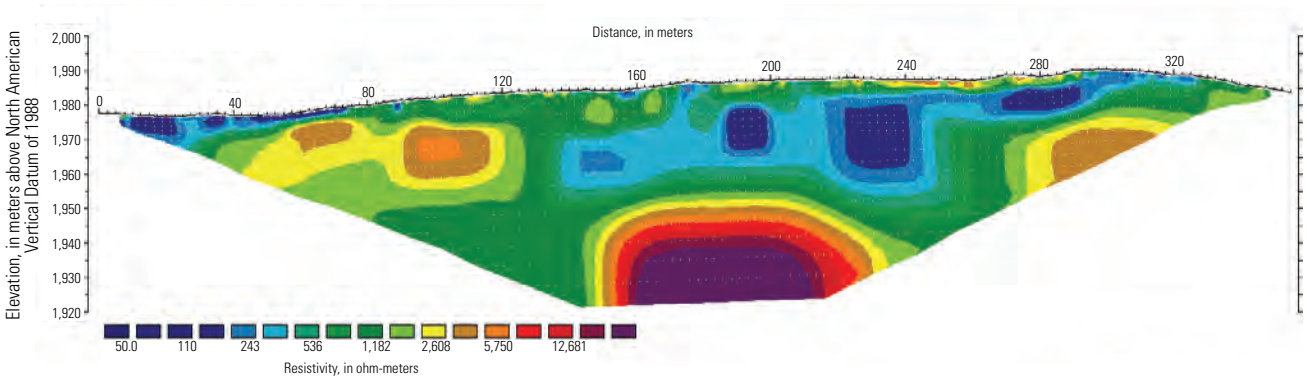

(*C*)

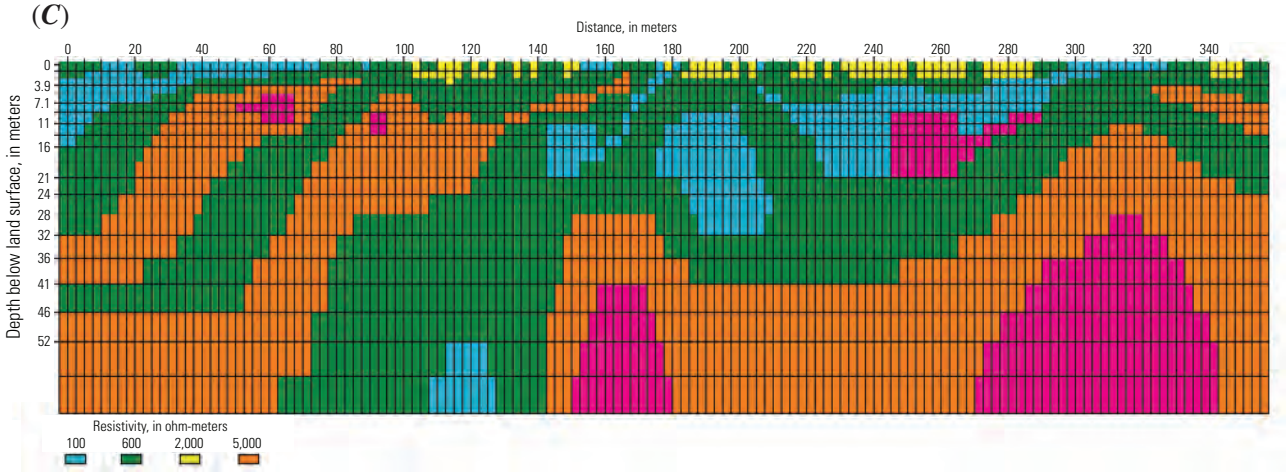

Appendix 5–2.4. Sections from line 3 showing inversion results of the *(A)* field data and *(B)* synthetic forward-model data for the Wenner-Schlumberger array, as well as *(C)* the forward model itself for the scenario without voids.

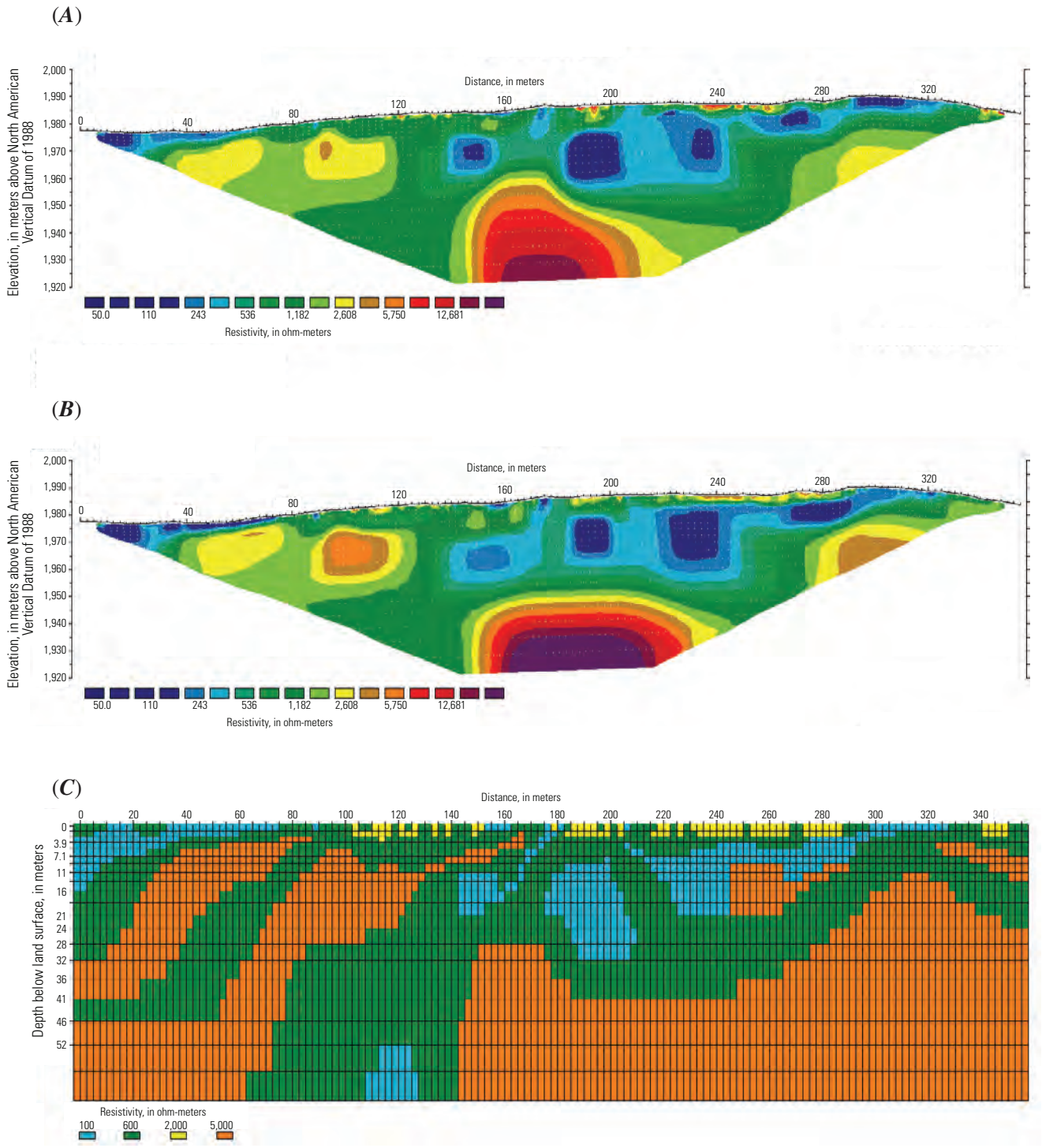

Appendix 5–3.1. Sections from line 4 showing inversion results of the *(A)* field data and *(B)* synthetic forward-model data for the dipole-dipole array, as well as *(C)* the forward model itself for the scenario with voids.

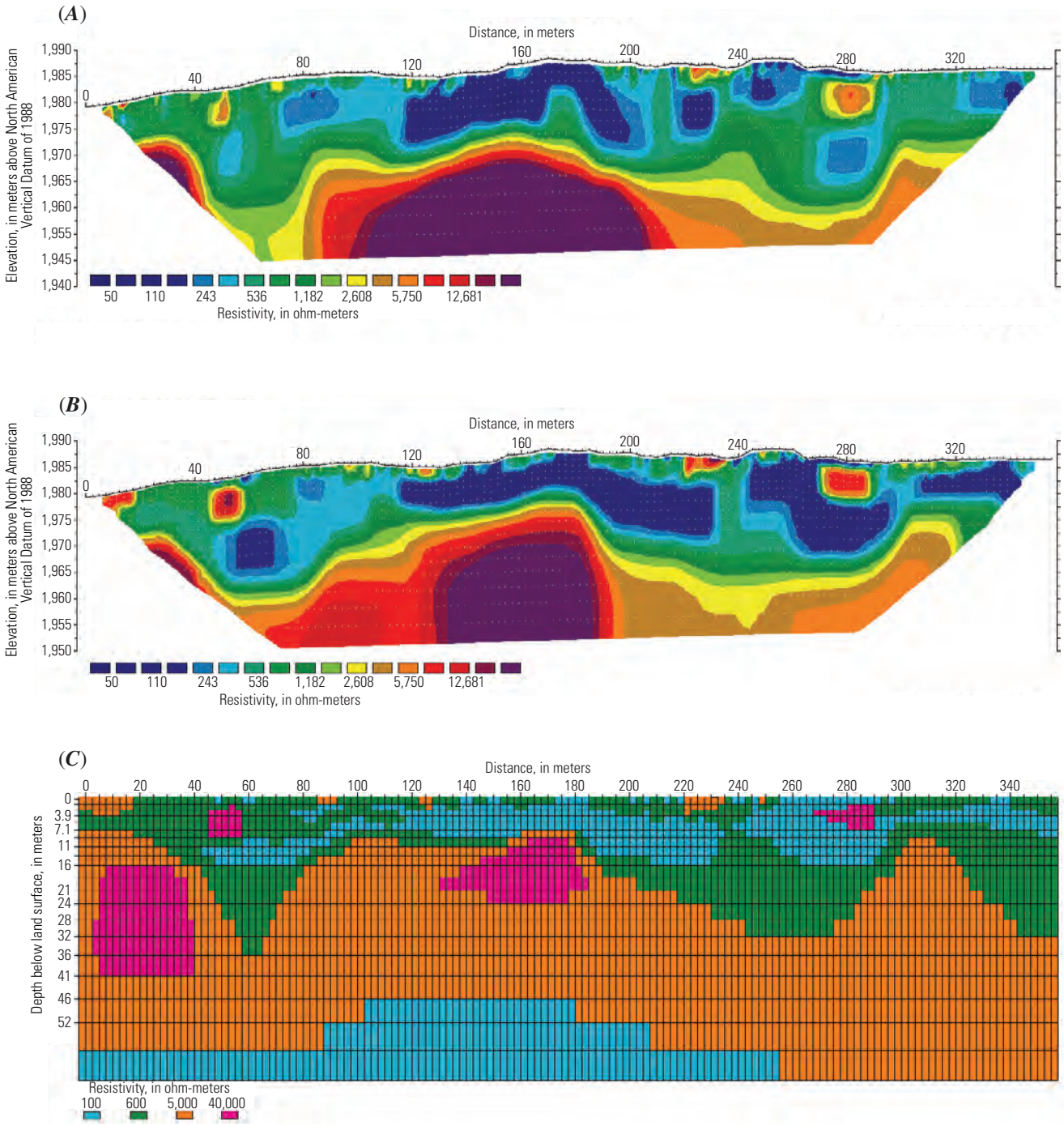

Appendix 5–3.2. Sections from line 4 showing inversion results of the *(A)* field data and *(B)* synthetic forward-model data for the dipole-dipole array, as well as *(C)* the forward model itself for the scenario without voids.

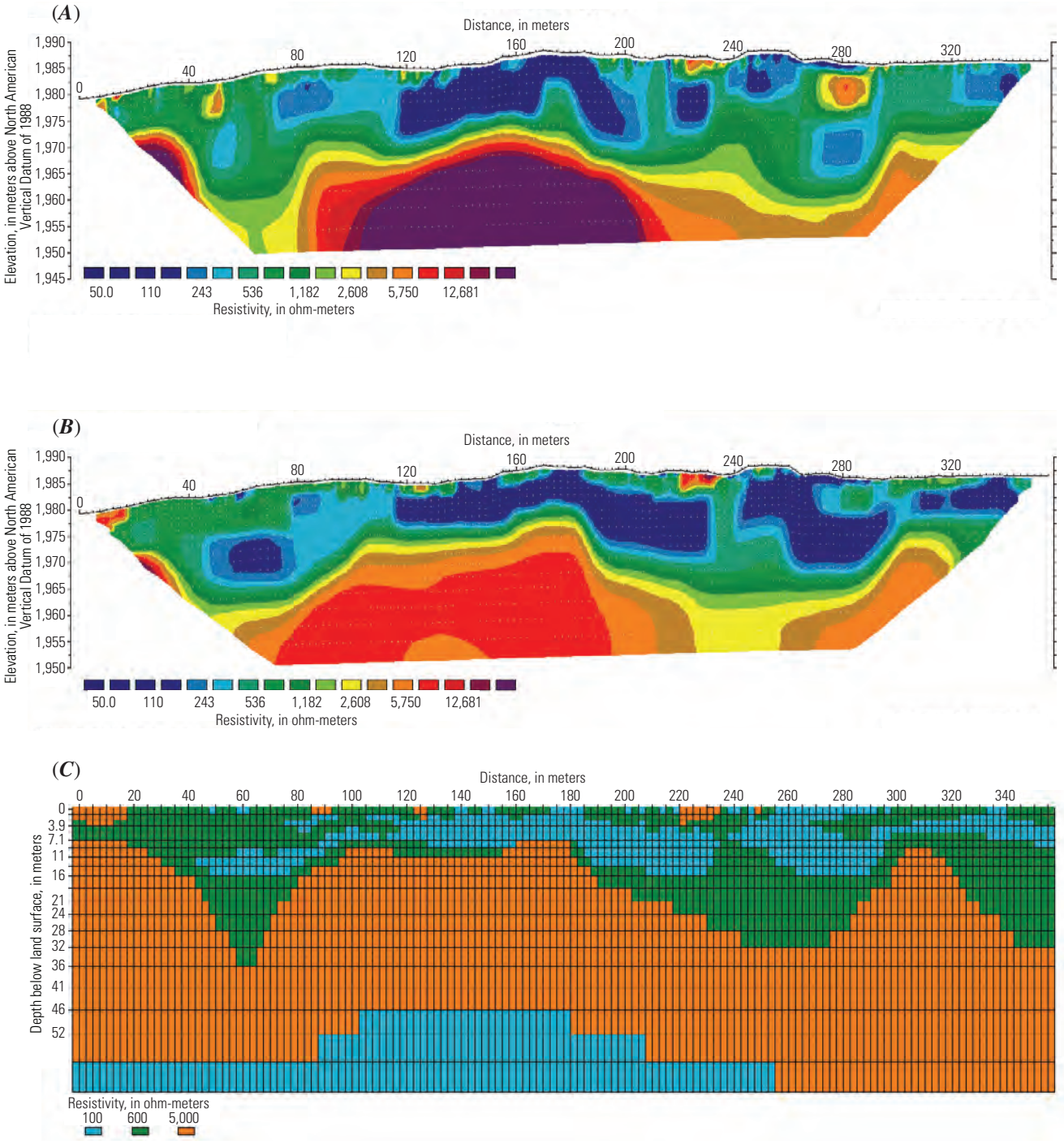

Appendix 5–3.3. Sections from line 4 showing inversion results of the *(A)* field data and *(B)* synthetic forward-model data for the Wenner-Schlumberger array, as well as *(C)* the forward model itself for the scenario with voids.

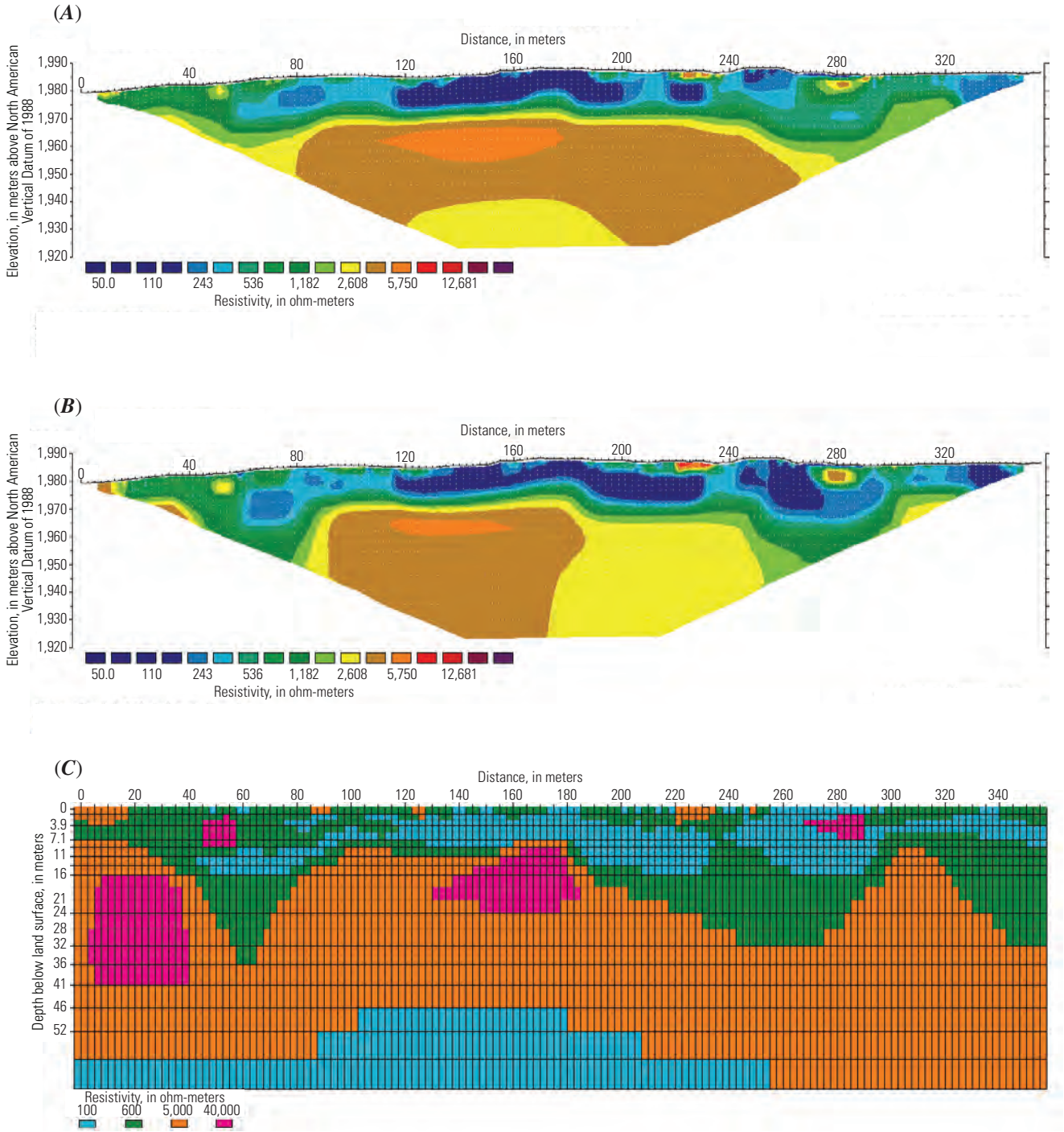

Appendix 5–3.4. Sections from line 4 showing inversion results of the *(A)* field data and *(B)* synthetic forward-model data for the Wenner-Schlumberger array, as well as *(C)* the forward model itself for the scenario without voids.

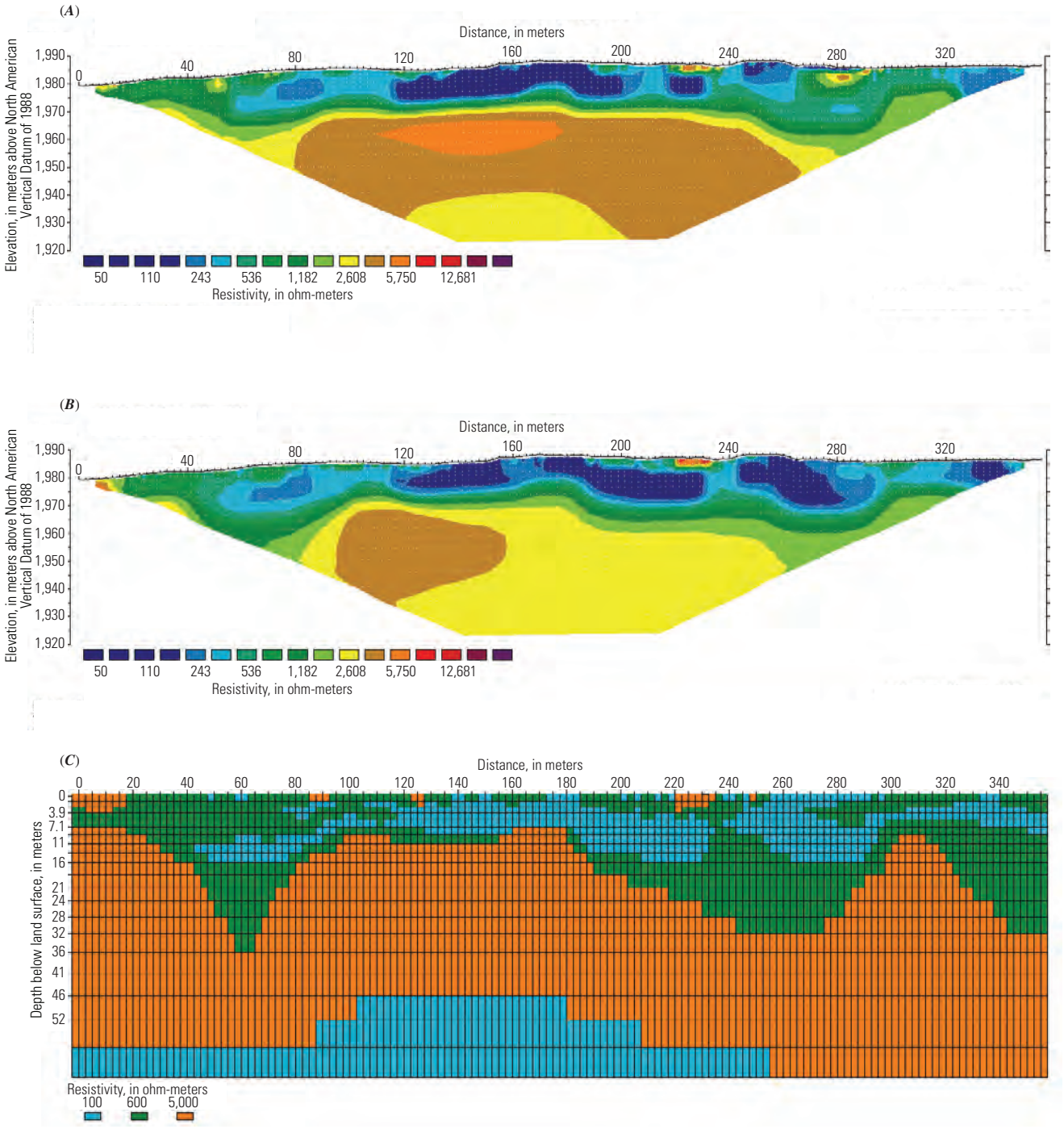

Appendix 5–4.1. Sections from line 7 showing inversion results of the *(A)* field data and *(B)* synthetic forward-model data for the dipole-dipole array, as well as *(C)* the forward model itself for the scenario with voids.

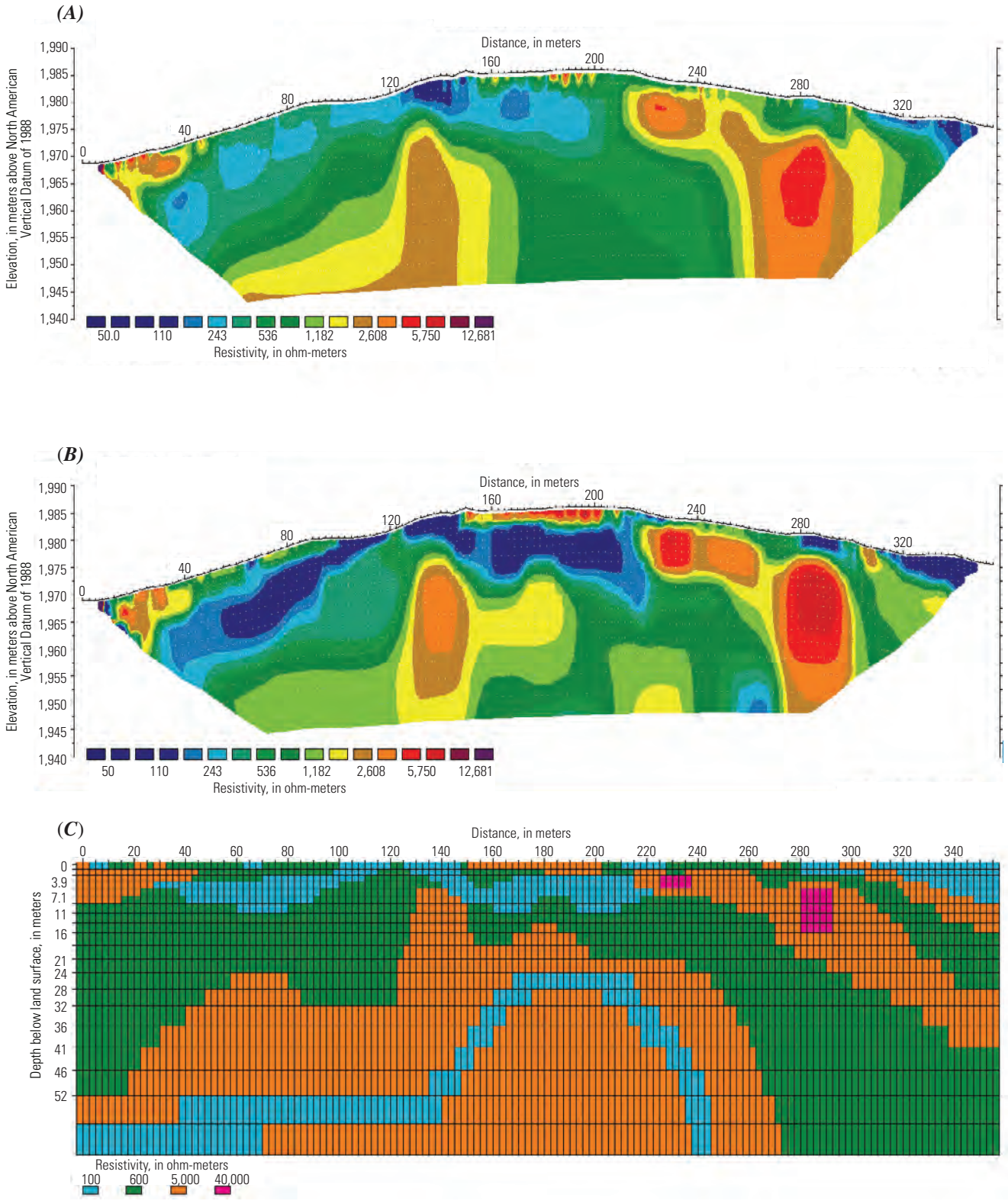

Appendix 5–4.2. Sections from line 7 showing inversion results of the *(A)* field data and *(B)* synthetic forward-model data for the dipole-dipole array, as well as *(C)* the forward model itself for the scenario without voids.

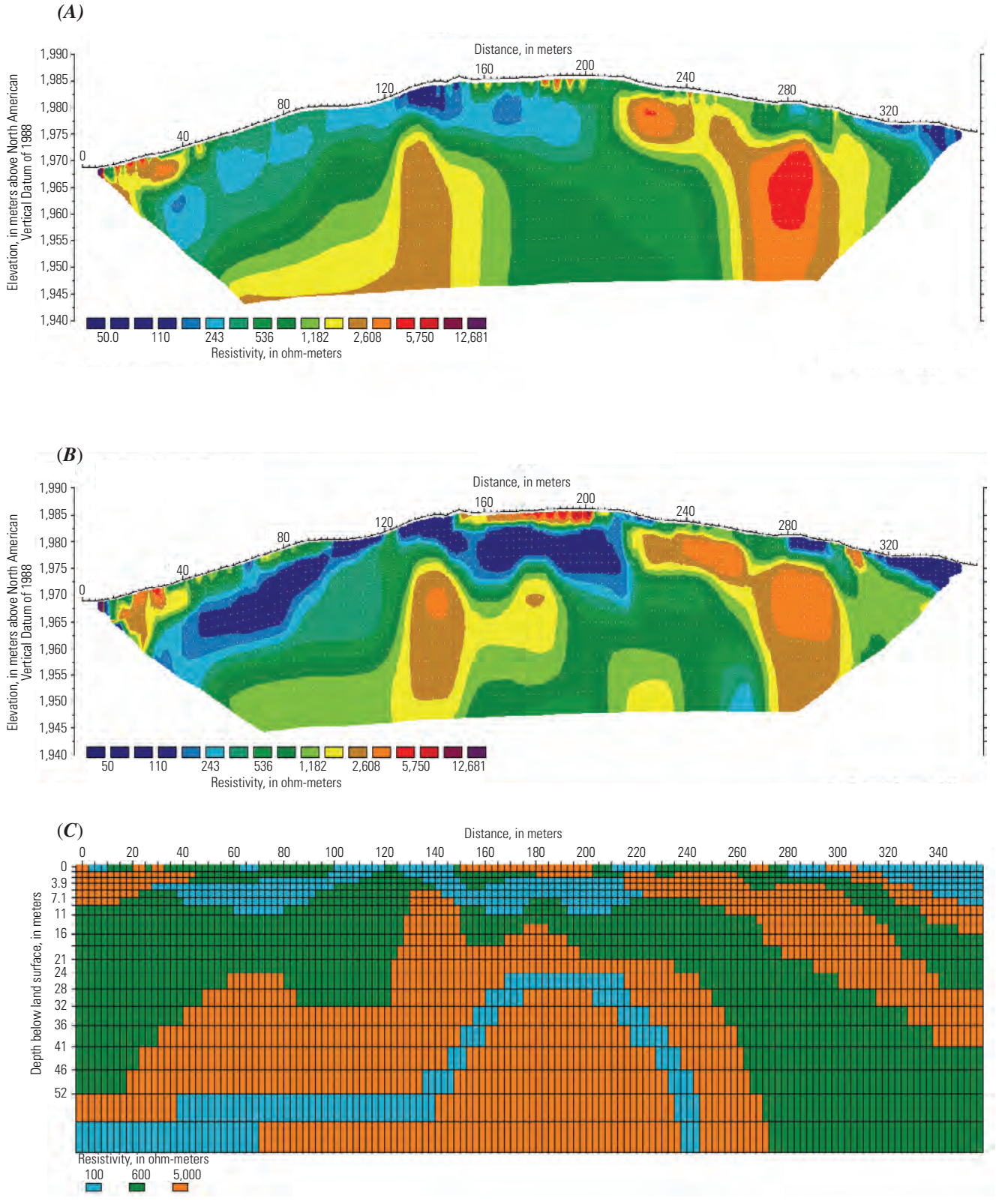

Appendix 5–4.3. Sections from line 7 showing inversion results of the *(A)* field data and *(B)* synthetic forward-model data for the Wenner-Schlumberger array, as well as *(C)* the forward model itself for the scenario with voids.

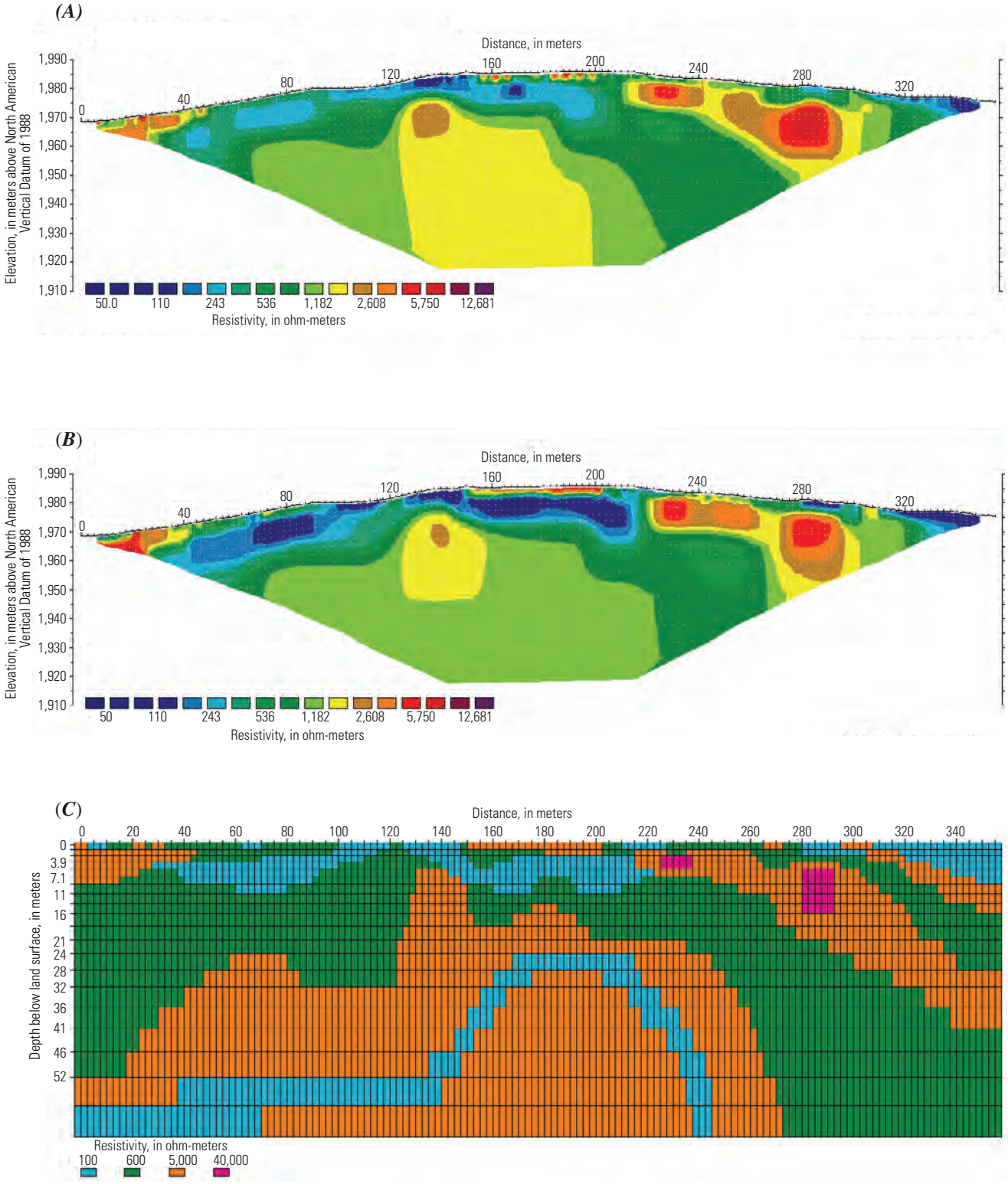

Appendix 5–4.4. Sections from line 7 showing inversion results of the *(A)* field data and *(B)* synthetic forward-model data for the Wenner-Schlumberger array, as well as *(C)* the forward model itself for the scenario without voids.

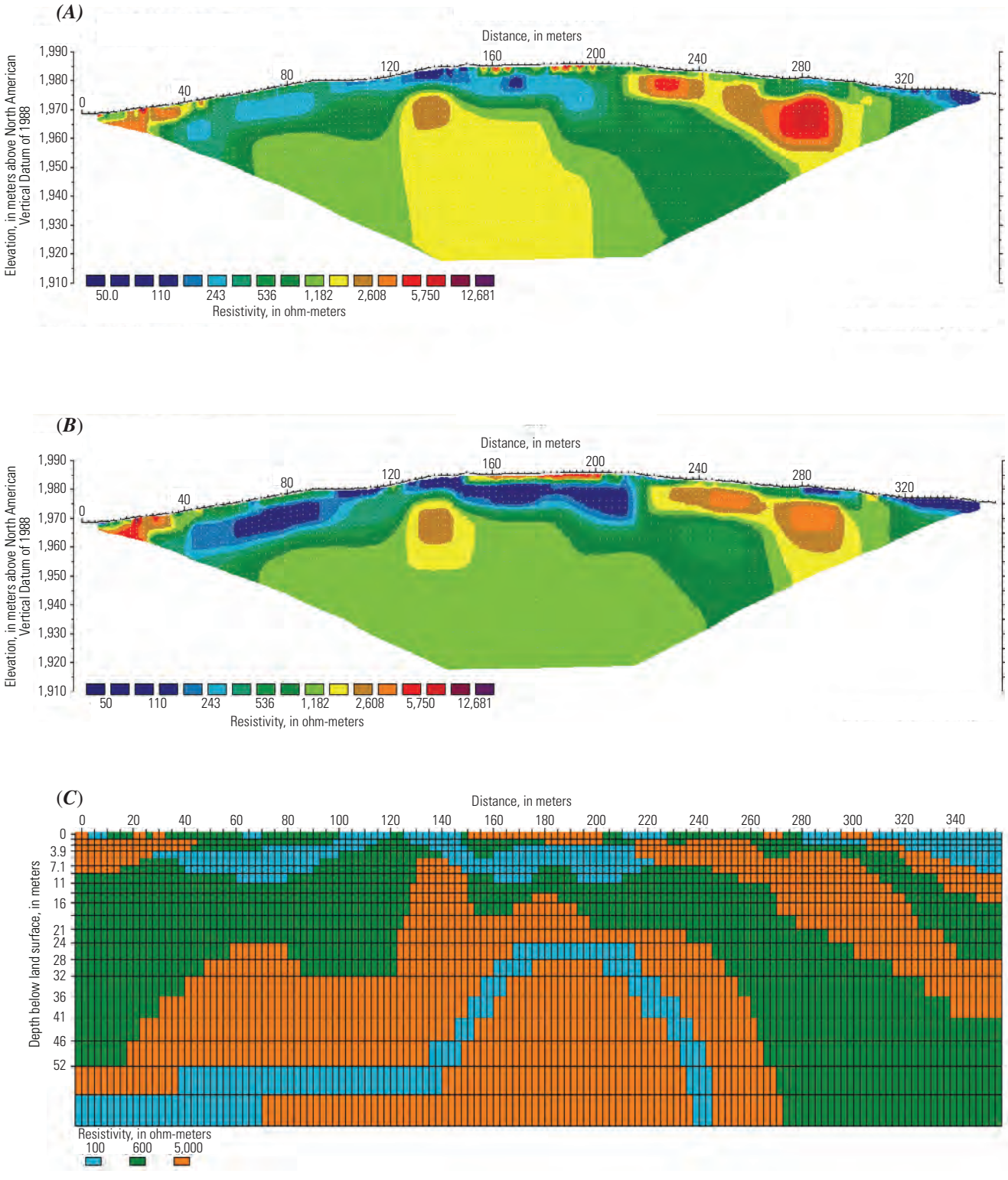

Appendix 5–5.1. Sections from line 1 showing inversion results of the *(A)* field data and *(B)* synthetic forward-model data for the dipole-dipole array, as well as *(C)* the forward model itself for the scenario with voids.

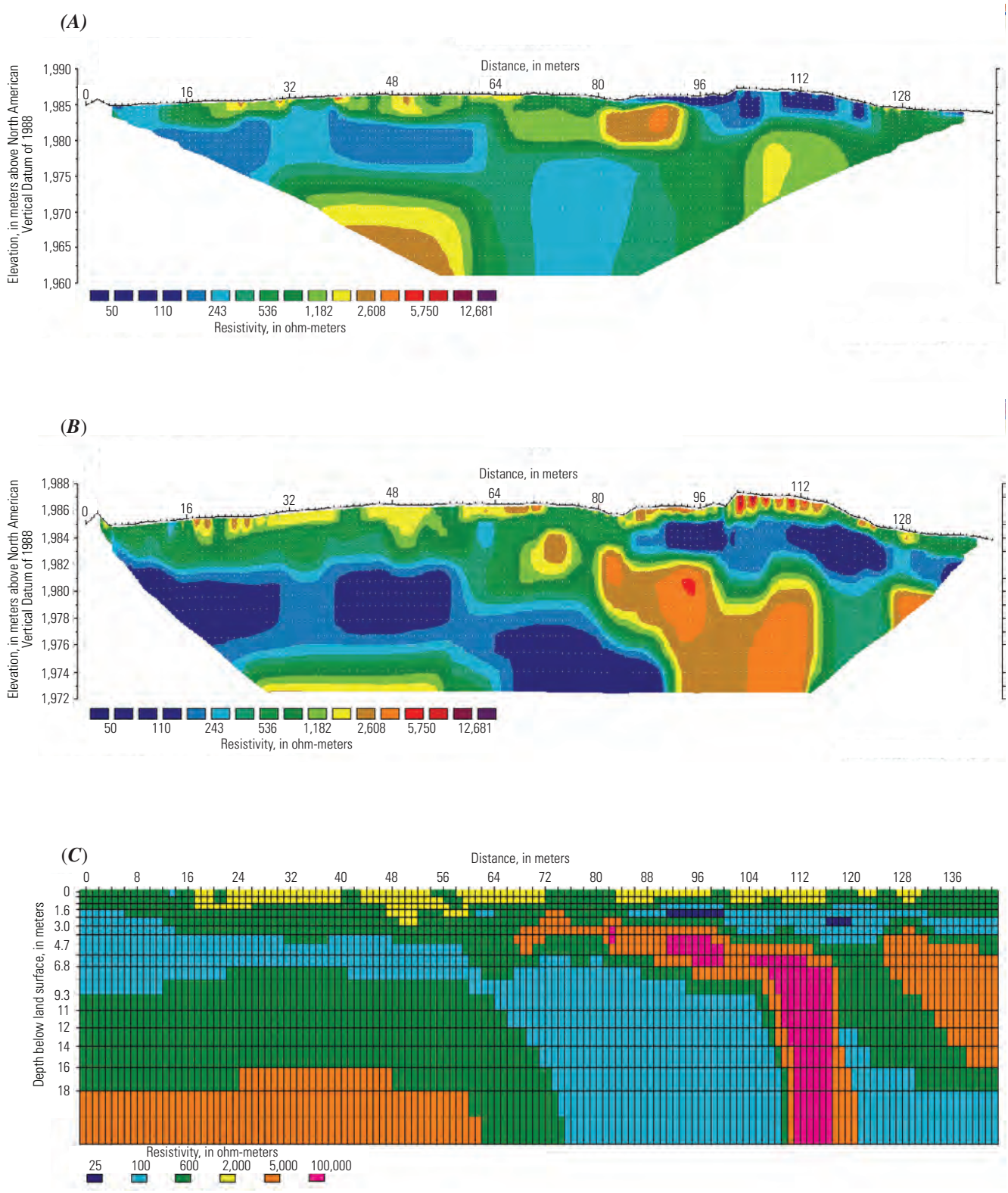

Appendix 5–5.2. Sections from line 1 showing inversion results of the *(A)* field data and *(B)* synthetic forward-model data for the dipole-dipole array, as well as *(C)* the forward model itself for the scenario without voids.

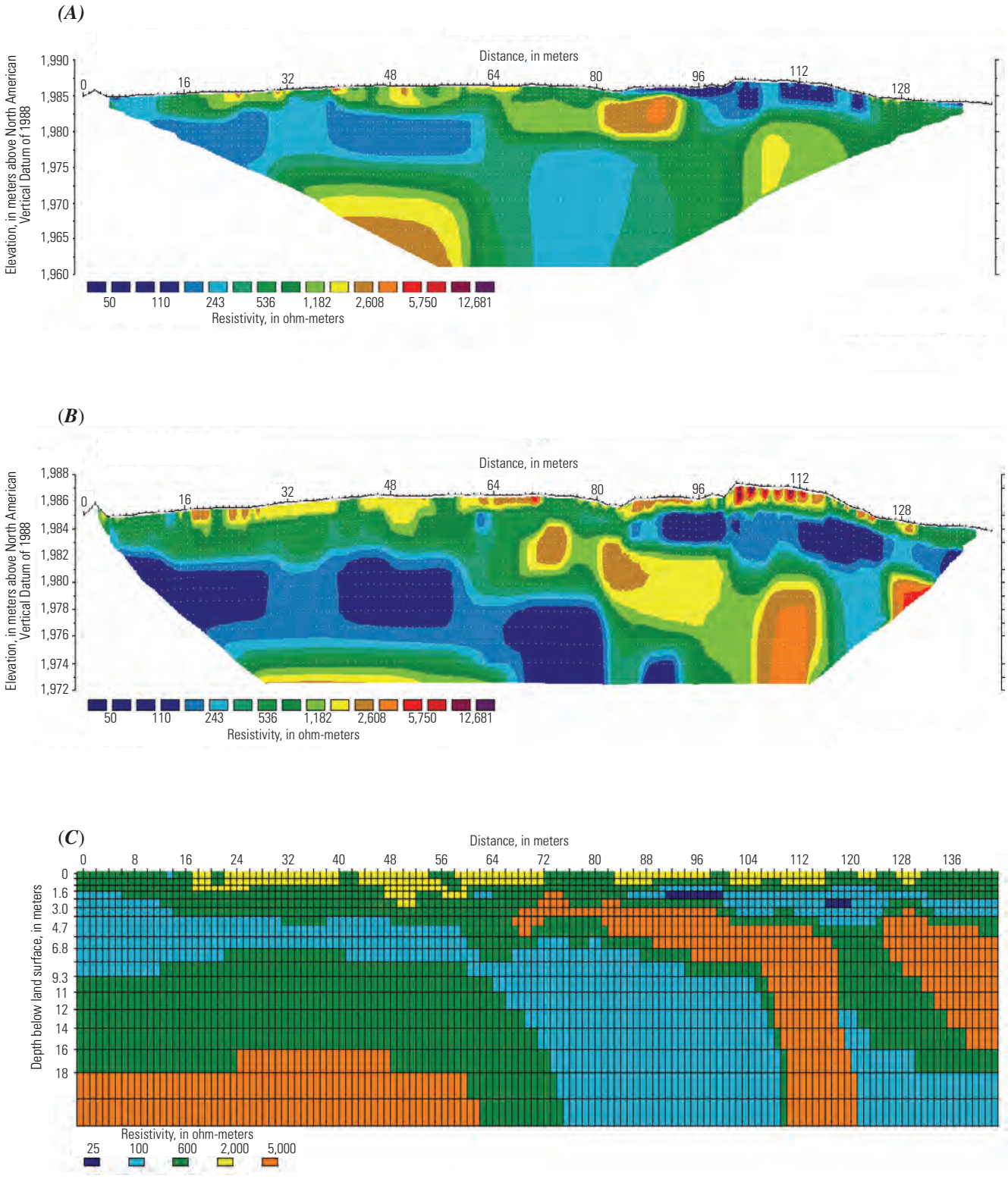

Appendix 5–5.3. Sections from line 1 showing inversion results of the *(A)* field data and *(B)* synthetic forward-model data for the Wenner-Schlumberger array, as well as *(C)* the forward model itself for the scenario with voids.

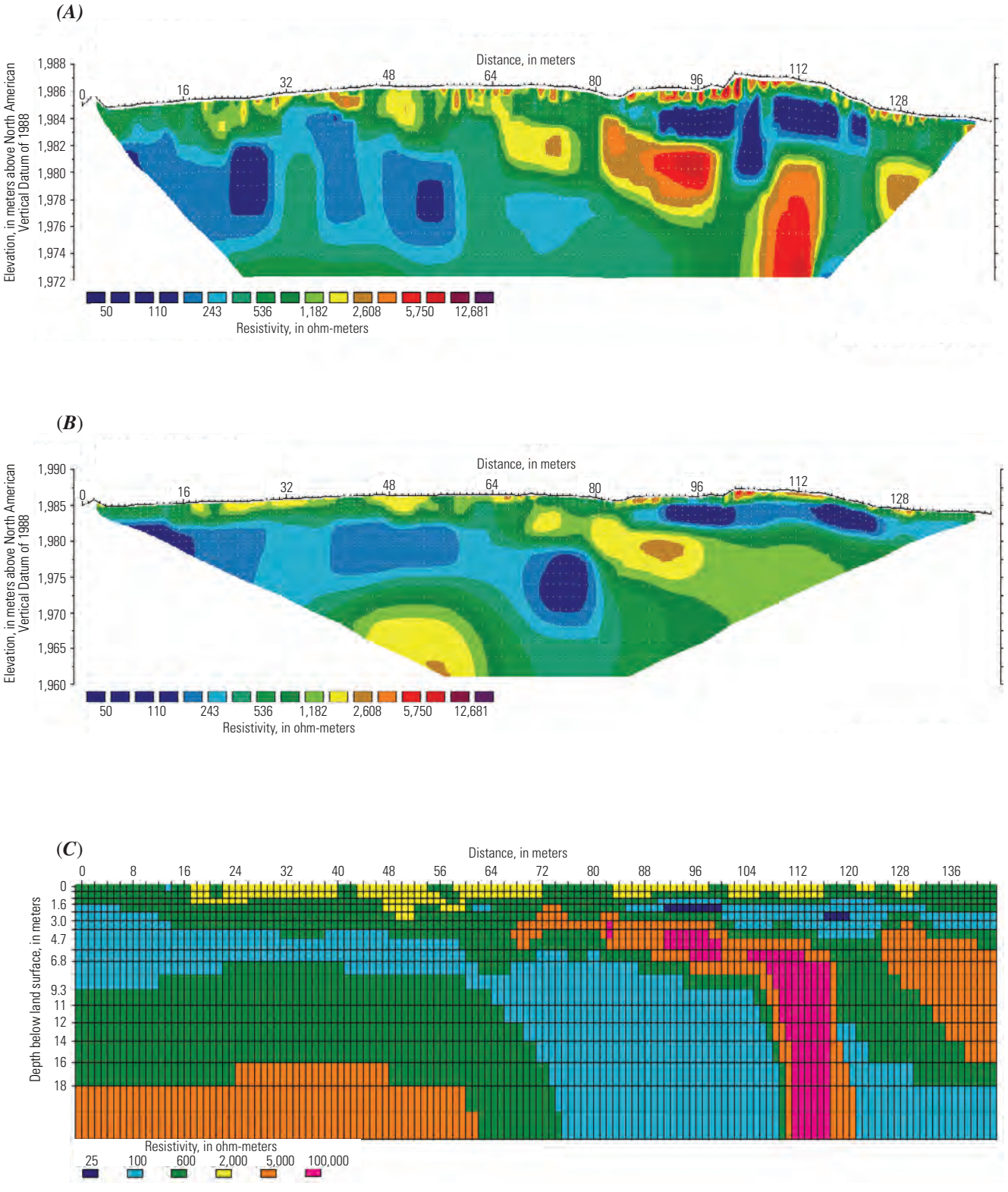

Appendix 5–5.4. Sections from line 1 showing inversion results of the *(A)* field data and *(B)* synthetic forward-model data for the Wenner-Schlumberger array, as well as *(C)* the forward model itself for the scenario without voids.

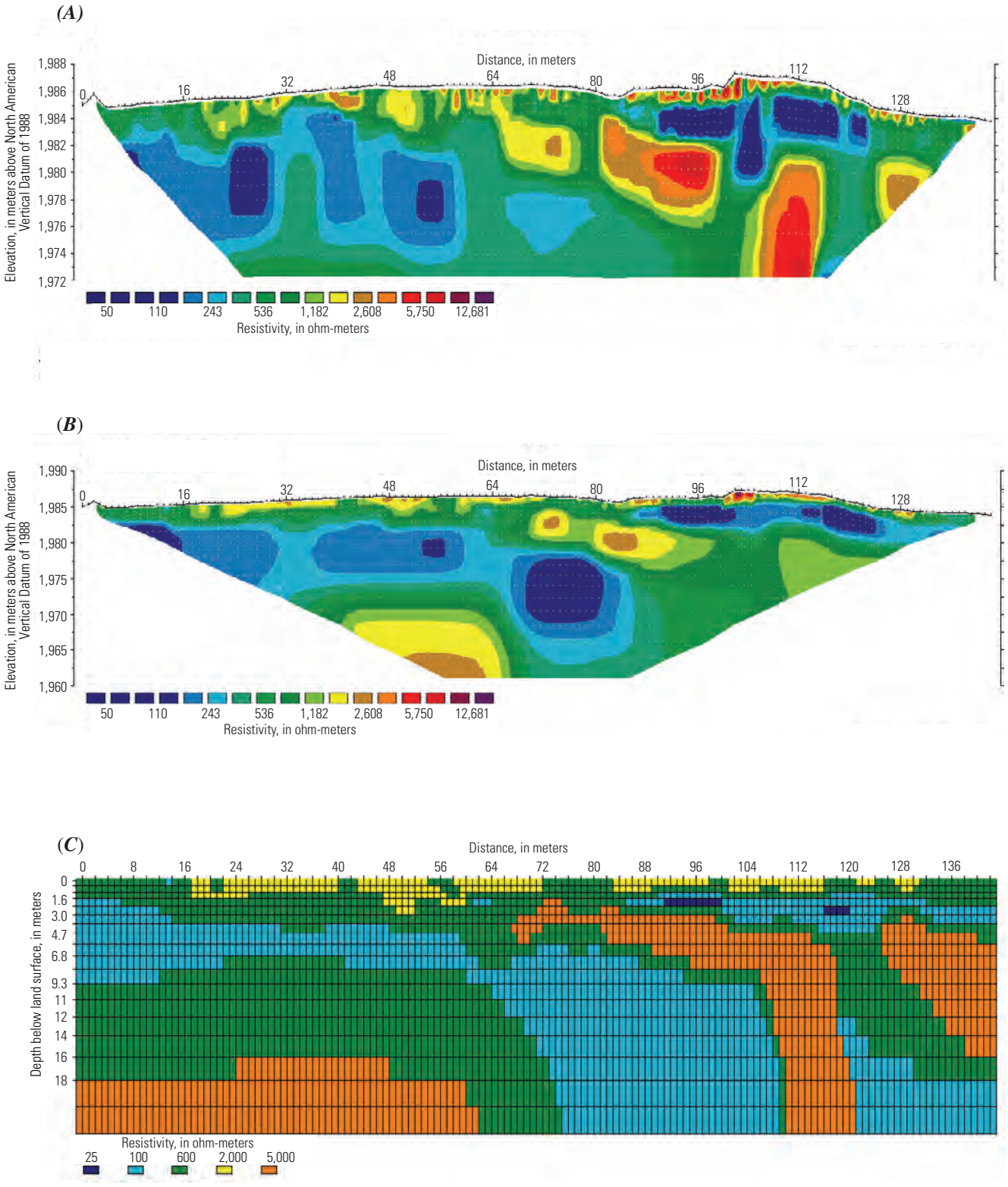

Appendix 5–5.5. Sections from line 1 showing inversion results of the *(A)* field data and *(B)* synthetic forward-model data for the high-resolution Wenner-Schlumberger array, as well as *(C)* the forward model itself for the scenario with voids.

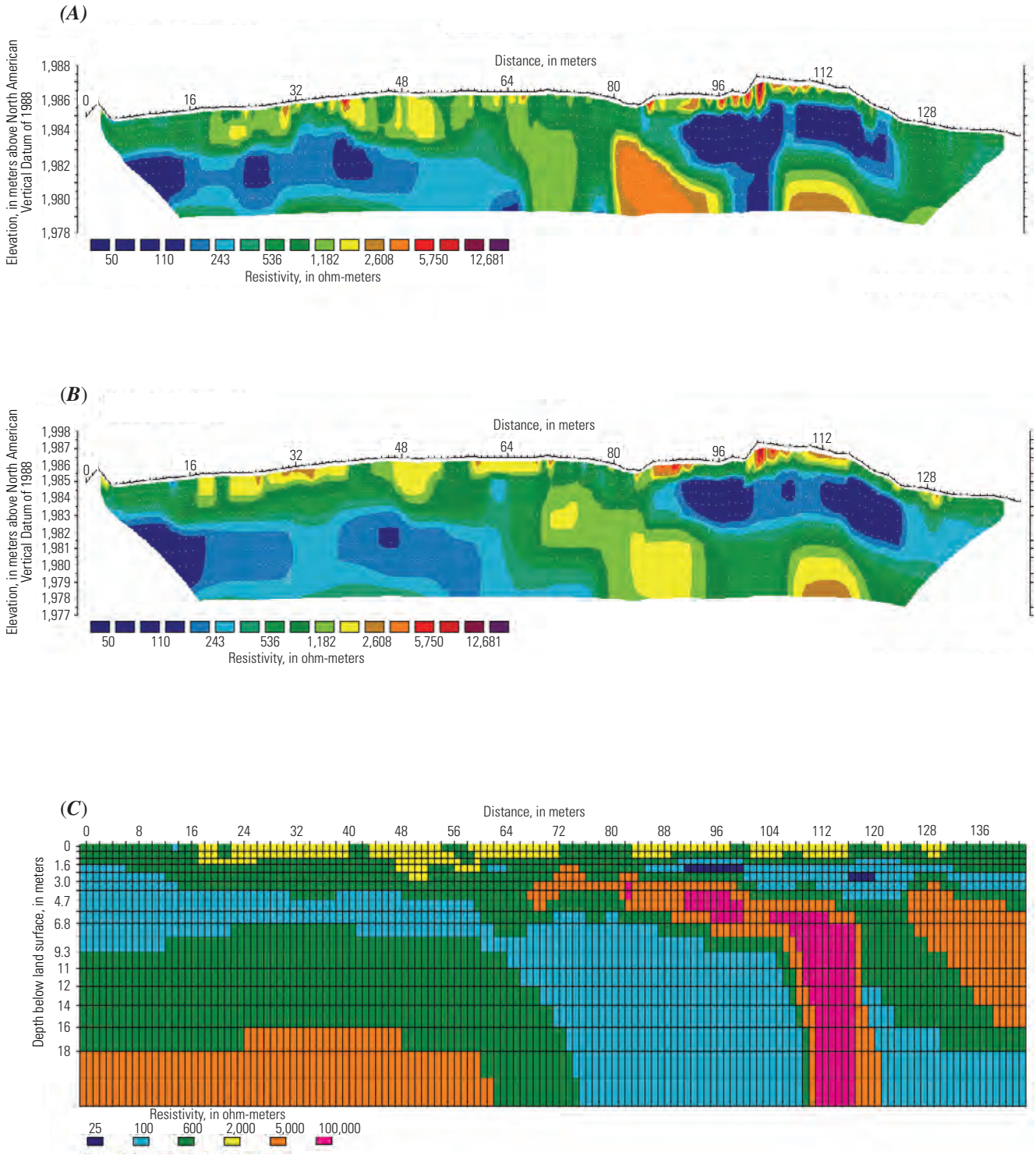

Appendix 5–5.6. Sections from line 1 showing inversion results of the *(A)* field data and *(B)* synthetic forward-model data for the high-resolution Wenner-Schlumberger array, as well as *(C)* the forward model itself for the scenario without voids.

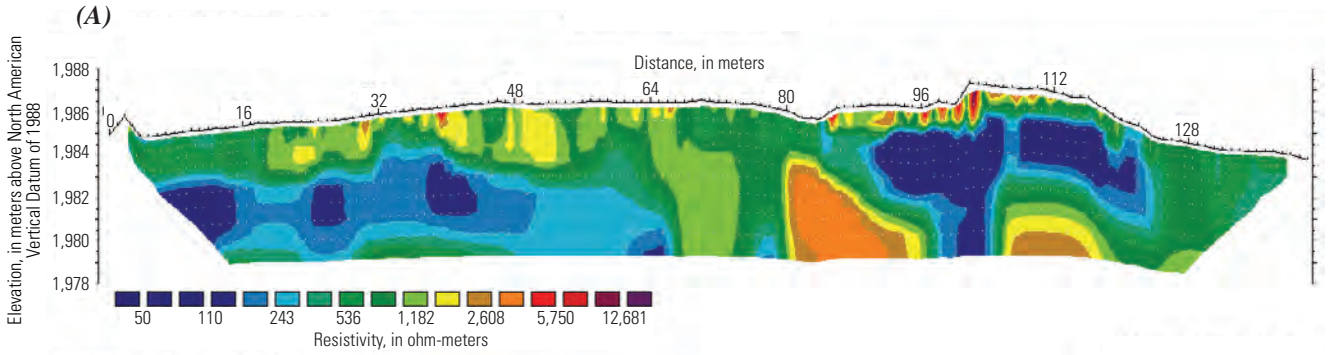

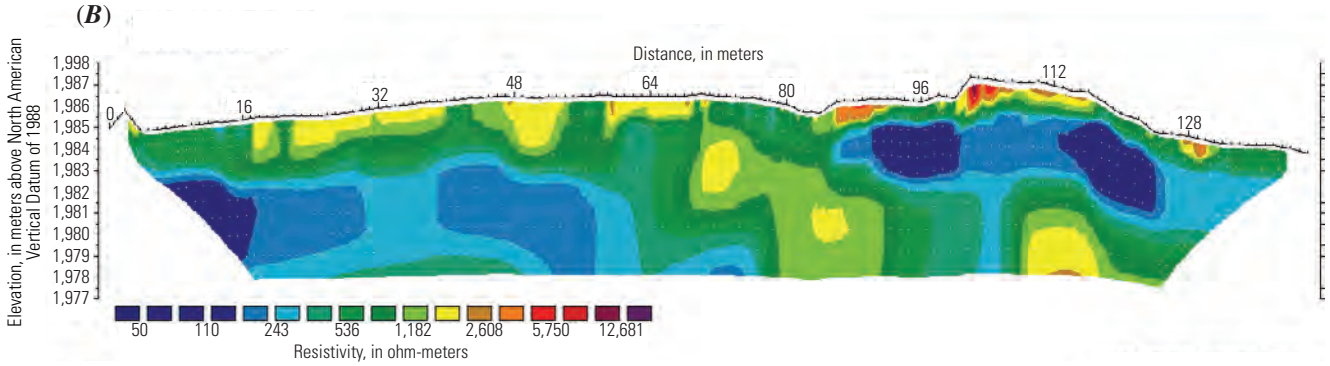

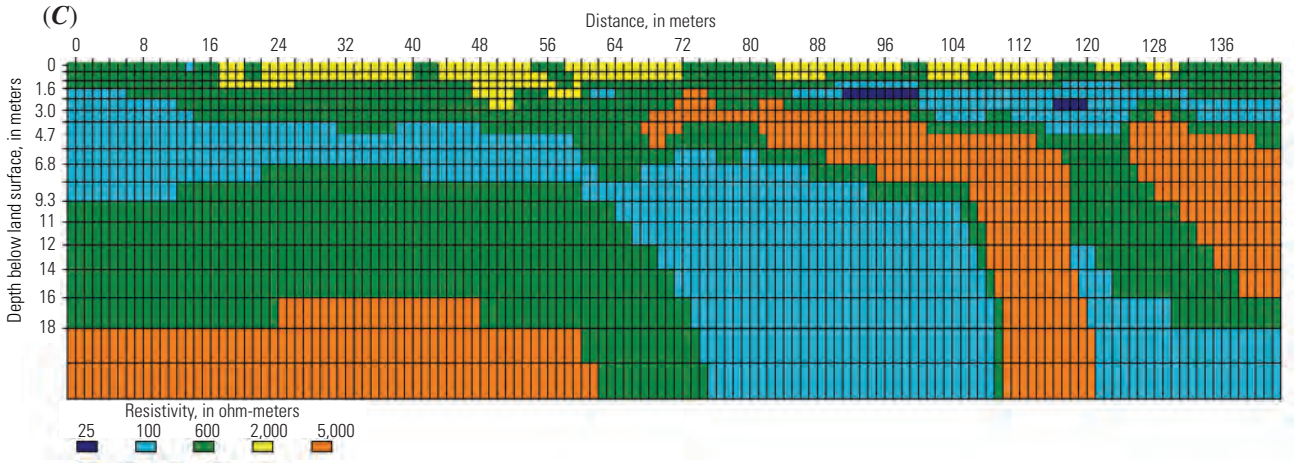

Appendix 5–6.1. Sections from line 5 showing inversion results of the *(A)* field data and *(B)* synthetic forward-model data for the dipole-dipole array, as well as *(C)* the forward model itself for the scenario with voids.

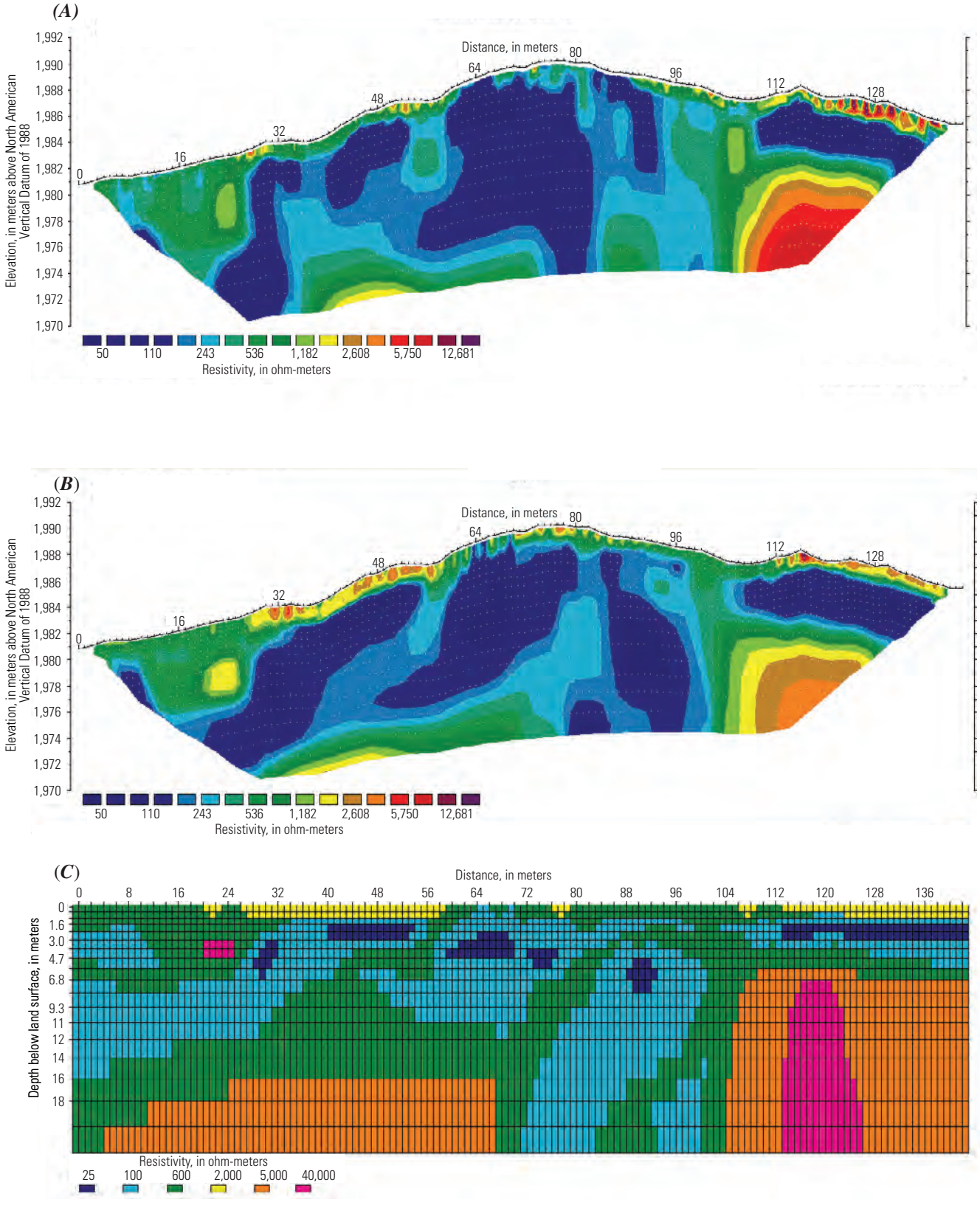

Appendix 5–6.2. Sections from line 5 showing inversion results of the *(A)* field data and *(B)* synthetic forward-model data for the dipole-dipole array, as well as *(C)* the forward model itself for the scenario without voids.

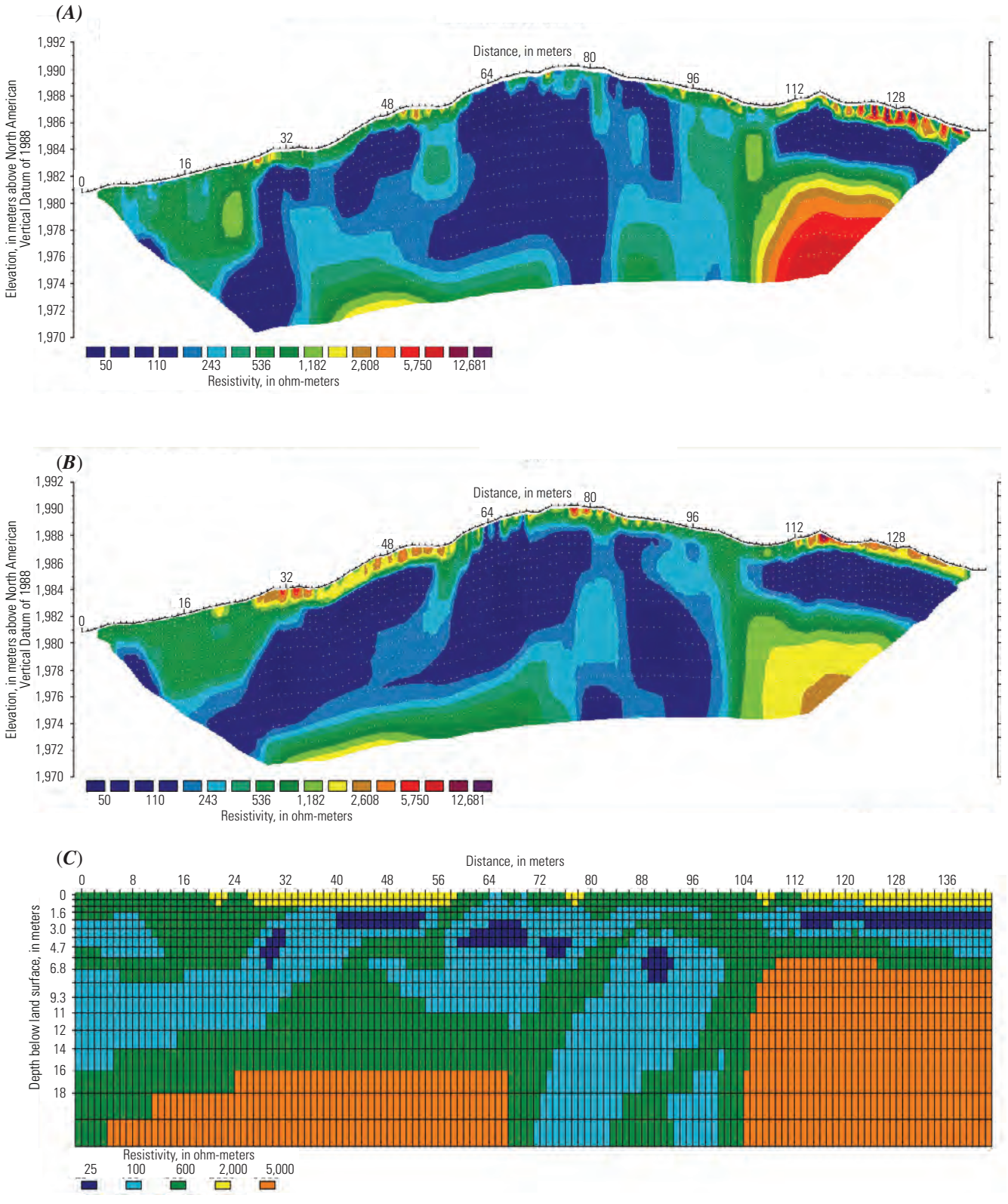

Appendix 5–6.3. Sections from line 5 showing inversion results of the *(A)* field data and *(B)* synthetic forward-model data for the Wenner-Schlumberger array, as well as *(C)* the forward model itself for the scenario with voids.

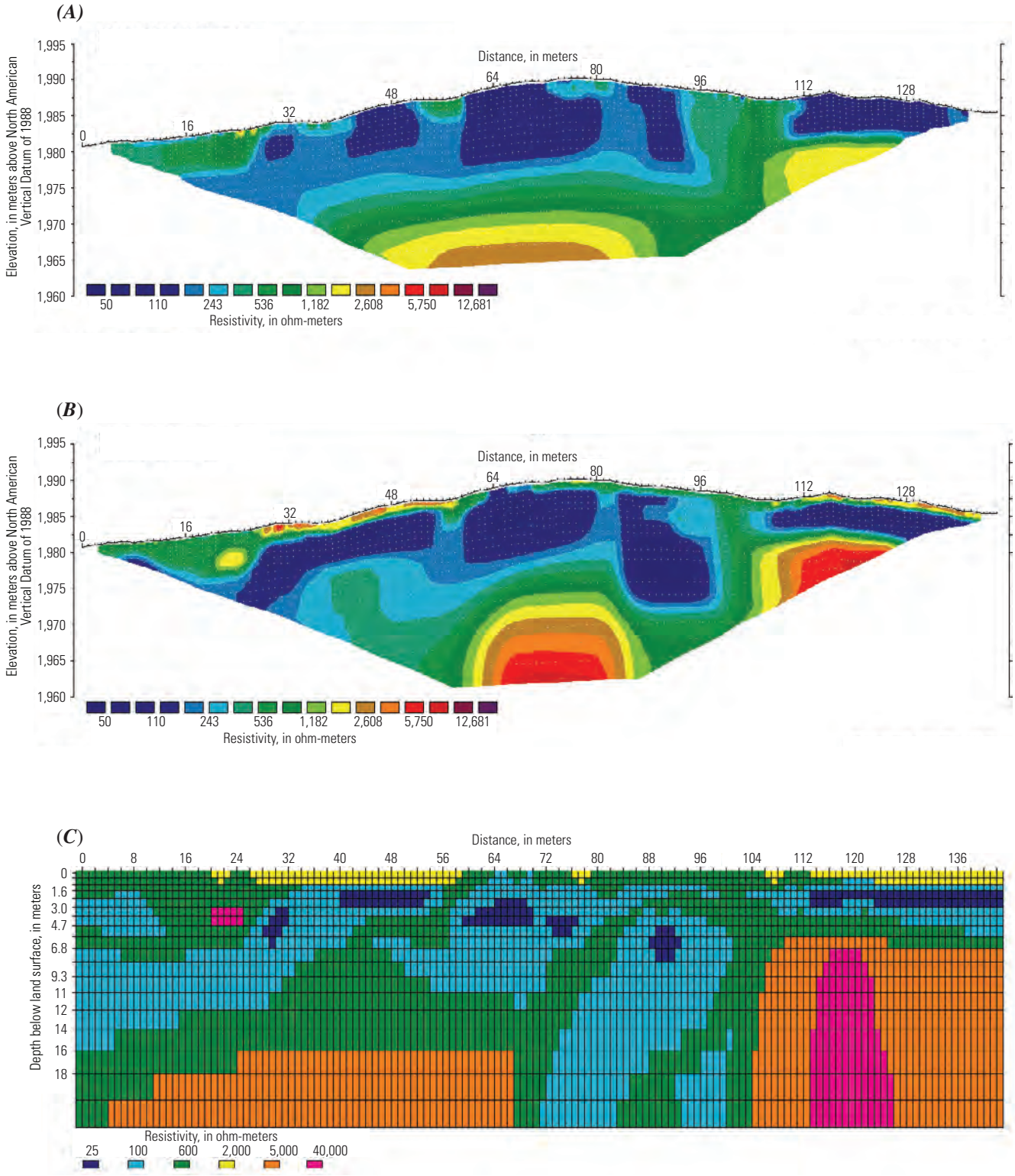

Appendix 5–6.4. Sections from line 5 showing inversion results of the *(A)* field data and *(B)* synthetic forward-model data for the Wenner-Schlumberger array, as well as *(C)* the forward model itself for the scenario without voids.

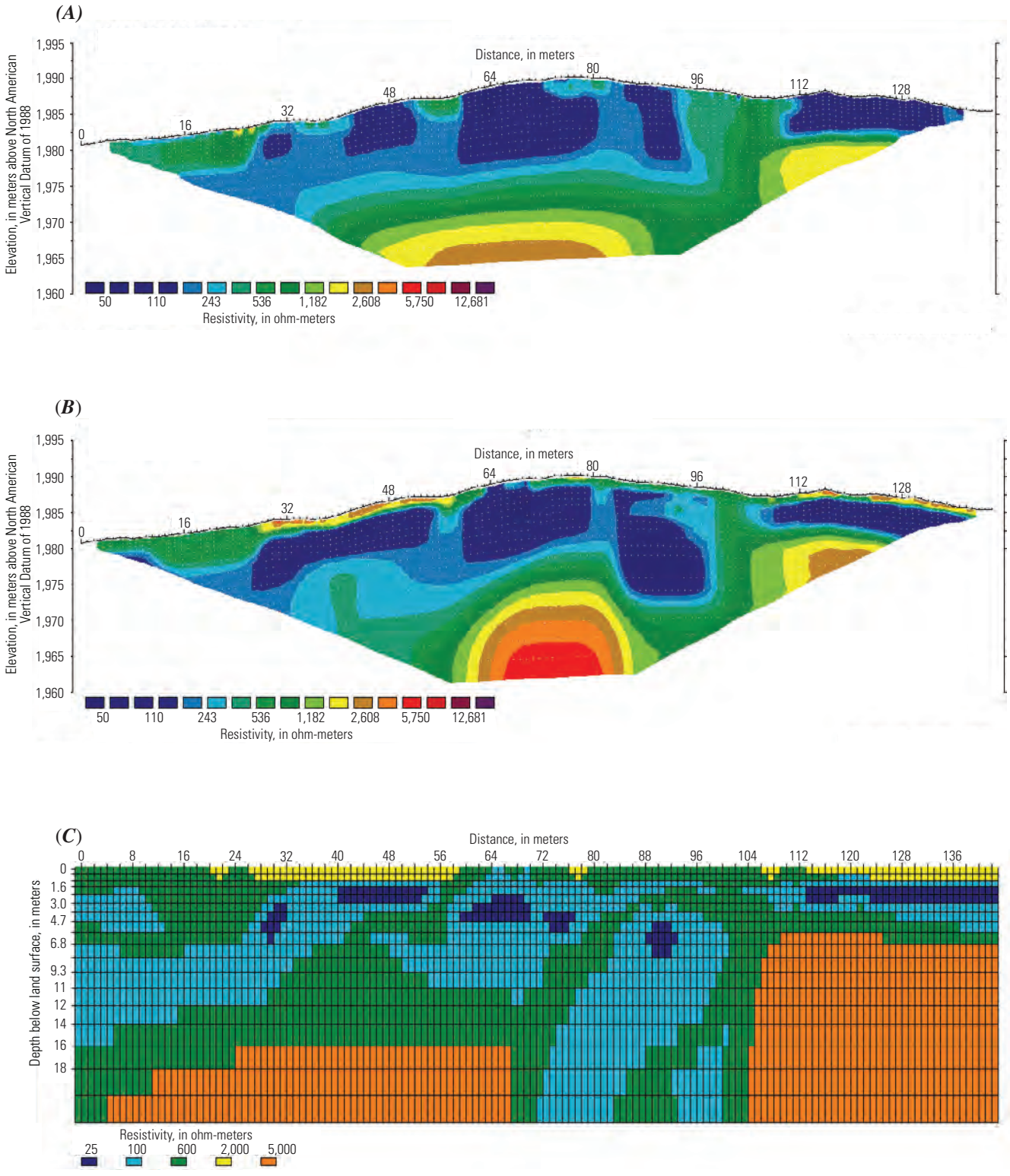

Appendix 5–6.5. Sections from line 5 showing inversion results of the *(A)* field data and *(B)* synthetic forward-model data for the high-resolution Wenner-Schlumberger array, as well as *(C)* the forward model itself for the scenario with voids.

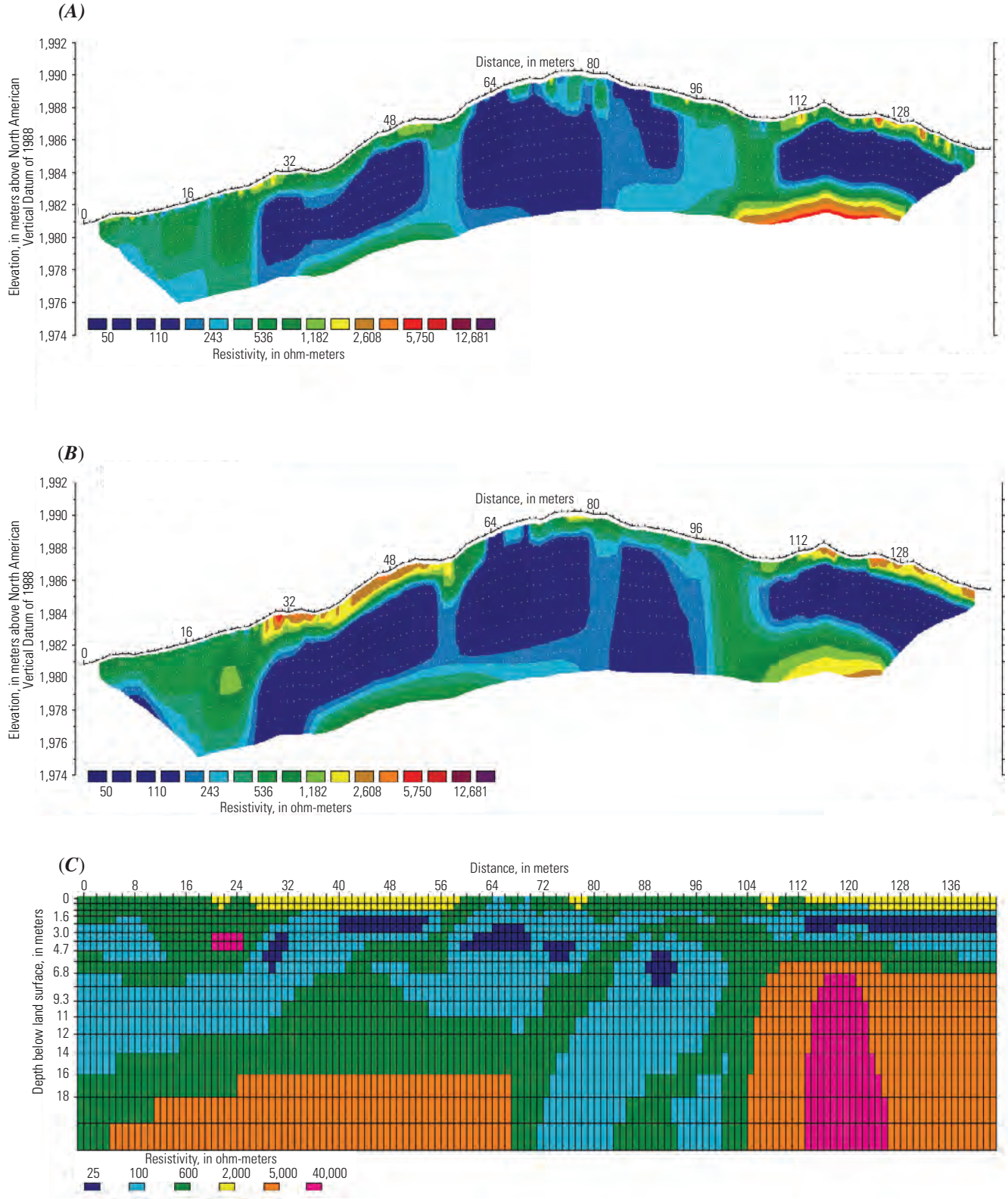

Appendix 5–6.6. Sections from line 5 showing inversion results of the *(A)* field data and *(B)* synthetic forward-model data for the high-resolution Wenner-Schlumberger array, as well as *(C)* the forward model itself for the scenario without voids.

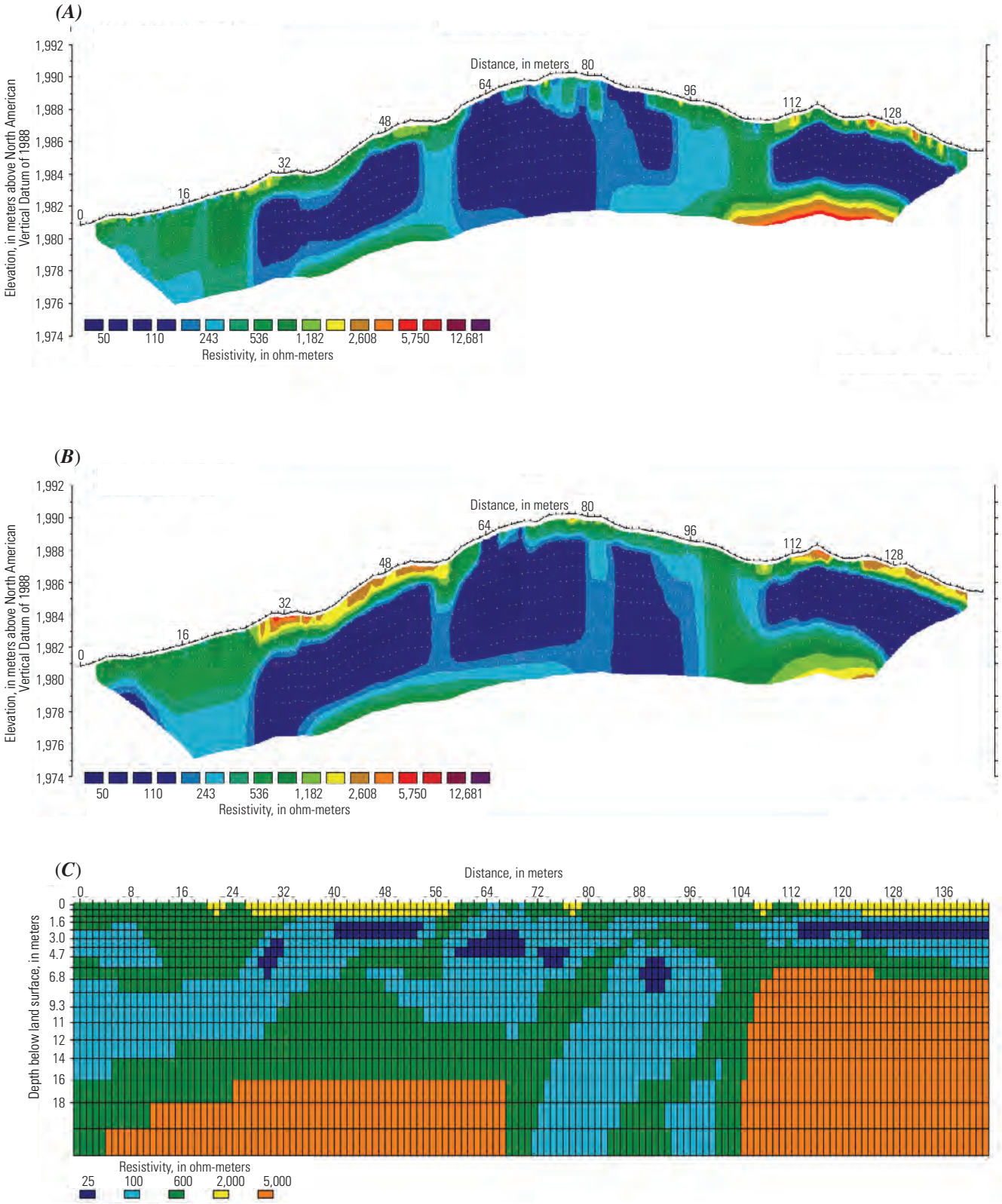

Appendix 5–7.1. Sections from line 2 showing inversion results of the *(A)* field data and *(B)* synthetic forward-model data for the dipole-dipole array, as well as *(C)* the forward model itself for the scenario with voids.

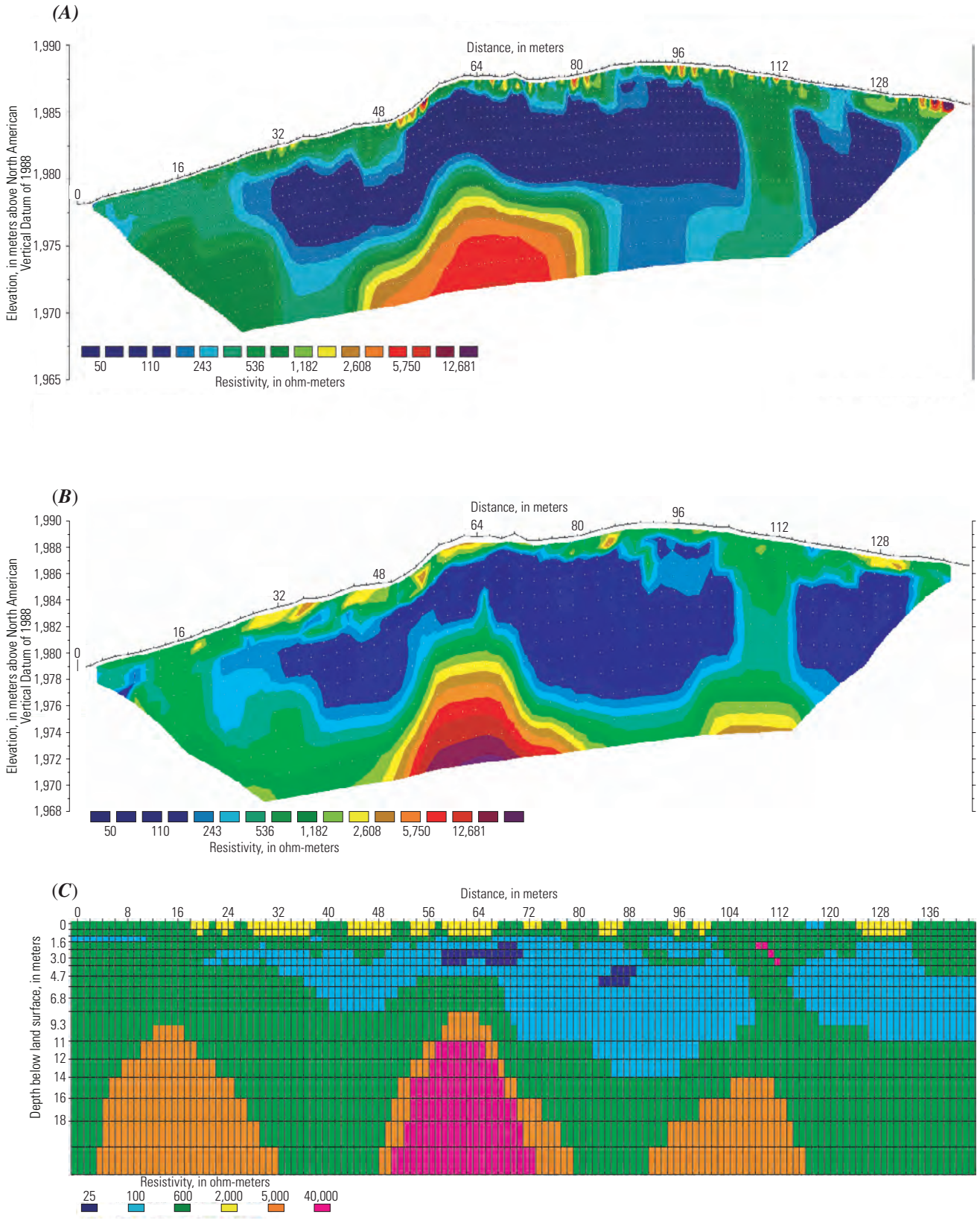

Appendix 5–7.2. Sections from line 2 showing inversion results of the *(A)* field data and *(B)* synthetic forward-model data for the dipole-dipole array, as well as *(C)* the forward model itself for the scenario without voids.

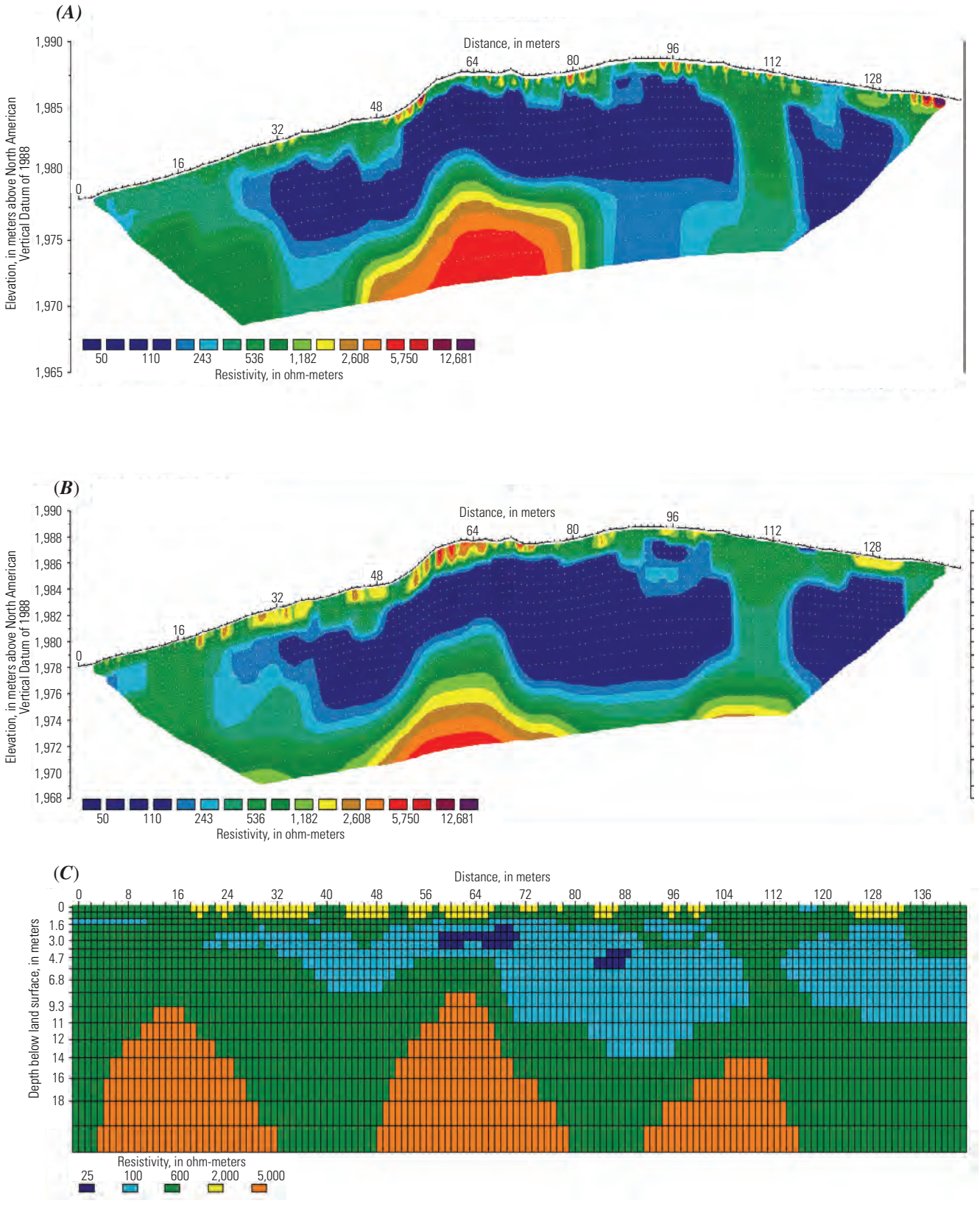

Appendix 5–7.3. Sections from line 2 showing inversion results of the *(A)* field data and *(B)* synthetic forward-model data for the Wenner-Schlumberger array, as well as *(C)* the forward model itself for the scenario with voids.

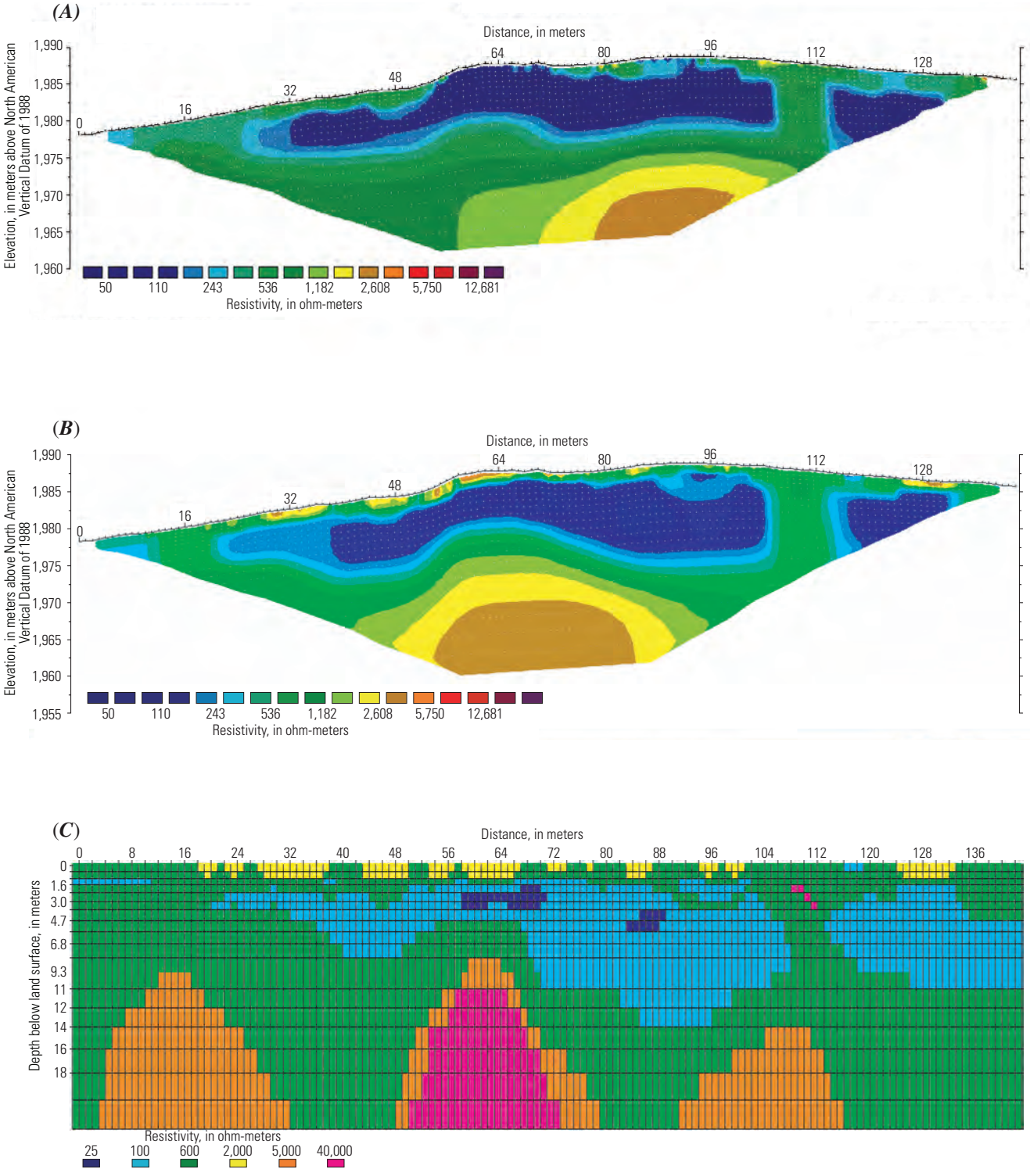

Appendix 5–7.4. Sections from line 2 showing inversion results of the *(A)* field data and *(B)* synthetic forward-model data for the Wenner-Schlumberger array, as well as *(C)* the forward model itself for the scenario without voids.

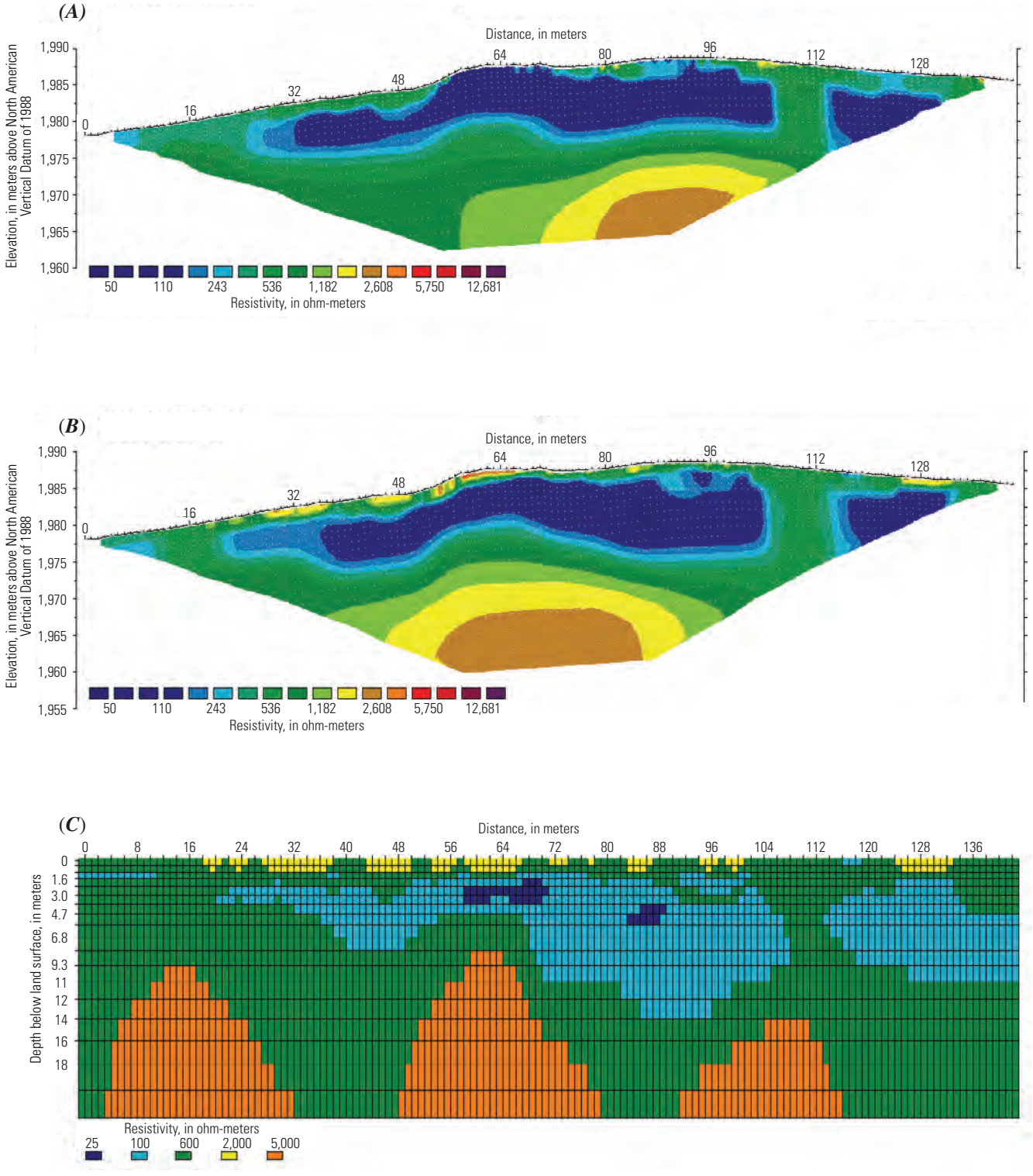

Appendix 5–7.5. Sections from line 2 showing inversion results of the *(A)* field data and *(B)* synthetic forward-model data for the high-resolution Wenner-Schlumberger array, as well as *(C)* the forward model itself for the scenario with voids.

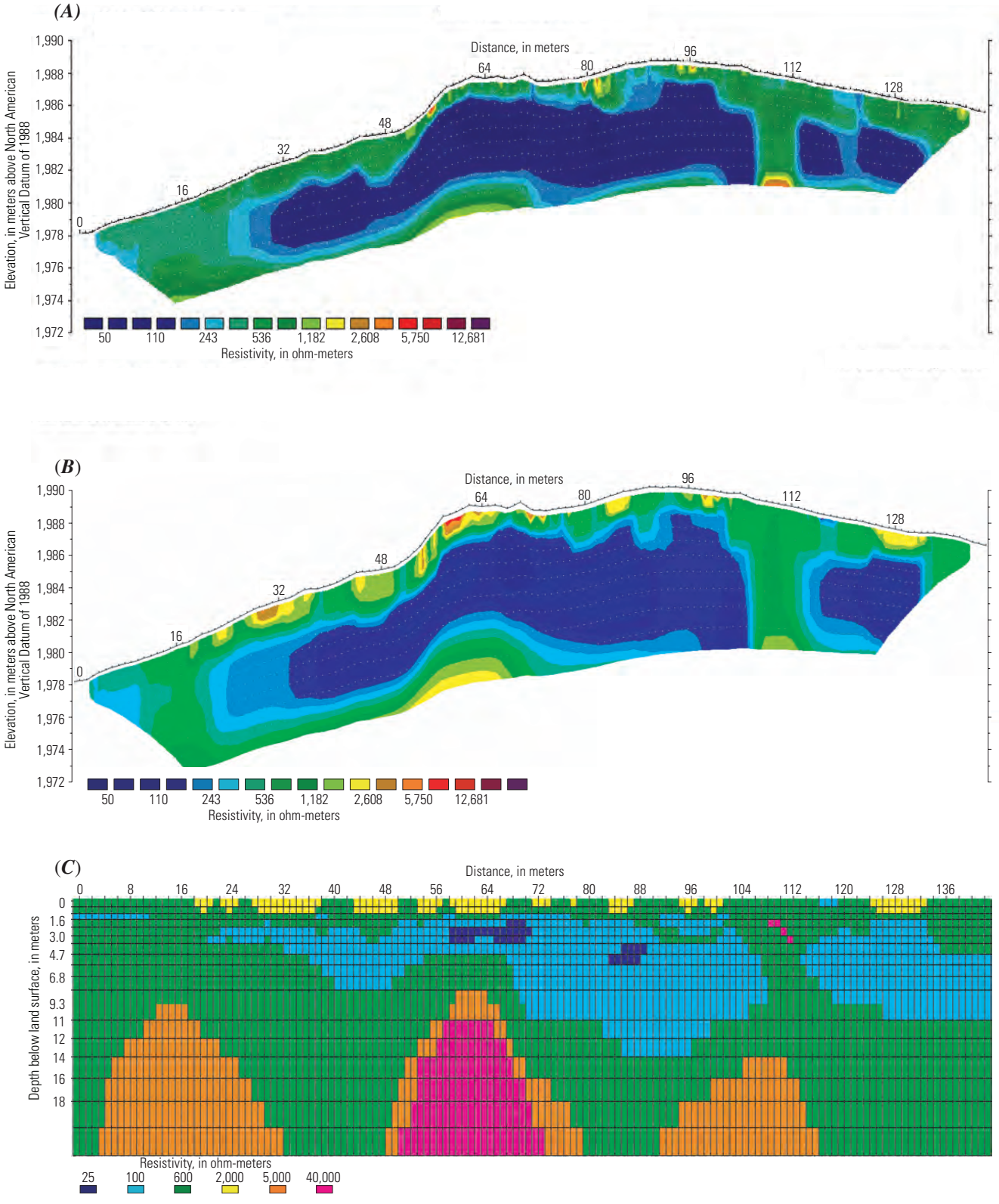

Appendix 5–7.6. Sections from line 2 showing inversion results of the *(A)* field data and *(B)* synthetic forward-model data for the high-resolution Wenner-Schlumberger array, as well as *(C)* the forward model itself for the scenario without voids.

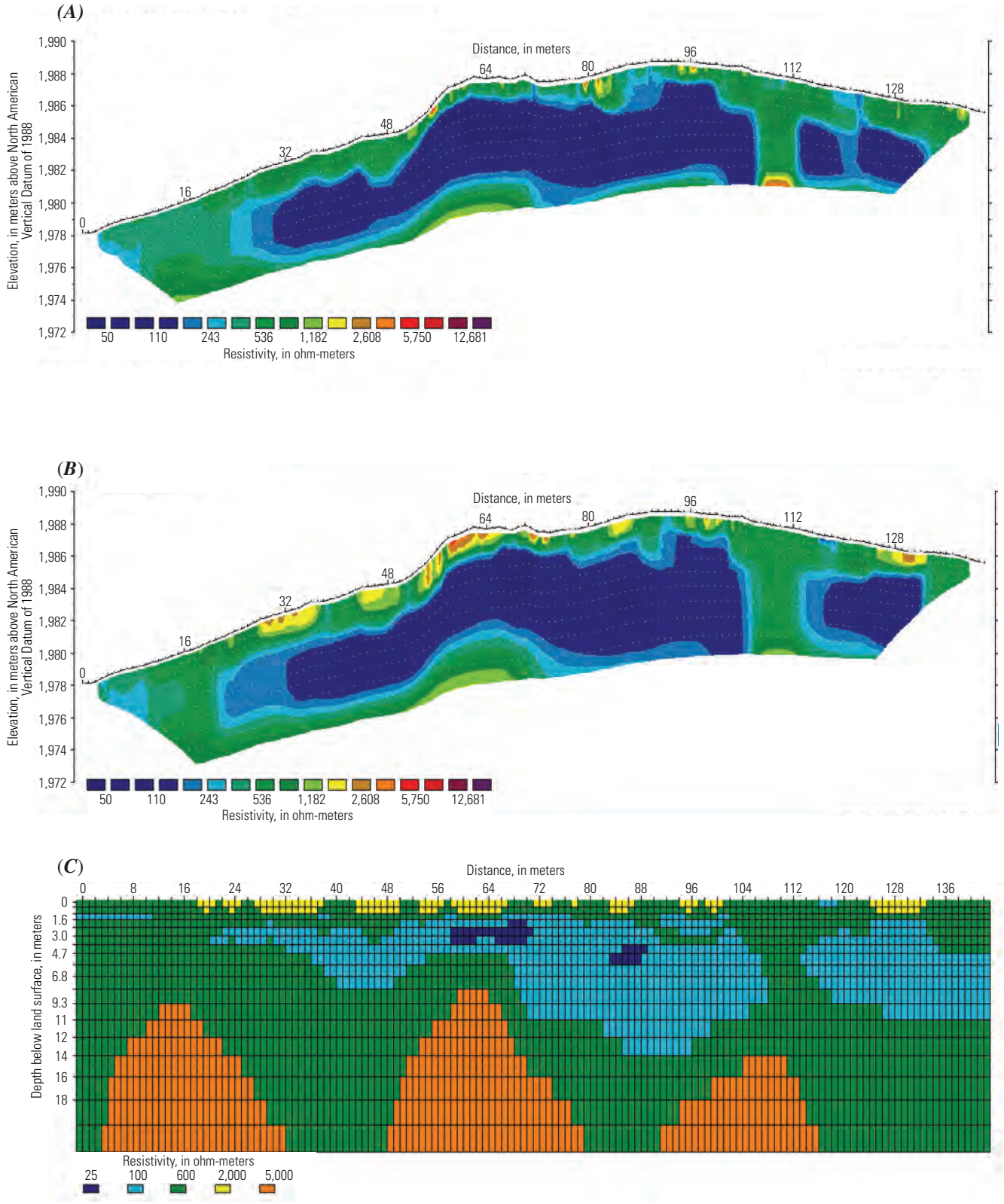

Prepared by Lawrence Publishing Service Center.
Edited by Lanna Combs.
Graphics by Jeff Hartley and Mike Kemppainen.
Layout and design by Kristi Hartley.

For more information concerning the research described in this report, contact:

U.S. Geological Survey
5231 South 19 Street
Lincoln, NE 68512
(402) 328-4100
http://ne.water.usgs.gov

USGS

Ball and others—**Characterization of Near-Surface Geology and Possible Voids Using Resistivity and Electromagnetic Methodsat the Gran Quivira Unit of Salinas Pueblo Missions National Monument, Central New Mexico, June 2005**—Scientific Investigations Report 2006–5176

Printed on recycled paper